GRI-CR-95-7110

FINAL REPORT

CONTRACT NAS8-39075

21 August 1991 through 30 June 1994

RADAR INVESTIGATIONS OF BARIUM RELEASES OVER ARECIBO OBSERVATORY, PUERTO RICO

Geospace Research, Inc.
550 N. Continental Blvd., Suite 110
El Segundo, CA 90245

Report Date: 7 July 1995

Institutional Authorization

Frank T Djuth

Frank T. Djuth, President
Geospace Research, Inc.
(310) 322-1160

Principal Investigator

Frank T Djuth

Dr. Frank T. Djuth
(310) 322-1160
FAX: (310) 322-2596
E-Mail: djuth@netcom.com

(NASA-CR-199197) RADAR INVESTIGATION OF BARIUM RELEASES OVER ARECIBO OBSERVATORY, PUERTO RICO Final Report, 12 Aug. 1991 - 30 Jun. 1994 (Geospace Research) 162 p

N96-12150

Unclas

G3/46 0071244

TABLE OF CONTENTS

Project Summary iii

1. Overview of Results Obtained during the CRRES *El Coqui* Campaign 1-1
   - 1.1 Campaign Diagnostics 1-1
   - 1.2 AA-3a Experiment 1-2
   - 1.3 AA-4 Experiment 1-2
   - 1.4 AA-3b Experiment 1-3
   - 1.5 NC-1 Experiment 1-4
   - 1.6 NC-2 Experiment 1-4
   - 1.7 AA-1 and AA-7 Experiments 1-4
   - 1.8 AA-2 Experiment 1-6

2. The CRRES AA-2 Release: HF Wave-Plasma Interactions in a Dense Ba^+ Cloud 2-1
   - Abstract 2-2
   - 2.1 Introduction 2-3
   - 2.2 Experiment Design 2-4
   - 2.3 Observations 2-6
   - 2.4 Discussion 2-18
   - 2.5 Conclusions 2-26

3. AA-4: The Ionospheric Focussed Heating (IFH) Experiment 3-1
   - Abstract 3-1
   - 3.1 Introduction 3-2
   - 3.2 Experiment Concept - Chemically Produced Cavity 3-5
   - 3.3 In Situ Measurements 3-9
   - 3.4 Incoherent Scatter Radar Measurements 3-15
   - 3.5 Ground-Based Optical and Radio Observations 3-18
   - 3.6 Conclusions 3-21

4. Incoherent Scatter Observations during Releases AA-1/AA-7 and AA-3b 4-1
   - 4.1 Arecibo Radar Measurements in Support of AA-1 and AA-7 4-1
     - 4.1.1 Description of the AA-1/AA-7 Releases 4-1
     - 4.1.2 Arecibo Radar Operations 4-3
     - 4.1.3 Radar Results 4-4
     - 4.1.4 Discussion and Conclusions 4-7

4.2 Arecibo Radar Measurements in Support of AA-3b 4-8
4.2.1 Description of the AA-3b Releases 4-8
4.2.2 Arecibo Radar Operations 4-9
4.2.3 Radar Results 4-9
4.2.4 Discussion and Conclusions 4-11
5. Spin-off Science Fostered by the *El Coqui* Campaign 5-1
Abstract 5-2
5.1 Introduction 5-3
5.2 Data-Taking Methodology 5-4
5.3 Aeronomic Observations 5-6
5.4 Conclusions 5-8

PROJECT SUMMARY

The NASA Combined Release and Radiation Effects Satellite (CRRES) *El Coqui* rocket campaign was successfully carried out in Puerto Rico during the period 18 May through 12 July 1992. This campaign was the last component of the larger CRRES program, which consisted of a primary CRRES spacecraft launched with an Atlas/Centaur vehicle, a Pagasus-borne small satellite, and two rocket campaigns performed from Kwajalein Atoll and Puerto Rico. The *El Coqui* campaign was conducted from Puerto Rico to take advantage of the large incoherent scatter radar at Arecibo Observatory, Puerto Rico and the Arecibo high-power, high-frequency (HF) facility. A total of eight rockets were launched into the ionosphere above Arecibo Observatory. Six of the rockets carried chemical release payloads that were used to actively modify the ionosphere and to examine physical processes in the laboratory-without-walls environment of space. The remaining two rockets were used to probe natural sporadic-E instabilities and to make *in situ* measurements of ionospheric modifications produced by the Arecibo HF facility.

This report describes five chemical release experiments supported by Geospace Research, Inc. (GRI) during the *El Coqui* campaign. These releases are designated as AA-1 (rocket 36-082), AA-2 (rocket 36-081), AA-3b (rocket 36-064), AA-4 (rocket 36-065), and AA-7 (rocket 36-083). GRI's efforts included the deployment of a new high-speed radar processor system at Arecibo Observatory, Puerto Rico. The special purpose processor allowed the full information content of the incoherent scatter radar data at Arecibo to be captured for the first time. This proved to be an important diagnostic tool for many of the studies related to the release experiments. In addition, a VHF (49.92 MHz) radar-interferometer was positioned on the island of Antigua to monitor the development of geomagnetic field-aligned striations in several of the release clouds (AA-1, AA-2, and AA-7). F. T. Djuth of GRI served as principal investigator on the AA-2 experiment; this release provided the focus for much of the analysis effort. The AA-2 experiment produced a variety of new and extraordinarily interesting results. The first detailed examination of these results has been completed, and the principal findings are described in a comprehensive journal article [Djuth *et al., J. Geophys. Res.*, in press, 1995]. In addition, close collaborations between personnel from the Naval Research Laboratory (NRL) and GRI yielded an extensive publication dealing with the AA-4 results [Bernhardt *et al., J. Geophys. Res.*, in press, 1995]. Radar data gathered by GRI in support of experiments AA-3b, AA-1, and AA-7 have also been fully analyzed. Journal publications on these three releases are pending; they will be submitted to

J. Geophys. Res. following the completion of data analyses by the respective principal investigators. Finally, radar tests performed by GRI and Arecibo Observatory in support of the *El Coqui* campaign yielded a powerful new diagnostic technique for studies of naturally occurring processes in the upper atmosphere [Djuth *et al.*, 1994]. This spin-off of the CRRES program is likely to have a significant and enduring impact on future studies of the earth's atmosphere and near-space environment.

REFERENCES

Bernhardt, P. A., C. L. Siefring, P. Rodriguez, D. G. Haas, M. M. Baumback, H. A. Romero, D. A. Sollin, F. T. Djuth, L. M. Duncan, D. E. Hunton, C. J. Pollock, M. P. Sulzer, C. A. Tepley, L. S. Wagner, and J. A. Goldstein, The ionospheric focussed heating (IFH) experiment, *J. Geophys. Res.*, in press, 1995.

Djuth, F. T., M. P. Sulzer, and J. H. Elder, Application of the Coded Long-Pulse Technique to Plasma Line Studies of the Ionosphere, *Geophys. Res. Lett.*, *21*, 2725-2728, 1994.

Djuth, F. T., M. P. Sulzer, J. H. Elder, and K. M. Groves, The CRRES AA-2 release: HF wave-plasma interactions in a dense Ba^+ cloud, *J. Geophys. Res.*, in press, 1995.

1. Overview of Results Obtained during the CRRES *El Coqui* Campaign

A general description of key results from all experiments conducted during the *El Coqui* campaign is provided below. This is intended to be a concise summary of campaign results. Particular attention is paid to experiments in which Geospace Research, Inc. (GRI) had active participation. These include five of the original CRRES investigations designated AA-4, AA-3b, AA-1, AA-7, and AA-2. The AA-2 barium release was of primary interest to GRI. Detailed studies of data acquired during the AA-2 and AA-4 experiments are presented in Sections 2 and 3, respectively. In Section 4, Arecibo radar results from experiments AA-3b, AA-1 and AA-7 are described and interpreted. Finally. an improved radar methodology was developed at Arecibo in anticipation of the CRRES program. This yielded a great deal of "spin-off" research in the atmospheric sciences. The new radar technique and its applications are described in Section 5

During the *El Coqui* campaign, GRI furnished a high-speed radar processor for use with the Arecibo incoherent scatter radar and deployed a VHF radar interferometer on the island of Antigua. All Arecibo radar data presented in this report were acquired by GRI in collaboration with M. P. Sulzer of Arecibo Observatory. K. M. Groves (Phillips Laboratory, Hanscom Air Force Base) also assisted in the collection of the Arecibo radar data and in the deployment of a VHF radar system on Antigua. Essential field support for the Antigua radar measurements was provided by J. W. Brosnahan (LaSalle Research Corporation), who worked closely with GRI personnel.

1.1 Campaign Diagnostics

Arecibo Observatory in Puerto Rico hosted many of the experimenters and served as a control center for most of the *El Coqui* chemical releases. Numerous groups established field sites throughout the Caribbean basin to support various aspects of the *El Coqui* project. Optical diagnostics were contributed by Arecibo Observatory, Los Alamos National Laboratory (LANL), the Naval Research Laboratory (NRL), and the Air Force Phillips Laboratory (PL). PL also supplied a KC-135 aircraft that was manned with personnel from PL and SRI, International (SRII). The airplane was used to map out irregularities in chemical release clouds with the aid of signals from satellite beacons. In addition, the PL aircraft served as a platform for optics and radio wave sounding of the ionosphere. Radars operating from HF to VHF were deployed and operated by Cornell University, Geospace Research, Inc. (GRI), LANL, PL, and SRII. Finally, supplemental radar processors were supplied by GRI and SRII to capture the full information content

of the Arecibo incoherent scatter radar and to furnish real-time data during several of the chemical releases. Summary charts identifying the primary *El Coqui* diagnostics, the principal investigators, chemical release payloads, and scientific objectives are presented in Tables 1-3. Brief descriptions of the principal results of each experiment are presented below.

1.2 AA-3a Experiment

The first launch of the campaign (rocket 18-224, L. M. Duncan/University of Tulsa, P.I.) occurred at dusk on May 25. Two small canisters of Ba were explosively released within the beam of the Arecibo HF facility at 251 and 271 km altitude. Each canister contained 1.1 kg of Ba. The two Ba clouds were viewed optically, and the lower of the two ion clouds was examined with the Arecibo incoherent scatter radar. This experiment was designed to map out large-scale ionospheric structures produced by the HF beam and provided the first glimpse of HF-induced Langmuir turbulence in a Ba^+ plasma. The studies of induced plasma turbulence proved to be rather intriguing. Initially very strong Langmuir and ion oscillations were detected in the Ba^+ cloud. However, after a short period of time (~15 s) these waves disappeared and the Ba^+ cloud effectively blocked the excitation of all HF-induced turbulence in the volume viewed by the radar. After several minutes, a normal pattern of HF-excited waves was established in the ionosphere. The total disappearance of the turbulence was completely unexpected and is currently the subject of a highly focused study.

1.3 AA-4 Experiment

On May 30, the second rocket of the campaign was launched (rocket 36-065, P. A. Bernhardt/NRL, P.I.). The payload consisted of a chemical canister and diagnostic instrumentation used to measure the properties of the modified ionospheric plasma. Approximately 30 kg of gaseous CF_3Br were vented at 284 km altitude near the center of the Arecibo HF beam. The purpose of the CF_3Br was to generate an electron density cavity in the ionosphere through dissociative attachment of free electrons. Once formed, the ionospheric cavity was used as a refractive lens to focus the HF beam. This greatly increased the power density of the beam near the point of HF reflection.

In Figure 1, backscatter power measured at 430 MHz with the Arecibo incoherent scatter radar during the CF_3Br release is displayed. The figure shows radar backscatter power (color scale) versus altitude and time relative to the launch at 04:11:00 AST. Radar power is expressed as a signal-to-noise ratio and plotted in dB; the ionospheric backscatter power is directly proportional to the density of free electrons. The tilted

streak between 150 and 190 s is the rocket as detected through a high order sidelobe of the radar beam. The chemical release occurred 170 s after launch. This figure illustrates the development of the ionospheric hole immediately after the release. The radar beam was pointed at the nominal release location for the first 312 s after launch; subsequently the beam was scanned in azimuth to map out the perimeter of the hole. The small trail extending from the rocket echo into the hole is thought to be backscatter from a piece of rocket debris.

Other observations made with the incoherent scatter radar clearly showed the subsequent intensification of HF-induced turbulence as the HF beam was focused. Radar backscatter from the turbulence increased by two orders of magnitude once the hole developed. An additional unanticipated discovery was made when *in situ* measurements of electron density were examined. Shortly after the release, small-scale (~2 m) electron density depletions developed in the plasma. The depth of some of the depletions relative to the background was very large (>90%). The source of these irregularities is currently unknown, but the mystery is likely to unravel as more data are examined.

A detailed discussion of the AA-4 experimental results is provided in Section 3.

1.4 AA3b Experiment

On June 6, rocket 36-064 (E. P. Szuszczewicz/SAIC, P. I.) was launched under dawn moon-down conditions to study multi-ion expansion processes and their coupling to the background ionosphere. Expanding clouds of Ba^+ and Li^+ with a mass ratio similar to that found in the high-latitude polar wind were diagnosed by a suite of *in situ* particle and field detectors and supporting radar/optical systems on the ground. Four canisters of chemicals were ejected from the mother payload, two parallel to the geomagnetic field and two perpendicular to the field. In the first release event, 712 gm of Ba and 38 gm of Li were discharged in the middle of the Arecibo radar beam at 290 km altitude. This release provided cross-field diagnostics of ion expansion along the geomagnetic field and surprisingly produced a decrease in radar backscatter rather than an increase expected because of the rapid ionization of neutral Ba. The second release occurred near ~350 km altitude where ion expansion parallel to the geomagnetic field could be viewed along field lines; the chemical mixture was the same as the first. The third release occurred on the downleg of the flight and involved the simultaneous discharge of two canisters, each containing 1.5 kg of Ba and 19 gm of Sr. The instrument package viewed the ionizing cloud as it expanded across the geomagnetic field. Preliminary examinations of the *in situ* data indicate that "snowplowing" of O^+ ions and forerunning Li^+ ions may have been detected. In addition, there is clear

evidence of gyro-kinetic effects on a Saha-like ionization source (i.e., an "instantaneous" ionization process that operates at the very earliest phases in the cloud's evolution).

The first release event occurred 180 s after launch. Approximately 712 gm of Ba and 38 gm of Li were explosively released in the middle of the radar beam at 290 km altitude. Surprisingly, this release produced a decrease in radar backscatter rather than an increase expected because of the rapid ionization of neutral Ba. This result is described in greater detail in Section 4.

1.5 NC-1 Experiment

Rocket 36-071 (M. C. Kelley/Cornell University, P.I.) was launched on June 9 at 01:39 AST. The payload contained a group of sensors specially designed to diagnose modifications to the natural ionosphere by the Arecibo high-power HF beam. The focus of the observations was on Langmuir turbulence excited near the reflection point of the HF radio wave. The rocket instrumentation detected packets of HF-induced ionospheric irregularities both below and above the nominal height of HF wave reflection. Individual irregularities had scale sizes in the range 20-30 m. Such medium-scale irregularities are not readily measured with ground-based radar systems. The newly detected irregularities are believed to play a central role in the evolution of HF-induced Langmuir turbulence, and the experiment as a whole is expected to provide much needed guidance for ongoing theoretical studies.

1.6 NC-2 Experiment

Rocket 21-105, (R. F. Pfaff/Goddard Space Flight Center, P.I.) was launched on the evening of June 22. It contained a heavily instrumented payload that was used to investigate sporadic-E plasma instabilities near 110 km altitude. Key *in situ* detectors included electron density and electric field sensors and an ion mass spectrometer. In addition to providing a detailed view of sporadic-E processes, the rocket payload also measured an intriguing wave structure at higher altitudes near 130 km. Continuing studies of this kilometer-size structure are likely to shed light on electrodynamic processes in the midlatitude ionosphere.

1.7 AA-1 and AA-7 Experiments

The chemical canisters onboard rockets 36-082 and 36-083 (E. J. Weber/PL, P.I.) were discharged at dawn near 255 km altitude on July 2 and 4. Optical observations made from the Space Shuttle on July 4 yielded the first space-based images of a high-

altitude chemical release. Each release consisted of ~22 kg of Ba and 276 gm of Sr with the Sr serving as a dopant for diagnostic purposes.

Backscatter power measured with the Arecibo incoherent scatter radar during the AA-1 Ba release is shown in Figure 2. Radar power (color scale) is displayed versus altitude and time relative to 05:01:15 AST. The actual launch time was 3 s earlier. The ionospheric backscatter power is directly proportional to electron density and inversely proportional to the quantity $[1 + T_e/T_i]$, where T_e and T_i are the electron and ion temperatures, respectively. The radar beam was initially positioned at a zenith angle of 15° and at the azimuth of the nominal release location. The faint, tilted streak seen near 120 s relative time is the rocket as seen through a high order sidelobe of the radar beam. The chemical release occurred at 138 s relative time at a point ~10 km outside of the radar beam. As expected, the Ba release produced a cloud of enhanced electron density shortly after the release (red/yellow region on left). The dark shadowing seen to the left and below the cloud is caused by a release-induced enhancement in the bulk temperature of background electrons. The electron temperature enhancement is approximately 1400 K above the ambient electron and ion temperature (~750 K). The dark regions of reduced radar cross section are dominated by background O^+ ions; no evidence of Ba^+ is found in these regions.

At 212 s relative time, beam scans in azimuth were initiated to map out the Ba^+ cloud. The radar beam is scanned out of the cloud and then back through it (enhancement seen at right). The slight darkening of the blue background above the cloud at right is caused by a reduction in electron density and an associated enhancement in electron temperature. The reduction in electron density is believe to occur along magnetic flux tubes behind the Ba^+ cloud. The origin of the early time bulk electron heating is not known. The late time density reductions may be related to electrodynamic processes occurring in the plasma.

Results from the AA-7 release are shown in Figure 3. Radar backscatter power (color scale) is displayed versus altitude and time relative to the launch at 04:58:00 AST. The radar beam was initially pointed at a zenith angle of 15° and at an azimuth near the actual release location. The release event occurred 141 s after launch. The tilted streak seen between 130 and 160 s is the rocket as it passes near the main lobe of the radar beam. Because of its proximity to the beam, the Ba release produced a cloud of enhanced electron density that was immediately detected as the rocket moved to altitudes above the release (red region on left). At 240 s, beam scans in azimuth were initiated to map out the Ba^+ cloud. The radar beam is scanned out of the cloud and then back through it (enhancement seen at right). The slight darkening of the blue background

above the cloud at left and the more pronounced darkening above the cloud at right is the same effect identified in Figure 2 (a reduction in electron density and an associated enhancement in electron temperature). More detailed discussions focusing on the depletions in radar cross section detected during AA-1 and AA-7 are provided in Section 4.

1.8 AA-2 Experiment

The final release of the *El Coqui* campaign (rocket 36-081, F. T. Djuth/GRI, P.I.) occurred at dawn (05:02 local time) on July 12. The purpose of the AA-2 experiment was to study the interaction between a powerful radio wave and a high ion mass (137 amu), "collisionless" plasma. Approximately 35 kg of Ba doped with 148 gm of Sr, 260 gm of Eu, and 24 gm of Li were released near 252 km altitude. The expected yield in Ba vapor was approximately 14 kg. This release was the largest of the CRRES program. It occurred near the center of the Arecibo HF beam, which was tilted northward over the Atlantic Ocean. AA-2 produced a distinctive ionospheric layer having a maximum plasma frequency of ~11 MHz. An extremely rich data set was obtained with the Arecibo incoherent scatter radar. The primary results of this release deal with microinstabilities excited in plasmas; these observations are discussed and interpreted by Djuth *et al.* [1994].

Figure 4 shows electron density measurements made with the Arecibo incoherent scatter radar during the AA-2 release. Electron density (color scale) is displayed as a function of altitude and time relative to the launch at 05:02:00 AST. The radar beam was initially positioned at the nominal release location at the center of the Arecibo high-power, high-frequency (HF) beam. The light vertical streak seen near 150 s is the rocket as viewed through a high order sidelobe of the radar beam. Light vertical streaks evident near 100 km altitude are caused by echoes from meteor trails. The release event occurred 152 s after launch. The position of the radar beam remained fixed until 229 s after launch; thereafter numerous azimuth and zenith angle scans were performed. Most of the temporal structure seen over time scales of 100 s or less is caused by beam movements across the cloud. Radar backscatter measured during the AA-2 experiment is shown on an expanded altitudinal scale in Figure 5. The gradual descent of the cloud over time scales of ~500 s is the result of gravitational forces.

An extremely rich data set was obtained with the Arecibo incoherent scatter radar. During the first two minutes after the release, the strongest ionospheric Langmuir turbulence ever measured at Arecibo was detected in the Ba^+ cloud. Moreover, the underlying symmetry of the basic wave-plasma interaction disappeared. Asymmetries

between upgoing and downcoming plasma waves greater than 10^5 in power were encountered in a process that theoretically should be symmetric. With the appearance of short-scale field-aligned irregularities monitored with a mobile VHF radar, wave symmetry was once again restored to the instability process. This experiment is expected to foster new theoretical efforts in an area that was once considered to be well-understood.

An in-depth discussion of the AA-2 results focusing on microinstabilities excited in the plasma is provided in Section 2.

REFERENCES

Djuth, F. T., M. P. Sulzer, J. H. Elder, and K. M. Groves, The CRRES AA-2 release: HF wave-plasma interactions in a dense Ba^+ cloud, *J. Geophys. Res.*, in press, 1995.

NASA/CRRES *El Coqui* Radar/Radio Diagnostics

Organization	Diagnostics
AO/NSF/Cornell University	430 MHz Incoherent Scatter Radar (Line Feed and Horn Feed)
Geospace Research, Inc. SRI, International	Supplemental Radar Processors, Arecibo
Los Alamos	Bistatic HF Radar, TX:Guadeloupe Rec: Providenciales and Grand Turk
NRL	Bistatic HF Radar (Channel Probe) TX: Guadeloupe, Ramay, Puerto Rico Rec: Grand Turk, Sabana Seca, Puerto Rico
Phillips Laboratory	Digisonde, Ramay, Puerto Rico
Phillips Lab/SRII	KC-135 Aircraft, FLTSAT Downlinks, Ionosonde
Cornell University	VHF Radar-Interferometer (CUPRI), St. Croix
Geospace Research, Inc.	VHF Radar-Interferometer, Antigua
SRI, International	HF Radar (FAR), Los Caños, Puerto Rico

Table 1

NASA/CRRES *El Coqui* Rocket Campaign

Launch Site: Tortuguero, Puerto Rico

Eight Rockets Launched in the Window May 18 - July 13, 1992

Rocket Designation	Principal Investigator	Launch Date/Time	
AA-3a	L. M. Duncan/University of Tulsa	May 25	Dusk
AA-4	P. A. Bernhardt/NRL	May 30	Before Dawn
AA-3b	E. P. Szuszczewicz/SAIC	June 6	Dawn
NC-1	M. C. Kelley/Cornell University	June 9	Post Midnight
NC-2	R. F. Pfaff/GSFC	June 22	Evening
AA-1	E. J. Weber/Phillips Lab	July 2	Dawn
AA-7	E. J. Weber/Phillips Lab	July 4	Dawn
AA-2	F. T. Djuth/Geospace Research	July 12	Dawn

Table 2

NASA/CRRES *El Coqui* Experiments

Experiment	Chemical Release	Objectives
AA-3a	2 x 1.1 kg Ba	Tracer of HF-Induced Irregularites Excitation of Langmuir Turbulence
AA-4	CF_3Br, 30 kg	Ionospheric Focussed Heating
AA-3b	2 x (712 gm Ba, 38 gm Li) 2 x (1.5 kg Ba, 19 gm Sr)	Single- and Multi-ion Expansions Parallel and Perpendicular to **B**
NC-1	None	Diagnostics of HF Modifications Langmuir Turbulence, Cavitons
NC-2	None	Sporadic-E Instabilities
AA-1	22 kg Ba, 276 gm Sr	Early-Time Phenomena, Cloud Structuring
AA-7	22 kg Ba, 276 gm Sr	Early Time Phenomena, Cloud Structuring
AA-2	35 kg Ba, 148 gm Sr 260 gm Eu, 24 gm Li	HF Modifcation of a High Ion Mass, "Collisionless" Plasma

Table 3

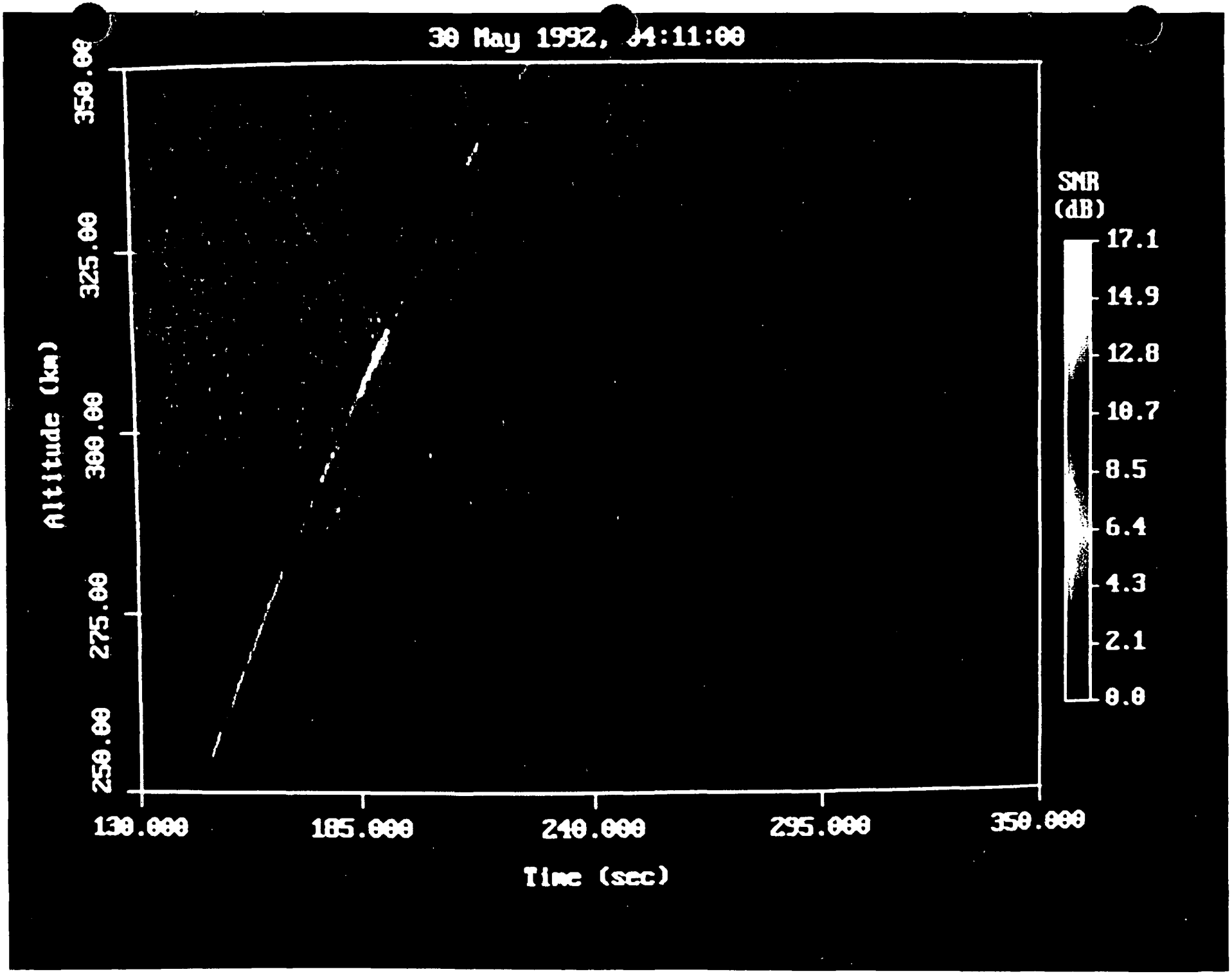
30 May 1992, 04:11:00
Altitude (km)
350.00
325.00
300.00
275.00
250.00
130.000
185.000
240.000
295.000
350.000
Time (sec)
SNR
(dB)
17.1
14.9
12.8
10.7
8.5
6.4
4.3
2.1
0.0

Figure 1

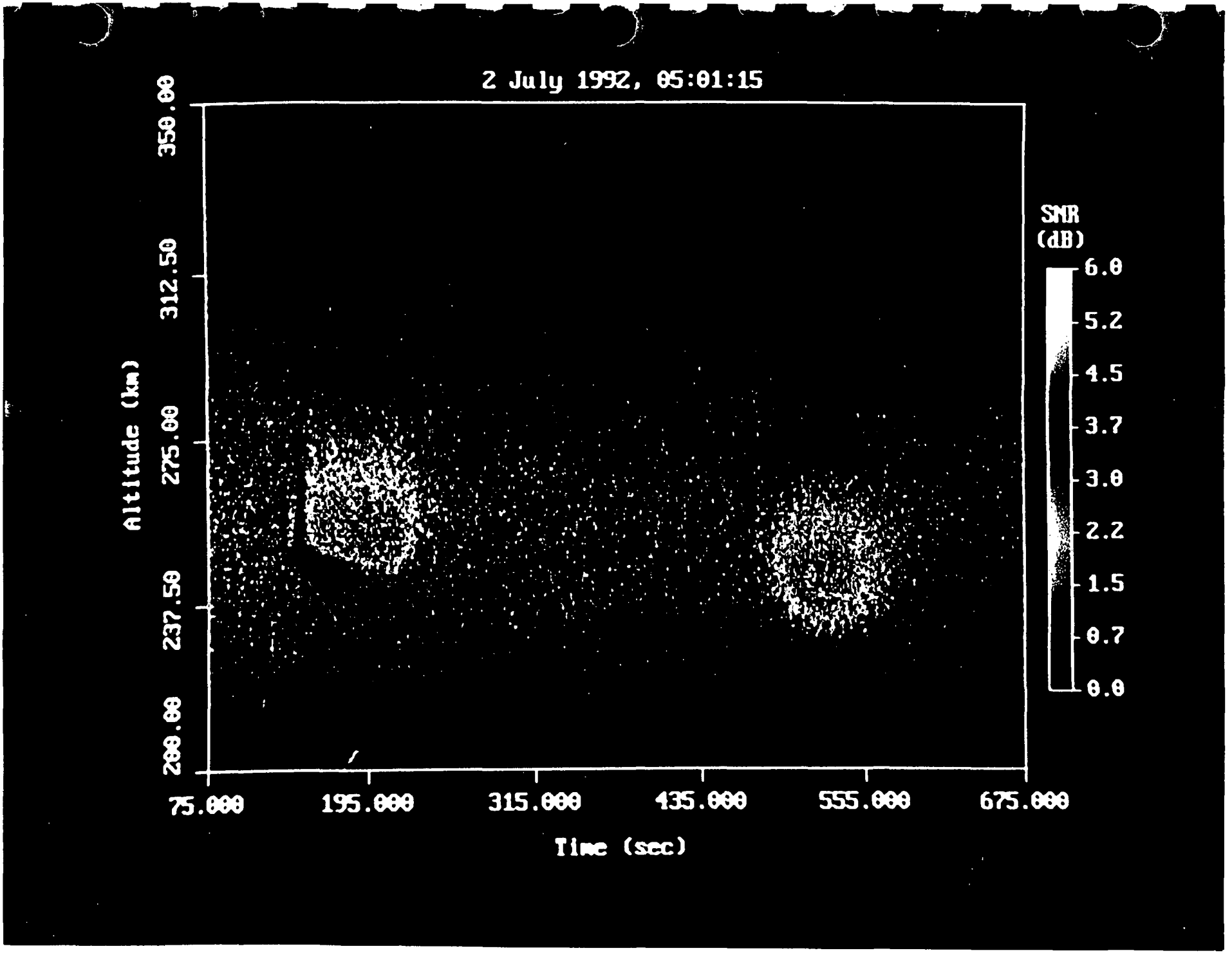
2 July 1992, 05:01:15
Altitude (km)
350.00
312.50
275.00
237.50
200.00
75.000
195.000
315.000
435.000
555.000
675.000
Time (sec)
SNR
(dB)
6.0
5.2
4.5
3.7
3.0
2.2
1.5
0.7
0.0

Figure 2

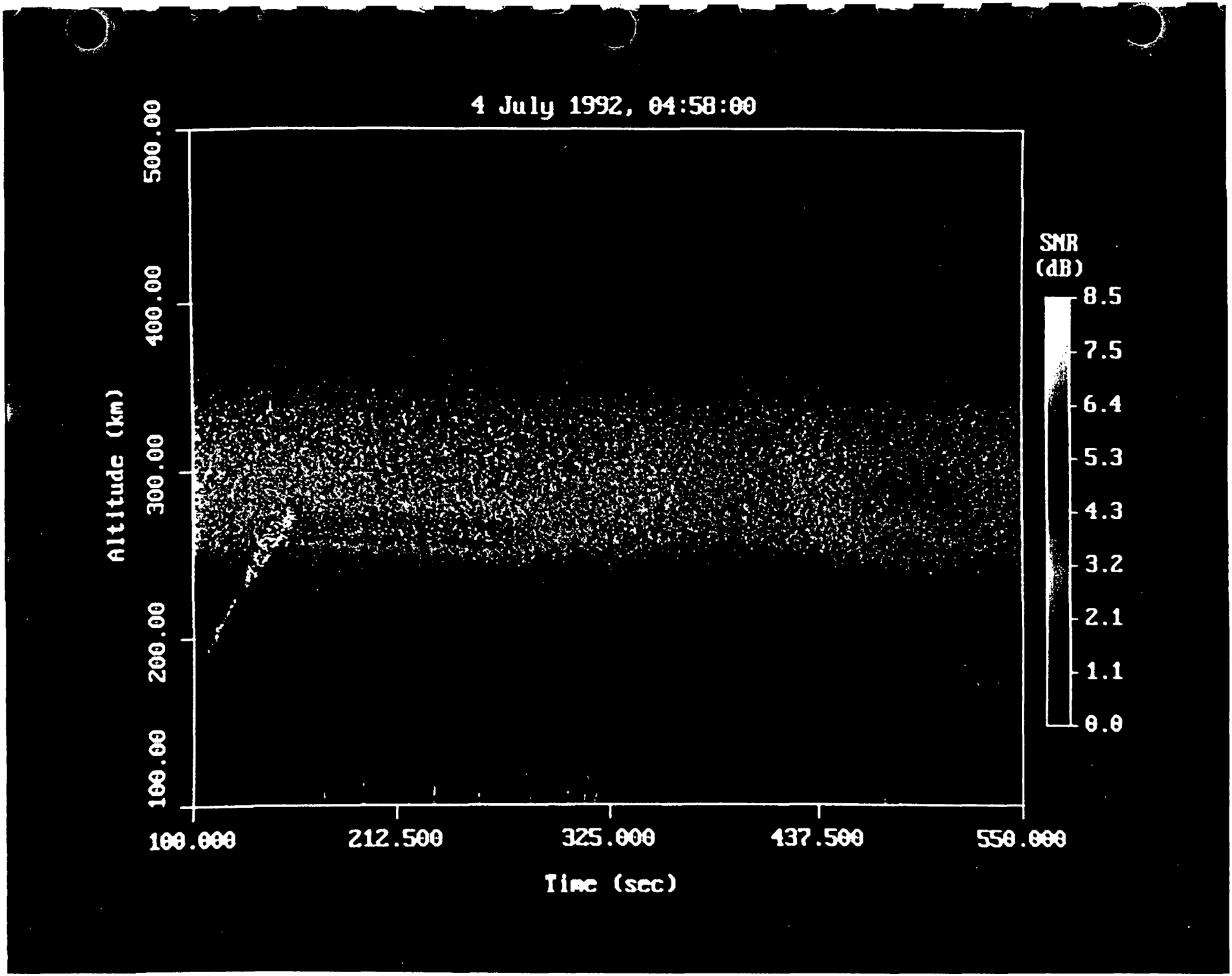
4 July 1992, 04:58:00
Altitude (km)
500.00
400.00
300.00
200.00
100.00
100.000
212.500
325.000
437.500
550.000
Time (sec)
SNR
(dB)
8.5
7.5
6.4
5.3
4.3
3.2
2.1
1.1
0.0

Figure 3

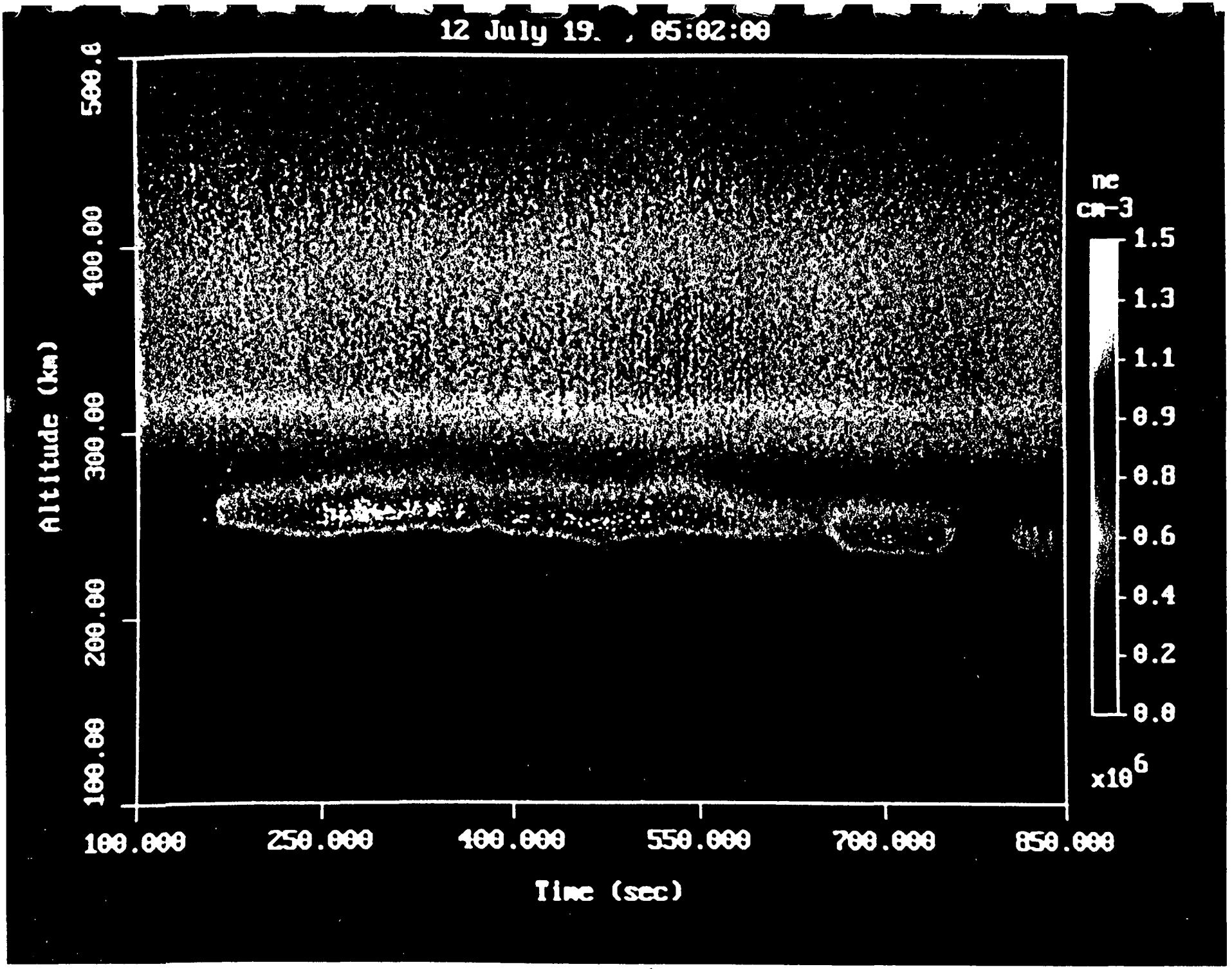
12 July 19. , 05:02:00
Altitude (km)
500.0
400.00
300.00
200.00
100.00
nc
cm-3
1.5
1.3
1.1
0.9
0.8
0.6
0.4
0.2
0.0
x10^6
100.000
250.000
400.000
550.000
700.000
850.000
Time (sec)

Figure 4

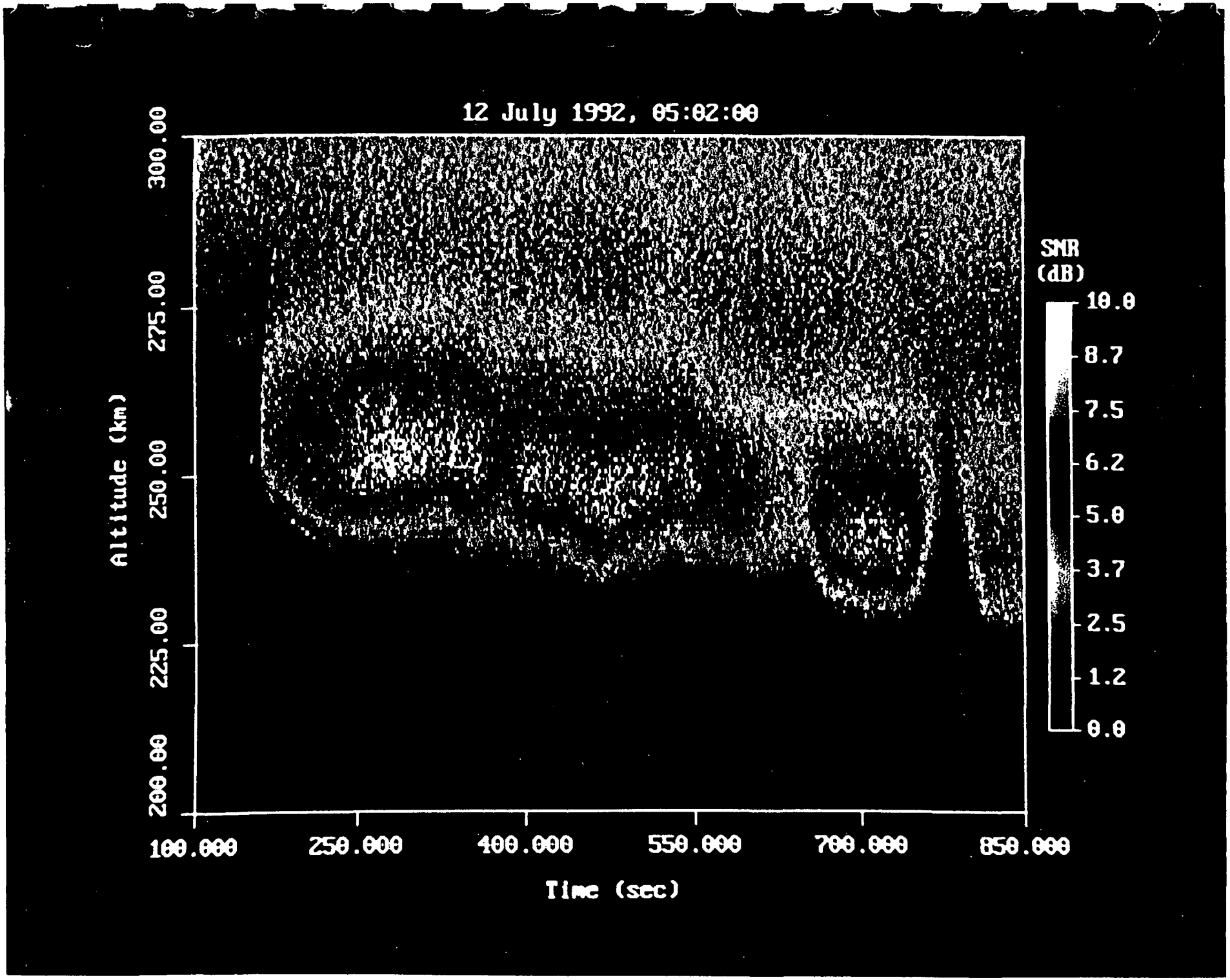
12 July 1992, 05:02:00
Altitude (km)
300.00
275.00
250.00
225.00
200.00
100.000
250.000
400.000
550.000
700.000
850.000
Time (sec)
SNR
(dB)
10.0
8.7
7.5
6.2
5.0
3.7
2.5
1.2
0.0

Figure 5

2. The CRRES AA-2 Release: HF Wave-Plasma Interactions in a Dense Ba^+ Plasma

The primary experiment conducted by Geospace Research, Inc. (GRI) during the *El Coqui* campaign involved radar observations in support of the AA-2 release. This release occurred on the last day of the campaign and yielded an extremely interesting data set. The principal diagnostics were the Arecibo incoherent scatter radar and a mobile VHF radar-interferometer positioned on the island of Antigua by GRI. A detailed description of the scientific results is provided in the article below. This paper is currently in press in the *Journal of Geophysical Research.*

The CRRES AA-2 Release: HF Wave-Plasma Interactions in a Dense Ba^+ Cloud

F. T. Djuth[1], M. P. Sulzer[2], J. H. Elder[1]
and K. M. Groves[3]

[1] Geospace Research, Inc., 550 N. Continental Boulevard,
El Segundo, CA 90245

[2] Arecibo Observatory, Arecibo, Puerto Rico 00613

[3] Phillips Laboratory, Hanscom Air Force Base, MA 01731

ABSTRACT

An ionospheric chemical release, designated AA-2, was performed on July 12, 1992 as part of the NASA Combined Release and Radiation Satellite (CRRES) *El Coqui* rocket campaign. The purpose of the AA-2 experiment was to study the interaction between a powerful radio wave and a high ion mass (Ba^+), "collisionless" plasma. Approximately 35 kg of Ba were explosively released near the center of the Arecibo high-frequency (HF) beam at 253 km altitude. This was the largest Ba release of the CRRES experiments; it yielded a distinctive ionospheric layer having a maximum plasma frequency of 11 MHz. At early times (less than one minute after the release), the HF beam produced the strongest Langmuir waves ever detected with the Arecibo 430 MHz radar. Resonantly enhanced Langmuir waves were observed to be excited principally at the upshifted plasma line (i.e., near 430 MHz + f_{HF}, where f_{HF} is the frequency of the modifying HF wave), and only weakly-excited waves were apparent at the downshifted plasma line (430 MHz - f_{HF}). The upshifted plasma line spectrum contained a dominant peak at the "decay line," that is, at the frequency 430 MHz + f_{HF} - δ, where δ is close to the Ba^+ ion-acoustic frequency (~2 kHz). Downshifted plasma line echoes occurred at frequencies near 430 MHz - f_{HF} and 430 MHz - f_{HF} - 1 kHz, and exhibited little or no signal strength at the decay line (430 MHz - f_{HF} + δ). During an initial period of intense upshifted plasma line excitation, the power asymmetry between the upshifted and downshifted plasma lines was of the order of 10^5 at the decay line. The upshifted plasma line was accompanied by strong HF-enhanced ion waves that were present only at the downshifted acoustic sideband. After geomagnetic field-aligned irregularities formed in the plasma, the amplitudes of the upshifted and downshifted plasma lines equalized, and each exhibited spectra characteristic of the parametric decay instability. At early times in the Ba^+ plasma, the symmetry of wave excitation anticipated for a parametric instability in a stationary, homogeneous plasma was absent. The experimental results indicate that the development of the parametric decay instability needs to be reexamined for a smooth plasma having a small (~5 km) vertical scale length. Moreover, ion flow down geomagnetic field lines appears to suppress instabilities responsible for the formation of field-aligned irregularities and may also have an impact on the way parametric instabilities are excited. New theoretical approaches are needed to resolve many of the issues raised by this experiment.

1. Introduction

The NASA Combined Release and Radiation Effects Satellite (CRRES) program consisted of a Pegasus-borne small satellite launched in April 1990, the principal spacecraft launched on an Atlas Centaur vehicle in July 1990, and two rocket campaigns: one from Kwajalein Atoll, Marshall Islands (August, 1990) and one from Puerto Rico (summer, 1992). All of the launch vehicles contained chemical payloads that were released in the ionosphere or magnetosphere. Results from the high-altitude releases are described in a review by Bernhardt [1992]. The Puerto Rico, or *El Coqui*, rocket campaign consisted of eight rocket experiments launched from Tortuguero, Puerto Rico during the period May 18 through July 13, 1992. Six of the rocket launches involved the release of chemicals in the ionosphere north of Arecibo Observatory, Puerto Rico. Of these, two entailed the modification of a Ba^+ plasma by transmissions from the Arecibo high-power, high-frequency (HF) facility, located 17 km northeast of Arecibo Observatory. Initial results from the largest of these two chemical releases, designated AA-2, are presented below.

The objective of the AA-2 experiment was to explore the interaction between a high-power HF beam and a high ion mass (Ba^+, 137 amu) plasma under conditions of low electron collisions. In addition, a moderate plasma scale length $H \equiv n_o/[dn_e(z)/dz]$ was highly desirable, where $n_e(z)$ is electron density as a function of altitude z and n_0 is the electron density at the point of reflection of the HF wave. Scale lengths of the order of 2 - 20 km were anticipated on the bottomside of the B^+ plasma cloud. The experiment design focused principally on the development of microinstabilities in the plasma. Originally, it was believed that it might be possible to suppress the parametric decay instability [e.g., Fejer, 1979] in a Ba^+ plasma and permit preferential growth of the oscillating two-stream instability. Such conjectures were made prior to the application of the strong Langmuir turbulence theory [DuBois et al., 1990; DuBois et al., 1991; Hanssen et al., 1992] to HF ionospheric modification experiments in the natural ionosphere at Arecibo. Subsequent experiments at Arecibo confirmed certain elements of the strong turbulence approximation [e.g., Fejer et al., 1991]. In light of a rapidly changing understanding of the HF modification process, the predicted outcome of the Ba^+ modification experiment became far less certain.

Prior to the AA-2 release, HF modification experiments had been performed in natural sporadic E regions [Gordon and Carlson, 1976; Djuth, 1984; Schlegel et al., 1987; Djuth and Gonzales, 1988]. In midlatitude sporadic E, Fe^+ ions having relatively

high mass (56 amu) often dominate the plasma. However, unlike the AA-2 experiment, electron collision frequencies are quite high (10-30 kHz), and vertical and horizontal electron density scale lengths are extremely small (H= 100 - 500 m). Indeed, the plasma parameters of sporadic E give rise to HF wave-plasma processes that are significantly different than those encountered at higher F-region altitudes [Djuth and Gonzales, 1988]. In general, the AA-2 experiment has no real analog in the natural environment; it provides a unique view of wave-plasma interactions in a previously unexplored plasma medium.

2. Experiment Description

Throughout this paper, time is referenced either to the launch of the AA-2 rocket at 05:02:00 AST on July 12, 1992 or to the time of the AA-2 chemical release. Both the HF facility operations and the data acquisition activities were closely tied to the launch time, whereas many of the experiment events were linked to the release time. When an L or an R is appended to a time, it designates the temporal reference (launch or release, respectively). For consistency, the times displayed in all figures are referenced to the launch time.

The AA-2 chemical release occurred approximately 152 s after launch at 05:04:32 AST. At this time, the solar depression angle was 12.2° at the release altitude (253 km); this permitted rapid ionization of the neutral barium cloud while preserving dark viewing conditions at ground level for optical observations. AA-2 entailed the explosive release of approximately 35 kg of Ba, doped with 148 gm of Sr, 260 gm of Eu, and 24 gm of Li to facilitate ground-based diagnostic measurements. This was the largest chemical release of the CRRES program. The chemicals were carried in six, rocket-borne canisters which were simultaneously discharged within the 3-dB power contour of the Arecibo high-power HF beam. All HF transmissions made during the AA-2 experiment were at an effective radiated power (ERP) of 60 MW with O-mode polarization. An overview of the release geometry and the locations of several essential ground sites is provided in Figure 1. The Arecibo HF beam was tilted 12° from vertical in the direction of geographic north to accommodate restrictions placed on rocket flight trajectories. The tilt was achieved through time-delay phasing with fixed delay lines. A frequency of 5.1 MHz was selected for *El Coqui* HF experiments because it satisfied all program requirements and yielded a favorable impedance match between the HF transmitter and antenna. The AA-2 release occurred approximately 14 km south-southeast of the center of the HF beam.

The AA-2 release point, like many of the *El Coqui* campaign chemical releases, was positioned well inside the viewing limits of the Arecibo radar beam (i.e. within 20° of the zenith). The 430 MHz radar was the principal diagnostic for AA-2 studies of plasma turbulence. Additional measurements were made with a wide variety of optical instrumentation, HF bistatic links that penetrated the release volume, and with a VHF radar-interferometer positioned on the island of Antigua. The VHF radar was tuned to 49.92 MHz, and was used to detect HF-induced geomagnetic field-aligned irregularities. The current work focuses primarily on results obtained with the 430 MHz radar.

In support of AA-2, special efforts were made to fully exploit the information available with the Arecibo incoherent scatter radar. The observing program was designed to provide wideband spectral information without compromising altitude resolution or system sensitivity. Three types of phase-coded radar pulses were employed. These included a 13-baud Barker-coded pulse (BKR) having a baud length of 4 μs; a three-baud Barker-coded pulse (1-μs bauds), referred to as a coded short pulse (CSP); and a 512-baud, pseudo-random phase-coded pulse (1-μs bauds), generically termed a coded long-pulse (CLP). The three pulses were cyclically transmitted within a "frame time" of 30 ms. A frame consisted of three 10 ms interpulse periods (IPPs), one for each type of pulse. Throughout the experiment period, ionospheric backscatter from each radar pulse was simultaneously sampled at the radar center frequency (430 MHz) and across both "plasma line" sidebands (430 MHz $\pm$ f_{HF}), where f_{HF} is the frequency of the HF transmissions (5.1 MHz). The plasma line bandpasses were centered near 430 MHz $\pm$ 5.1 MHz. Appropriate filters were selected to optimize measurements made with a particular type of pulse. The spectral bandwidths of the data channels ranged from 250 kHz on the BKR ion line to 2 MHz at the downshifted CLP plasma line. The three pulse types were used to extract different kinds of information about the processes occurring in the Ba^+ plasma. Power profile (i.e. power versus range) measurements made with the BKR pulse had the best detection sensitivity with moderately good altitude resolution (600 m). Better altitude resolution (150 m) and wideband spectral information were obtained with the CLP with some loss of sensitivity when signals were strong. The CSP yielded power profile measurements with good range and temporal resolution when strong HF-enhanced plasma lines/ion lines were present.

An important feature of the AA-2 radar data-taking program was that raw, unintegrated voltage samples were preserved on all data channels throughout the experiment period (~ 45 min). This made it possible to optimize temporal integration periods after the fact, change digital processing techniques as desired, and examine radar returns on a pulse-by-pulse basis to explore interesting events.

3. Observations

The background F-region just prior to the AA-2 release had a peak plasma frequency of ~8 MHz at a height of 345 km. As noted earlier, the release occurred at ~253 km altitude at 05:04:32 AST on July 12, 1992. The Arecibo HF facility made continuous transmissions for 30 min prior to the release; it was operated at an effective radiated power (ERP) of ~60 MW and tuned to a frequency (f_{HF}) of 5.1 MHz. The height of the HF-excited Langmuir waves and ion waves provided a convenient and continuous calibration of the electron concentration profile. HF-enhanced backscatter detected with the Arecibo 430 MHz radar occurs relatively close to the so-called critical altitude, that is, near the altitude at which $f_{ep} = f_{HF}$, where f_{ep} is the electron plasma frequency. With f_{HF} = 5.1 MHz, the critical layer has an electron concentration of 3.2×10^5 cm^{-3}. One of the go/no-go launch criteria required that the critical layer in the natural ionosphere be located above the projected release altitude. This was done to ensure that the HF beam would undergo total reflection in a predominantly Ba^+ plasma. At the time of release, the background electron concentration at the discharge height was 1.6×10^5 cm^{-3}.

Ba Ion Cloud Formation

At 151.9 s into the AA-2 flight, six chemical canisters were simultaneously ignited producing a spherically expanding neutral cloud centered on the rocket. The thermite consisted of a Ti/B mixture successfully used in other CRRES releases. At the time of release the rocket was at 252.5 km altitude, and its speed was 1.486 km/s. The westward, northward and vertical components of the rocket velocity were 0.182 km/s, 0.313 km/s, and 1.441 km/s, respectively. A thermite release of this type produces shells of neutral gas that expand radially relative to the rocket velocity. During prior CRRES releases involving the Ba/Ti/B mixture [e.g., Bernhardt *et al.*, 1993], the mean radial expansion speed was found to be ~1.4 km/s with a thermal spread of roughly ± 0.3 km/s relative to the mean. The AA-2 release canisters contained a total of 35.3 kg Ba, 148 g Sr, 260 g Eu, and 24 gm Li. The vaporization efficiency is estimated to be ~40%, based on test measurements from rocket-borne Ba/Ti/B releases at Wallops Island, VA. For the AA-2 experiment, the predicted yield is $\sim 6 \times 10^{25}$ atoms of Ba vapor. Under full solar illumination of the cloud at UV wavelengths between 310 and 200 nm, the Ba ionization time constant is 28 s [e.g., Carlsten, 1975]. Because the neutral Ba cloud becomes optically thin within a few seconds of the release, one expects the cloud as a whole to ionize with an e-fold time of about 30 s.

During the AA-2 release period, optical viewing conditions from many ground-based sites were poor because of the passage of a tropical wave across the Caribbean. This prevented accurate inventories of Ba^+ ion production from being performed, as had been done in many of the prior CRRES releases. Additionally, cloud cover hampered efforts aimed at determining the expansion velocity of the neutral cloud experimentally. Optical measurements at Arecibo Observatory were made under hazy observing conditions, with cloud cover occasionally obscuring the release. This notwithstanding, the optical data showed that the Ba cloud development was not unlike that observed in the past for a release of this type. The spherically expanding neutral cloud became almost completely ionized over a time scale of ~1 min, and, as expected, the resulting Ba^+ cloud was aligned with the geomagnetic field. The fully-developed ion cloud appeared to be smooth with no evidence of field-aligned irregularities. At the release altitude, the ion-neutral collision frequency and the background neutral wind speed (~50 m/s) were low. Under these conditions, the gradient drift instability is expected to give rise to, at most, very weak striations in the cloud over long time scales (tens of minutes).

In Figure 2, the AA-2 release event recorded with the Arecibo 430 MHz radar is illustrated with BKR data acquired at the ion line. The range-corrected ion-line power is proportional to $n_e/[1 + T_e/T_i]$, where n_e is electron density, and T_e and T_i are electron temperature and ion temperature, respectively. Photoelectron-enhanced plasma lines similar to those in the natural daytime ionosphere [e.g., Djuth *et al.*, 1994] were not detected in the Ba^+ cloud with the CLP technique. During AA2, the photoelectron phase energies (i.e., $E_\phi = \frac{1}{2} m_e v_\phi^2$, where $v_\phi = \frac{1}{2} f_r \lambda$, f_r is plasma wave frequency, and λ is radar wavelength) monitored with the 430 MHz radar ranged from 5.8 to 12.9 eV. However, determinations of absolute electron density before and after the release were aided by the presence of strong HF-enhanced ion waves and Langmuir waves. The height of these enhancements is close to the 3.2×10^5 cm^{-3} point in the plasma. Errors associated with this calibration technique are dictated primarily by the detailed microphysics of the excitation process. In general, HF-enhanced backscatter observed at Arecibo occurs between the critical altitude, where $f_{ep} = f_{HF}$, and the so-called "matching altitude," where the Langmuir wave frequency (determined by the linear dispersion relation) is approximately equal to f_{HF} [e.g., Fejer *et al.*, 1991]. For the electron temperatures measured during the AA-2 experiment, the electron density at the matching altitude is calculated to be ~4-5% less than the density at the critical layer. This type of calibration is available in the natural ionosphere prior to the release and in the Ba^+ cloud for approximately 300 s after the release.

The critical layer observations are augmented by measurements of T_e/T_i obtained in the natural F region and in the Ba^+ plasma. These measurements allow the electron density profile to be calculated at altitudes far away from the critical layer and at times when no HF-enhanced waves are present. In the Ba^+ cloud, it is extremely difficult to make an accurate determination of T_e/T_i because of the potential presence of two ions (O^+, Ba^+) of dissimilar mass, and because of significant vertical gradients in electron concentration. To obtain T_e/T_i in this environment, we must rely on the CLP ion line observations, which are severely clutter-limited. The clutter is generated by the Ba^+ cloud itself and the overlying *F* layer. Our approach to this problem is to measure T_e/T_i near the peak of the Ba layer, where the signal-to-clutter ratio is greatest. We then assume that this ratio does not vary markedly at other altitudes within the cloud because of the importance of electron heat conduction along the magnetic field. The necessary temperature data were obtained by integrating the ion line spectrum across a 7.2 km altitude interval (48 consecutive range gates) for a time period of 6 s (200 radar pulses). Precautions were taken to avoid HF-enhanced ion lines on the bottomside of the Ba^+ cloud. Our studies indicate that T_e/T_i was ~1.1 prior to the release at 253 km altitude but increased to 1.8 at 173 s L (21 s R) and 2.2 at 225 s L (73 s R). Incoherent scatter spectra from the release cloud were analyzed assuming 100% Ba^+ ions. Electron concentration values obtained from measurements of the critical altitude were found to be consistent with values calculated under the assumption of constant T_e/T_i ratio throughout the Ba^+ cloud.

In Figure 2, the light vertical streak/speckles seen near 150 s L is the rocket as viewed through a high order sidelobe of the radar beam. Temporal changes in the structure of the Ba cloud are caused mostly by changes in the pointing direction of the radar beam. For the first 228 s after launch, and at all times prior to launch, the 430 MHz beam was pointed at the center of the HF beam at a nominal altitude of 250 km (see Figure 1). The radar beam was then moved across the Ba cloud in an effort to adjust for the ~14 km horizontal displacement between the projected release point and the actual one. Concurrent efforts were made to spatially map out the locations of resonantly-excited Langmuir and ion waves. In addition, continuous pointing adjustments were made to keep the radar beam on a critical surface in the Ba cloud as the cloud drifted toward the perimeter of the HF beam. Optical data indicated that the cloud drifted toward the northwest at an average speed of ~50 ± 5 m/s. A similar value was obtained from incoherent scatter radar measurements of F-region ion drifts made 45 min before the release. Moreover, VHF radar observations of the drift speed of HF-induced F-region irregularities were made from Antigua throughout the experiment period. This

radar had a line-of-sight directed towards the northwest. Just prior to the release, the radial drift speed of irregularities near 270 km altitude was measured to be 47 m/s ± 3 m/s.

The location of the radar beam versus time after launch is shown in Figure 3. An altitude of 240 km was selected for the horizontal projection of position because the majority of the resonantly enhanced Langmuir/ion waves were detected near this height. The only exception comes during a ~60-s period following the release. Resonant waves are first detected in the Ba^+ plasma near 250 km altitude but then rapidly move downward to the 240-km level. Once the beam motion is initiated, beam locations are indicated with the symbol (+) at 12-s intervals. Temporal integrations (12 s in duration) centered on these times were used to construct the temporal evolution of the electron density profile shown in Figure 4. Forty profiles are shown beginning with the launch of the rocket. In this data display, strong HF-enhanced ion lines are apparent near 272 km prior to the release. An echo from the rocket is also evident in the integration period just before the release. The Ba plasma initially expands over a 30-km altitude interval. Once the cloud is fully formed, it slowly sinks in altitude at the rate of ~25 m/s.

The BKR ion line data of Figure 4 can be combined with CLP observations of the HF-enhanced plasma line and ion line to determine the temporal history of the critical altitude. As noted above, the critical altitude can be accurately established using resonant ion line enhancements and/or enhancements measured at either of the two plasma lines. Enhanced plasma lines generally provide signals having the greatest strength, whereas the weaker ion line enhancements offer the convenience of having the enhancements embedded in the power profile used to determine electron concentration versus height.

Throughout the AA-2 experiment period, the power at the upshifted plasma line was either comparable to or much greater than the power measured at the downshifted line. This made the upshifted plasma line preferable in determining critical layer height. Figure 5 shows backscatter power at the upshifted plasma line versus altitude and time after launch. The altitude resolution of the measurements is 150 m. Notice that the echo detected in the natural *F* region prior to the release at 152 s is structured and spread in altitude. This is caused by HF-induced electron density irregularities that form in the plasma [e.g. Djuth *et al.*, 1990]. From the time of the rocket launch to the release 152 s later, the HF-enhanced waves are detected over the altitude range of ~272 km ± 1.8 km. Enhancements are observed near altitudes where critical points exist in the plasma (i.e., the altitude at which $f_{ep} = f_{HF}$, where f_{ep} is the electron plasma frequency). In this irregular environment, it is difficult to determine whether the observed enhancements occur exactly at the critical point or at locations where the frequency matching condition

is satisfied for weakly-driven parametric instabilities. The matching condition can be expressed as

$$\omega_r^2 = \omega_{ep}^2 + \sin^2\theta\,\omega_{ec}^2 + \frac{3k^2\kappa T_e}{m_e} \approx \omega_{HF}^2, \qquad (1)$$

where ω_r is Langmuir wave frequency, ω_{ep} and ω_{ec} are the electron plasma frequency and electron cyclotron frequency, respectively, θ is the angle between the radar line-of-sight and the geomagnetic field, k is radar wavenumber, T_e is electron temperature, m_e is electron mass, and Boltzmann's constant is represented as κ. This situation is complicated by the fact that Langmuir waves propagating in geomagnetic field-aligned irregularities can satisfy (1) at multiple locations along a single irregularity [e.g., Muldrew, 1978a]. As noted above, electron density at the matching height is ~4-5% less than that at the critical altitude.

The presence of HF-induced irregularities within the Arecibo radar beam (~800 m diameter at 272 km altitude) gives rise to most of the altitude spread in the observed enhancements. Additionally, the 15° tilt of the radar beam from zenith generates a small amount of false altitude spread. The radar wavefront subtends an altitude interval of ~200 m because of its finite beamwidth. Given the measured scale length H=40 km near the critical point, perturbations with a maximum variation of 8% relative to the background profile would produce the observed 3.6 km spread in the enhanced plasma line.

Following the Ba release at 152 s L, a discontinuous step downward in plasma line altitude is evident in Figure 5. This corresponds to the formation of a critical layer within the Ba cloud. The plasma line altitude rapidly decreases during the first minute after the release. During this period the size of the Ba^+ cloud is increasing in all directions as the neutral Ba gas becomes fully ionized. At times greater than about 240 s L the plasma line echo is observed to fade in and out several times. This is primarily the result of the HF pulsing program employed during the AA-2 experiment (discussed below). Changes in the plasma line height after 228 s L arise because of the movement of the radar beam across the Ba^+ cloud (see Figure 3).

Prior to the Ba release, enhanced ion lines were readily detected in the natural F region with BKR pulses (Figure 4). Detectable BKR enhancements were also evident in the Ba cloud during the first 120 s after the release. The altitude and temporal scales of the data presented in Figure 2 are greatly expanded in the display of Figure 6. In Figure 6, HF-enhanced ion lines are clearly evident on the bottomside of the Ba^+ cloud. The ion line enhancements are generally confined to a single 600-m range cell at any

given time. These echoes are not evident in Figure 4 because of the long (12-s) temporal integrations used for that presentation. During a 12-s period, the enhanced ion line backscatter is distributed across many range cells, and as a result, sharp peaks cannot be discerned in the profiles.

The temporal history of the critical altitude, its vertical velocity, and the ionosphere scale length H at the critical altitude is plotted in Figure 7. The critical heights were determined from both the 430 MHz ion line observations (Figures 4 and 6) and resonant enhancements at the upshifted plasma line (Figure 5). In the former case, HF-enhanced ion lines were used to define the critical layer prior to the release at 152 s L. After the release, the combination of HF-enhanced ion lines and electron concentration profiles were used. Each profile was least-squares-fit to a cubic so that the critical height could be accurately determined. As expected, the ion line and plasma line observations yielded similar results. However, the upshifted plasma line data provided the best measure of the critical altitude and its rate of change in the Ba^+ cloud because of the strong echoes and better range resolution of the plasma line observations.

It is presumed that the vertical velocity of the critical layer is equal to the rate of change in the ion/plasma line altitude. Because the radar beam was pointed at 15° zenith angle, this entails an implicit assumption that the vertical gradient is dominant in the Ba^+ plasma. In Figure 7, vertical velocity in the Ba^+ plasma is shown only at times when the 430 MHz beam is stationary. During beam scans, erroneous values are generated by even mild gradients across the Ba^+ cloud.

The scale length H plotted in Figure 7 was determined from the first derivative of the fitted electron density profile at the critical height. In the Ba^+ cloud, the scale length at the critical layer ranges between 4 and 6 km throughout the period of observations. This contrasts markedly with the scale length encountered in the natural ionosphere prior to the release (~40 km).

HF-Induced Plasma Turbulence

The temporal history of the HF-induced backscatter at the plasma lines is presented in Figure 8 beginning 100 s after launch. CLP measurements were chosen for this display because they have good sensitivity in the time domain. The total power received at the upshifted plasma line, PL+ (430 MHz + f_{HF}), and the downshifted plasma line, PL- (430 MHz - f_{HF}), is plotted in the figure as a signal-to-noise ratio. Because the CLP bandwidths of the PL- and PL+ channels were 2 MHz and 1 MHz, respectively, the total noise power in the PL- channel was roughly twice that of the PL+. The PL- results presented in Figure 8 have been compensated for this disparity in plasma line noise level

and for differences in the gain of the Arecibo line feed system at 430 MHz - f_{HF} and 430 MHz + f_{HF}. Thus, the relative strength of PL+/PL- backscatter from Langmuir oscillations is accurately represented in the figure. Prior to the release at 152 s L, the PL+ and PL- power levels in the natural ionosphere are approximately the same. Following the release, it is clear that a large asymmetry develops between the two plasma lines.

Modes of HF facility operation are indicated at the bottom of Figure 8. They include continuous wave transmissions (CW), high duty cycle pulsing (HD), low duty cycle pulsing (LD), and 2-s periods of no transmissions. All transmissions were at a level of 60 MW ERP. The HD mode consisted of the repetitive transmission of 1.595-ms pulses within an interpulse period of 1.995 s. The unusual period (1.995 s) was chosen so that the Arecibo 430 MHz radar (restricted to a 30 ms frame time) could probe the Ba^+ plasma over a range of times (separated by 5 ms) relative to HF turn-on. Transmissions designated LD employed 195-ms pulses followed by HF-off periods of 1800 ms. In the current study, only plasma line data acquired under CW conditions are presented.

Extremely strong HF-enhanced plasma lines were detected at the upshifted plasma frequency (430 MHz + f_{HF}) during the AA-2 release. The largest echoes occurred during two periods: 175-230 s L (23 - 78 s R, period P1) and 278 - 291 s L (126 - 139 s R, period P2). Indeed, in terms of absolute signal strength in the spectral domain, these periods include the strongest enhanced plasma line echoes ever recorded at Arecibo. The largest signals measured at the decay line are approximately 10 times greater than those detected at the peak of the plasma line "overshoot" in the natural F region with 80 MW HF ERP [e.g. Djuth *et al.*, 1986]. During P1, echoes at the downshifted plasma line (430 MHz -f_{HF}) are not visible in the time domain display of Figure 8. However, spectral analyses reveal very weak echoes at the downshifted plasma line throughout this time interval. During P2, significant enhancements at the downshifted plasma line are observed for the first time. At this stage in the experiment, the power levels of the downshifted plasma line enhancements are approximately 20 times less than those at the upshifted line. Strongly enhanced ion lines are present throughout P1 and P2; the strength of the ion-line enhancements is closely correlated with PL+ amplitude.

The appearance of the downshifted plasma line enhancements at 283 s L coincided with the first detection of HF-induced, geomagnetic field-aligned irregularities in the Ba^+ cloud. A VHF radar-interferometer sensitive to irregularities having a spatial scale of 3-m across geomagnetic field lines (discussed in Section 2) was used to make

this measurement. The VHF radar was deployed on the island of Antigua, where it had an optimum viewing geometry for detection of field-aligned irregularities at ~250 km altitude in the Ba^+ cloud. The formation of such irregularities may in fact be responsible for the equalization of the upshifted and downshifted plasma line power after 340 s L (188 s R). This situation is not unlike that encountered in the natural F region at Arecibo. Indeed, prior to the release at 152 s L, strong echoes from HF-induced field-aligned irregularities were detected in the natural ionosphere near 272 km altitude.

As noted in Section 2, the principal purpose of the CLP observing program was to provide wideband spectral coverage with good altitude resolution (150 m). Throughout the experiment period, simultaneous CLP measurements were made at the PL-, PL+, and ion line across spectral bandwidths of 2 MHz, 1 MHz and 1 MHz, respectively. All spectral observations displayed in the present work have been corrected for the frequency-dependent response of the Arecibo line feed. Correction factors relative to PL- have been applied to signals at PL+ and the ion line. The intrinsic frequency resolution of the spectral measurements as determined by pulse width (512 μs) is 1.95 kHz. However, the Fast Fourier Transforms (FFTs) used to compute spectra displayed below have been zero-padded to fill a 1024-μs window. This yields a point separation of 0.98 kHz, which allows the positions of very sharp spectral peaks to be more easily located. However, only points separated by 1.95 kHz are statistically independent.

During period P1, the altitude band of plasma wave and ion wave enhancements quickly decreased with time. At any given moment, the strongest echoes in all three frequency bands generally occurred in the same 150-m altitude cell. An example of the plasma line/ion line enhancements typically observed in the Ba^+ cloud during P1 is presented in Figure 9. The spectra shown in the figure have been truncated in frequency for display purposes. No other spectral features were present in the PL+, PL-, and ion-line bands. The peaks of the signals are represented as signal-to-noise ratios, where the noise power is the sum of contributions from the sky and the radar receiver system. If this were the only contribution to the random fluctuation level, one would expect the mean spectral baselines to lie close to a signal-to-noise ratio (S/N) of 0 dB. However, a "noise-like" clutter contribution is generated by the CLP technique [Sulzer, 1986] because of the presence of signals at other radar ranges. This technique randomizes signals at unwanted ranges and thereby converts them into "white noise" at the decoded radar range. The resulting signal-to-clutter ratio is not indicative of absolute signal strength. At the ion line, signal-to-clutter ratios may be quite small, depending on the relative amplitudes of signals at other ranges. For weak signals having signal-to-clutter ratios less than unity, the statistics are governed by the clutter fluctuations. A pedestal

near 20-dB signal-to-noise ratio is evident at the PL+ in Figure 9. This is the combined effect of the spectral windowing function and CLP clutter from other radar altitudes. At the ion line, the "noise" baseline is elevated above 0 dB S/N. This is due to clutter produced by incoherent scatter returns from the Ba^+ cloud and overlying F region. The downshifted plasma line is very weak and has no clutter contributions from other radar ranges; its baseline lies at 0 dB S/N.

The spectral observations shown in Figure 9 were taken from the 242.34 km altitude cell containing the strongest signals at 188.5 s L. In general, the upshifted plasma line exhibits a large spectral peak offset from (430 MHz + f_{HF}) by -2.0 ± 0.5 kHz. This corresponds to the expected location of the "decay line" [e.g. Showen and Kim, 1978] in the barium plasma. If excited, decay lines appear at 430 MHz ± (f_{HF} - δ), where δ is approximately equal to the ion-acoustic frequency. The enhanced ion line exhibits a single peak displaced from 430 MHz by -1.4 ± 0.4 kHz. At the downshifted plasma line, a very weak peak is often present exactly at 430 MHz - f_{HF}. However, this weak feature may also be found at 430 MHz - f_{HF} - 1 kHz. At the frequency offset of the decay line (δ~2 kHz), the power asymmetry between the signals at PL+ and PL- is ~10^5. In the past, power asymmetries of this magnitude have not been encountered during any HF modification experiments conducted in the natural ionosphere at Arecibo. This includes observations made in the F region, the E region and sporadic E [e.g., Djuth *et al.*, 1986; Djuth, 1984; Djuth, 1979].

Altitude-resolved spectra at 188.5 s L are presented in Figure 10. At this point in the experiment, the PL+ was confined to a total of four range cells, whereas the PL- and ion line scatter were restricted to one or two cells at most. The 430 MHz radar beam was stationary and pointed 15° from vertical. The altitude extent of the PL- and ion line scatter must therefore be very small because the 15° tilt of the radar wavefront, in itself, introduces an altitude smearing of ~180 m at 242 km altitude. A short data integration period (300 ms) was chosen for Figure 10 because the echoes were rapidly descending in altitude. For presentation purposes, we selected a data segment where the strongest PL+ echo was centered on single range cell. The strength of all signals vary somewhat (a factor of ~3 in power) from one 300-ms integration period to the next. In part, this is a product of the scattering statistics and the occasional sharing of signal between two range cells. However, slow variations in mean signal strength over time scales of 1-2 s account for about half of the power fluctuation.

The result of efforts to improve the signal statistics at the ion line by lengthening the integration time to 3 s (100 pulses) is shown in Figure 11. For the purpose of comparison, the integration period was centered on the time of the observations in

Figure 10. It is clear that the random fluctuations from the clutter are reduced, but the enhanced ion line has now crossed three range cells. This limits the signal integration time at any given range cell to about 300 ms. The weak scatter centered near zero frequency displacement at the highest and lowest ranges is caused by incoherent scatter from the unmodified Ba^+ cloud.

An example of spectra obtained during period P2 (278 - 291 s L) is presented in Figure 12. At this juncture of the experiment, the rapid altitude decline of the enhancements has halted, and therefore longer integration periods could be employed. Moreover, data were selected from a time interval centered on 285.0 s L when the radar beam was stationary. This avoids range smearing of signals as the beam scans across spatial gradients in electron concentration. Moderate to large echoes are present at both the PL- and the PL+ in Figure 12. As in Figure 10, the plasma line enhancements are confined to 4-5 altitude cells. Convincing ion line enhancements are present in only two altitude cells (239.79 km and 239.94 km); the weak signals at other altitudes are caused by incoherent scatter from the Ba^+ plasma. The PL+/PL- power asymmetry noted earlier is still present at a somewhat reduced level. Decay line peaks at ~2 kHz offset from 430 MHz + f_{HF} are prevalent in the PL+ spectra, but the PL- spectra exhibit peaks at larger offsets (3-5 kHz) from 430 MHz - f_{HF}.

In Figure 13, altitude-resolved spectra are shown at a later stage in the experiment (340.8 s L) when the resonant backscatter at PL+ was comparable to that of the PL-. At 340.8 s L, weak ion-line signals may be present in a few ranges, but these detections are far less convincing than those shown earlier. Because the radar beam was steered toward the center of the Ba^+ cloud, the CLP clutter level at the critical altitude increased markedly. This made it difficult to detect features such as the unmodified Ba^+ ion line spectrum with 100 pulses of integration. The echo returns at the plasma lines generally exhibit peaks near the decay line offset in the Ba^+ plasma (~2 kHz), although slightly greater offsets of ~3 kHz are present in a few ranges.

The altitude extent of the PL- echoes in Figure 13a is 1.35 km, whereas the PL+ signals span an altitude interval of 1.05 km (Figure 13c). The difference in the two altitude intervals arises because of the presence of weak signals in the two lowest altitude cells of the PL- display and the absence of these signals in the PL+ panel. This disparity may be the result of the greater sensitivity of the radar line feed at PL- than at PL+. (The larger S/N value indicated for the PL+ includes a factor of ~2 increase to compensate for the line feed response of the radar.) The altitude spread of the plasma line echoes in Figure 13 is greater than that shown in previous figures of this type. In part, this is due to the fact that the radar beam was quickly scanned in azimuth during the 3-s integration

period of the data. By studying changes in the altitude of the largest signal with shorter (300 ms) temporal averages, we conclude that 300 m is the upper limit of the altitude spread contributed by changes in the critical height across large-scale spatial gradients scanned by the radar beam. With this correction factor, the PL- altitude expanse is 1.05 km, which is still significantly greater than that recorded at earlier times (i.e. 600 m and 750 m, respectively, in Figures 10 and 12). Thus, there is evidence that a wider altitude interval of excitation accompanies the equalization of the PL+/PL- amplitudes.

An overview of the locations of the HF-enhanced spectral peaks versus time after launch is provided in Figure 14. Data from CLP range cells containing the strongest spectral peaks were selected for this display. The range cell containing the largest spectral peak is generally the same for the PL+, PL-, and ion-line enhancements. At late times ($\geq$ 280 s L) differences in ranges are occasionally found, but even under these circumstances the peaks are confined to an interval of two range cells (300 m). To avoid spurious noise spikes and ion-line echoes from the unmodified barium cloud, we imposed a requirement that the maximum spectral peak be at least 3.3 σ above the mean (noise + clutter) level. Data interpolation between 0.98-kHz FFT points was performed using model fits to the $(\sin x/x)^2$ spectral windowing function under the assumption that the bandwidth of the actual signal was infinitely narrow. The "quantized" frequency bands evident at 0.98 kHz increments in Figure 14 indicate that this narrow-bandwidth model is not completely correct. Other modeling efforts made with signals of finite bandwidth produced additional ambiguities and uncertainties that are difficult to resolve without a firm theoretical description of peak width versus time. For simplicity, the narrow-bandwidth (monochromatic) model was adopted for the present analysis.

As expected, the best temporal coverage in Figure 14 is provided by the PL+ echo (upper panel). Between ~163 s and 170 s L, the frequency of the PL+ signal has a positive frequency offset, δ, from 430 MHz + f_{HF}, but with increasing time the peak migrates to δ = -2.0 $\pm$ 0.5 kHz. This behavior is discussed in Section 4; in part, it is the result of a Doppler shift caused by the downward motion of the Ba^+ plasma. In the current work, spectra recorded prior to ~188 s L are not emphasized because plasma dynamics are thought to play an important role in determining the frequency of the peak. This greatly complicates the interpretation of the observations and is beyond the scope of the current work. The ion line observations of Figure 14 indicate that the strongest enhancements consistently occur at a negative frequency offset from 430 MHz (δ = -1.4 $\pm$ 0.4 kHz). In addition, the PL- measurements made between 180 s and 210 s L reveal that the weak echo shown in Figures 9 and 10, can occur near δ = -1 kHz (referenced to 430 MHz - f_{HF}) as well as at δ = 0 kHz. At 280 s L and later, the PL- spectral peaks

occupy a band extending from approximately δ = -1.5 kHz to δ = -6.0 kHz. This band includes the decay line and the first cascade line of the parametric decay instability [Perkins et al., 1974; Fejer, 1979].

Data acquired with the Antigua 49.92 MHz radar indicate that some of the plasma line events may be linked to the formation of HF-induced field-aligned irregularities in the Ba^+ cloud. The first detection of 3-m field-aligned irregularities (FAIs) occurred at 283 s L. Backscatter from the HF-induced irregularities was initially very weak, but moderate signal strengths were evident at later times during the period 296 - 309 s L. The initial detection of FAIs occurred very close to the time when moderate PL- enhancements appeared in the Arecibo data base (e.g., Figure 8). Moderate to strong FAI scatter was observed between 339 and 370 s L when the HF facility was operating CW. During this interval, the amplitudes of the PL+ and PL- were first observed to equalize. At later times (404 - 493 s L), only weak FAI backscatter was detected. During this period the PL+/PL- signals also became weaker, but their relative strengths remained comparable.

Summary

The observations presented in this section provide an overview of the most prominent features of the Arecibo radar data acquired during the AA-2 release. Many aspects of the experiment, such as the temporal development of the enhanced Langmuir oscillations/ion waves, are not addressed in the current study. Moreover, measurements from several of the supporting diagnostics (e.g., the Antigua 49.92 MHz radar) will be described in greater detail in a future publication. The principal results reported here may be summarized as follows. During the first 150 s after the Ba release, a large power asymmetry exists between PL+ and PL-, with most of the backscatter return residing at the PL+. Peaks at the decay line are commonly observed in the PL+ spectrum. The enhanced ion line spectrum contains a single peak at a sideband downshifted from 430 MHz by 1.0 to 1.5 kHz. For the first 120 s following the release, the PL- spectrum contains a very weak peak located either exactly at 430 MHz - f_{HF} or in the vicinity of 430 MHz - f_{HF} - 1 kHz. Beginning ~131 s after the release, significant enhancements are evident at the PL-. Initially, the PL- spectra contain strong peaks at frequency offsets of 3-5 kHz from 430 MHz - f_{HF} with some signs of unresolved structure near the decay line. At later times, peaks at the decay line dominate the PL- spectrum. The altitude interval of the PL+/PL- enhancements is smallest at early times, but increases markedly at ~186 s after the release. Within this same time frame, the PL+ and PL- amplitudes

equalize. Both effects appear to be related to the formation of 3-m field-aligned irregularities in the plasma.

4. Discussion

HF modification studies conducted in the natural F region at Arecibo provide an important frame of reference from which to view the results of the AA-2 release. In the past, experiments have always been performed at Arecibo using a vertically directed HF beam. However, with the CRRES experiments, the HF beam was tilted 12° from the vertical in the direction of geographic north to accommodate the rocket launch requirements. The 12° tilt is well within the Spitze angle (15.7°) calculated for $f_{HF} = 5.1$ MHz and the geomagnetic field geometry of Arecibo. During the AA-2 release, the 430 MHz radar beam was initially pointed towards the center of the HF beam in the ionosphere but later moved to various locations south of that point. Consequently, it is reasonable to assume that the microphysics near the critical layer remains intact with the tilted HF beam, provided that the plasma is for the most part horizontally stratified. To within reasonable limits, this applies to the AA-2 Ba^+ cloud.

Throughout the period of AA-2 observations, the 430 MHz radar viewing angle, A, relative to the geomagnetic field ranged from 53.0° to 55.1°. This is not greatly unlike the value A ≅ 44° used in many of the past investigations of HF-induced Langmuir oscillations in the natural F region. For AA-2 studies, the value A=55.1° applies to all observations made prior to 228 s L. Thereafter, values between 55.1° and 53.0° are appropriate, depending on the specific pointing direction of the 430 MHz radar beam.

Because the scale length H is shorter in the Ba^+ cloud (H ~ 5 km) than in the typical F-region environment (H = 30 - 70 km), vertical distances to reference points in the plasma are greatly compressed in the AA-2 experiment compared to the natural ionosphere. For example, the altitude of the upper hybrid resonance ($f_{HF} = [f_{ep}^2 + f_{ec}^2]^{1/2}$, where f_{ep} is the local electron plasma frequency at the resonance, and f_{ec} is the electron cyclotron frequency) and the so-called "matching height" [Fejer *et al.*, 1991] (where one would expect to detect Langmuir waves with the 430 MHz radar based on frequency-matching of the Langmuir wave dispersion relation to f_{HF}) are both located in a zone 200-250 m below the critical height.

Experimentally, if the 430 MHz radar were pointed vertically, 1 - 2 altitude cells (150 - 300 m) would cover most of the resonance region thought to be responsible for HF-enhanced plasma lines/ion lines at Arecibo. However, because the 430 MHz radar

beam was positioned at zenith angles between 15° and 13° during the CRRES observations, the altitude interval spanned by a single 150-m range cell is greater than 150 m. This situation arises because of the finite beamwidth of the tilted radar beam. At 240 km altitude the half-power beamwidth of the 430 MHz radar is approximately 700 m. At 15° zenith angle, the radar wavefront at the half-power point occupies an altitude interval of 181 m. If strongly excited waves were confined to an infinitely narrow altitude interval, and these waves were detected only out to the half-power points of the radar beam, one would expect to find signals in 2-3 consecutive range cells. If the strongest echo is centered on a range cell (e.g., Figure 10, PL+ echo at 242.34 km), one would expect to find weaker echoes of comparable strength in range cells above and below the cell containing the strongest signal. Moreover, if a range cell contains an extremely strong signal, contributions from signals beyond the 3-dB power points of the radar beam may become important. A strong enough signal could readily penetrate into 4 or more range cells. In Figure 10, PL+ backscatter is detected in two range cells above the range of strongest scatter and in one range cell below it. The asymmetry in the altitude span is consistently observed at early times (175-230 s L) when the PL+ is particularly strong. We believe that this occurs because the shape of the radar beam is asymmetric relative to the pointing direction at large (~15°) zenith angles. For the AA-2 observations, the effective beamwidth is wider to the north of the beam axis than to the south. The distortion is caused by "spillover" in the illumination of the reflector dish. Weak signals, such as those at the ion line and PL- in Figure 10, are observed in only one range cell because the signal contributions near the perimeter of the radar beam are below the clutter/noise floor of the measurement.

On the basis of the above arguments, the altitude-resolved spectral measurements of Figure 10 are consistent with the excitation of PL+, PL-, and ion line enhancements in a single, very narrow (<< 150 m) altitude interval. In Figure 12, the altitude interval may be slightly broader. However, in Figure 13 the significant increase in the range spread of the echoes is probably caused by appreciable irregularities in the critical surface viewed by radar. Corroborative results obtained with the 49.92 MHz radar on Antigua indicate that these irregularities are most likely HF-induced.

As noted in Section 3, the Ba^+ cloud is formed from neutral Ba vapor expanding radially relative to the rocket velocity at the moment of release. The travel time of the Ba/Ba^+ cloud to the radar viewing location was roughly 11 s, which yields a travel speed of ~1.3 km/s. This speed is somewhat greater than the estimate of ~0.9 km/s based on the velocity distribution function of Ba measured during the high-altitude CRRES releases [Bernhardt *et al.*, 1993]. If the initial Ba^+ ions have a horizontal speed of

1.3 km/s, then the ion flow speed projected down geomagnetic field lines is ~850 m/s. One would expect this flow speed to rapidly decrease because of collisions between Ba^+ and atmospheric O and O^+. The total collision frequency between Ba^+ and O/O^+ is ~0.5 s^{-1}. The initial rate of descent of the critical layer in Figure 7 (roughly 600 m/s) is consistent with high ion flow speeds along the geomagnetic field. However, the velocity of the critical layer decreases substantially over time scales of 10 - 20 s following the arrival of the Ba^+ in the radar field-of-view. This time constant most likely applies to the ion flow velocity as well.

It is difficult to determine the purity of the Ba^+ plasma on the basis of the incoherent scatter spectra alone. The reason for this is the trade-off between ion temperature (T_i), ion mass (m_i), and electron temperature (T_e) in the analysis of the incoherent scatter spectrum [e.g., Sultan, *et al.*, 1992] and limitations in the spectral resolution needed to define a narrow Ba^+ ion-line spectrum. The AA-2 observations are consistent with a high (90% or greater) fractional composition of Ba^+ ions to total ($O^+ + Ba^+$) ions in that "reasonable" values of T_i and T_e are obtained under this condition. In addition, enhanced ion line/plasma line measurements made in the ionization cloud (Figures 10 and 11) also point toward a dominant Ba^+ contribution. On physical grounds, one expects the Ba release to produce an electrostatic snowplow that excludes O^+ ions from the Ba^+ cloud [Schunk and Szuszczewicz, 1988, 1991; Ma and Schunk, 1991, Bernhardt *et al.*, 1991].

The locations of many of the spectral features in Section 3 resemble those expected for the parametric decay instability. The value of the offset δ for the decay line peaks at (430 MHz $\pm$ (f_{HF} - δ)) and the enhanced ion line at (430 MHz $\pm$ δ) can be estimated using parametric instability formalism [e.g., Perkins et al., 1974; Fejer, 1979]. For a 100% Ba^+ plasma and averaged data values of T_e = 2350 K and T_i = 1100 measured ~1 minute after the release, one obtains δ = 1.7 kHz. This is reasonably close to the average location/frequency interval of the PL+/PL- peaks (2.0 $\pm$ 0.5 kHz) and the offsets (δ = 1.4 $\pm$ 0.4 kHz) of the downshifted ion line peak at 430 MHz - δ. These values are representative of measurements made 35 s after the release (187 s L) and later.

In Section 3, we noted that the PL+ spectral peak undergoes a rapid frequency change between 163 s and ~185 s (top panel in Figure 14). In part, this may be the result of a Doppler shift brought about by the fact that the excited waves are in a plasma moving towards the radar. To test this hypothesis, we assume the PL+ peak is generated directly by the parametric decay instability and that the rate of change in the PL+ range is approximately equal to the line-of-sight plasma velocity. Moreover, to obtain a realistic time-dependent estimate of the decay line frequency, we assume that electron

temperature can be approximated as T_e = 987 K + 1363 x [1 - exp(t/30 s)], where t is time referenced to the release, and the time constant (30 s) is a rough estimate based on the AA-2 release results. This formula yields the measured background electron temperature at the time of the release (987 K) and reproduces the late-time temperature T_e=2350 K used above. Ion temperature is initially set equal to 910 K but allowed to increase to 1100 K as T_e increases. The result of this calculation is shown as a continuous line in the upper panel of Figure 14. The calculation reproduces the general downward trend of peak frequency at times between 163 s and 185 s L, but the theoretical estimate does not agree with the data in detail. This indicates that either the line-of-sight ion flow speed is significantly greater than the rate of change of the PL+ range or that the excitation of the decay mode proceeds somewhat differently in a rapidly moving plasma. At times after 200 s L, the calculated location of the decay line lies near the upper boundary of the measured range of peak frequencies. In this case, the interpolated frequency locations may have been influenced by the presence of unresolved spectral structure in FFT cells adjacent to, and on the 430 MHz side of, the peak (see e.g., Figure 13c). This effect could readily move the interpolated frequency of the peak by -0.5 kHz. A correction factor of this magnitude would bring the observations in line with the calculated decay mode frequency.

Before a threshold for the parametric decay instability can be determined, an accurate estimate of the Langmuir wave damping decrement in the Ba^+ plasma is needed. The usual assumption is that the damping is controlled by collisions between electrons and ions. Near the critical layer in the AA-2 plasma, the electron-ion collision frequency, ν_{ei}, is ~150 s^{-1}, assuming T_e = 2350 K. However, because many photoelectrons are created by the ionization of the neutral cloud, questions arise concerning the contribution of electron Landau damping to the overall damping decrement. To address this issue, we have examined PL- data during the period 155-280 s L for evidence of enhancements by suprathermal electrons. This method is similar to that used to detect photoelectrons in the daytime ionosphere [Carlson *et al.*, 1977, Djuth *et al.*, 1994]. During the period selected for analysis, only a weakly enhanced plasma line was present at 430 MHz - f_{HF} (Figure 10). Measurements in the presence of strong PL+ enhancements are not feasible because of poor system sensitivity. (The clutter from the CLP technique greatly elevates the level of random fluctuations at ranges of interest to the study.) Our investigation yielded no detections of photoelectron-enhanced plasma lines over a 2-MHz band centered on 430 MHz - f_{HF}. This frequency band corresponds to radar phase energies (electron energies) between 5.8 and 12.9 eV. In general the PL- is used to detect electrons moving up geomagnetic field lines (away

from the radar). However, even though most Ba photoelectrons are initially directed downwards along geomagnetic field lines through the bottom of the cloud, about one-third of the flux is expected to be scattered back up field lines because of elastic and inelastic collisions with the neutral atmosphere [e.g., Carlson et al., 1982]. On the basis of our study, we can set an upper limit on the upgoing flux of 2×10^5 electrons cm^{-2} s^{-1} eV^{-1} at phase velocities comparable to those of the HF-enhanced plasma lines. This is more than two orders of magnitude less than the daytime photoelectron flux, and the corresponding Landau damping decrement is very small for any comparable electron energy distribution. We conclude that the appropriate damping decrement for Langmuir waves is specified by ν_{ei}.

The parametric decay threshold calculated for a homogeneous plasma using the Ba^+ plasma parameters is E_o~0.2 V/m, where E_o is the amplitude of the pump electric field. This can be compared with estimates of the HF electric field in the plasma. Under the assumption that a standing wave pattern is generated near radio wave reflection, the predicted HF electric field at the first standing wave maximum is 1.7 V/m. At lower heights near the upper hybrid resonance/430-MHz-radar matching height (~250 m below the critical layer), the standing wave maximum has a value of 1.2 V/m. Thus, the estimated HF electric field strengths in the resonance region are well above the threshold for the parametric decay instability in a homogeneous plasma. However, in the present case where the ionospheric scale length is rather small (~5 km), the homogeneous plasma approximation may be inappropriate. In a horizontally-stratified medium, excited Langmuir waves decouple from the HF pump wave as they propagate down the plasma gradient [Perkins and Flick, 1971; Fejer and Leer, 1972]. This can lead to a substantial increase in the instability threshold. Unfortunately, the assumptions implicit in the work of Perkins and Flick [1971] and Fejer and Leer [1972] are not appropriate for AA-2 experimental conditions. Further theoretical studies are needed to address the role played by plasma inhomogeneity in the AA-2 experiment.

In general, the spectra presented in this paper are intended to show typical behavior during the AA-2 experiment. Displays of unique and/or transient features have been avoided. Most of the enhanced plasma line/ion line measurements appear to contain elements of the parametric decay instability, but some major inconsistencies are also evident in the data. Figure 10 shows a very strong decay line in the PL+ spectrum and the expected enhancement at the downshifted sideband of the ion line. Indeed, the concept of oppositely propagating ion waves and Langmuir waves is central to the parametric decay process. However, one would also expect the strong PL+ decay waves in Figure 10 to saturate by generating oppositely propagating Langmuir waves though the

ion nonlinear Landau damping process [Perkins *et al.*, 1974]. No such cascade line is present in the PL- spectrum. Instead, one finds a weak spike located at frequencies between 430 MHz - f_{HF} and 430 MHz - f_{HF} - 1 kHz (Figure 14). The feature at 430 MHz - f_{HF} may be the result of linear mode conversion [Morales and Lee, 1977] along the steep vertical gradient in the Ba^+ cloud. The echoes offset by -1 kHz are harder to explain, but could be produced by Langmuir waves scattered off the strongly enhanced ion waves traveling away from the radar.

The spectra of Figure 10 are characteristic of the initial period of strong PL+ enhancements between 170 s and 235 s L. These observations suggest that strongly excited Langmuir waves with radar wavevectors **k** ($|\mathbf{k}| = 18\ m^{-1}$) directed toward the radar are coupled to ion-acoustic waves having oppositely directed wavevectors. Absent in the data are decay line/cascade line waves with wavevectors directed away from the radar and ion-acoustic waves with **k** directed toward the radar. The observations seem to indicate that only half of the oppositely propagating waves expected for a parametric decay instability [e.g., Fejer, 1979] are present in the plasma with no signs of wave saturation. In Figure 12, the PL+ is weaker than in Figure 10, but the anticipated cascade line in the PL- spectrum (offset by 3-5 kHz) appears in the data. Moreover, the expected enhancement of the downshifted sideband in the ion line spectrum is readily discernible. In Figure 13, the plasma lines have only moderate amplitudes, and, at most, weak ion-line enhancements are present. Nevertheless, when the PL- decay line is strong (altitude 240.69 km), an unresolved cascade line appears to be present in the PL+ spectrum. Similarly, an unresolved cascade line is present in the PL- spectrum when a strong decay line appears in the PL+ spectrum (range 240.54 km). Figure 14 shows that the first PL- cascade line can exceed the amplitude of the decay line, but that this is usually not the case at the PL+. The results of Figures 12-14 support the idea that parametric decay processes are operative in the plasma.

Clearly, the most curious feature of the observations is the large power asymmetry in the backscatter from radar wavevectors directed toward the radar (PL+) versus those directed away from the radar (PL-). This asymmetry is most evident at early times following the release (18 s - 83 s R, 170 - 235 L), but it doesn't completely disappear until about 145 R (297 s L). The observed power ratio between PL+ and PL- is greater than 10^5 at the decay line. Moreover, the absolute strength of the PL+ decay line is greater than any plasma line signal seen in previous ionospheric modification experiments at Arecibo. Observations made in the past in the natural ionosphere at Arecibo have yielded no large, systematic asymmetries between the power at the

upshifted and downshifted plasma lines. At F-region altitudes, the time-averaged power is roughly comparable at the upshifted and downshifted plasma lines. In sporadic E, either the PL+ or the PL- may be dominant. The ratio of PL+ power to PL- power ranges from 10^{-1} to 10^{2}, but very few cases are encountered near the extrema of this range [Djuth, 1979].

During part of the time when a large asymmetry in plasma line power was observed, substantial Ba^+ flow velocities existed along geomagnetic field lines. This is mirrored by the rapid decrease of the critical layer in Figure 7. Initially, the estimated ion flow velocity projected along the geomagnetic field (~850 m/s) exceeded the ion-acoustic velocity in the Ba^+ plasma (~550 m/s). As noted above, this ion flow velocity is not determined from incoherent scatter observations, but is calculated from the initial expansion rate of the neutral Ba cloud. If the ion flow velocity parallel to the geomagnetic field is scaled according to the rate of change in the critical altitude, one finds that the flow becomes subsonic at ~12 s after release (164 s L). Under these assumptions, all of the observations of the plasma line power asymmetry discussed herein were made under conditions of subsonic ion flow. Moreover, there does not appear to be any correlation between the rate of descent of the critical layer and the magnitude of the asymmetry.

The strongest plasma line asymmetries were observed at times when the Antigua 49.92 MHz radar detected no 3-m field aligned irregularities in the Ba^+ cloud. At later times (339 s - 370 s L) when moderate/strong backscatter from 3-m irregularities was detected, the amplitudes of PL+ and PL- were roughly equal. This situation is not unlike that observed in the natural F region. The data presented in Figure 8 between 100 s L and 150 s L were, in fact, acquired in the natural F region in the presence of strong scatter from 3-m irregularities. The plasma line asymmetry encountered during AA-2 may be associated with the smoothness of the Ba^+ plasma at early times following the release. In the natural F-region at Arecibo, this situation never exists for long periods of time because HF-induced field-aligned irregularities (FAIs) quickly develop in the plasma [e.g., Coster *et al.*, 1985].

The suppression of instabilities responsible for the production of HF-excited FAIs may be related to the plasma flow down geomagnetic field lines during AA-2. At Arecibo, short-scale FAIs are believed to be excited by instability processes occurring near the upper hybrid resonance [Noble and Djuth, 1990]. At early times following the AA-2 release, the altitude of the upper hybrid resonance moves rapidly downwards in altitude because of the build-up of Ba^+ ions along geomagnetic field lines. However, unlike the case of a slowly descending ionization layer in thermal equilibrium, the

plasma in the upper hybrid resonance zone does not simply move down in altitude while maintaining the frequency matching conditions necessary for instability growth. In the AA-2 experiment, the altitude zone of the upper hybrid resonance is continuously formed and then reformed by arrival of fresh plasma from greater heights. This situation arises because of the broad distribution of ion velocities parallel to the geomagnetic field. In effect, the resonance region is continuously recreated by the downward ion flow. This limits the residence time of the HF wave in the region of instability growth. If the HF wave is not present in the resonance region over time scales of the instability growth period, then the production of short-scale irregularities will be inhibited. Moreover, the effect of the rather short scale length $H \sim 5$ km in the Ba^+ plasma is to increase the instability threshold for the short-scale irregularities and to decrease their growth rate [Grach *et al.*, 1977; Das and Fejer, 1979]. Assuming a nominal instability growth time of ~1 s and a 50-m resonance zone, one finds that even a relatively slow (70 m/s) field-aligned ion flow may interfere with the production of field-aligned irregularities. In light of this, it is not surprising that AFAIs are detected only at late times during the AA-2 experiment when the vertical velocity of the critical layer is small.

No specific explanation for the plasma line power asymmetry is offered here. The plasma line asymmetry may be caused by processes sensitive to the downward ion flow, the smoothness of the Ba^+ plasma and/or the shortness of plasma scale length. A reexamination of the development of the parametric decay instability in this type of environment is needed. In addition, it is important to recognize that Langmuir wave propagation in an inhomogeneous medium can greatly influence observations made from a limited range of viewing angles with the Arecibo 430 MHz [Muldrew, 1978a, b]. Throughout the experiment, the radar viewed the excited plasma/ion waves at 53.0° to 55.1° relative to the geomagnetic field. Additional studies are required to determine whether propagational geometries exist that can exclude PL- scatter at the 50 dB level while maintaining strong PL+ and ion line enhancements.

5. Conclusions

During the AA-2 experiment, the Arecibo 430 MHz radar detected some of the strongest HF-enhanced plasma lines ever recorded at Arecibo Observatory. At early times, within 83 s of the Ba release, extremely strong plasma lines were observed near 430 MHz + f_{HF} - δ, where δ = 2.0 ± 0.5 kHz. These echoes are caused by HF-excited Langmuir oscillations with wavevectors **k** ($|k|$ = 18 m^{-1}) pointed toward the radar. The observed value of δ is close to the frequency offset calculated for the parametric decay instability in a Ba^+ plasma; the spectral peak is commonly referred to as the decay line [Showen and Kim, 1978]. The upshifted plasma line was accompanied by strong HF-enhanced ion waves that were present only at the downshifted acoustic sideband, that is, at 430 MHz - δ, where δ = 1.4 ± 0.4 kHz. Only very weak echoes were detected at the downshifted plasma line. The spectral peaks were either centered exactly at 430 MHz - f_{HF} or located near 430 MHz - f_{HF} - 1 kHz. The power asymmetry between the upshifted and downshifted plasma line enhancements was greater than 10^5 at the decay line. No explanation for this remarkable asymmetry is provided in the present work. However, the current results indicate that the development of the parametric decay instability needs to be reexamined in a smooth Ba^+ plasma having a short scale length (5 km). An assessment of the impact of ion flow along geomagnetic field lines may be essential to understanding the AA-2 plasma line observations. Finally, propagation of Langmuir oscillations into the field-of-view of the 430 MHz radar cannot be ruled out as a source of the power asymmetry. However, a propagational model must also account for the presence of a strongly-enhanced downshifted sideband in the ion line spectrum.

In support of the AA-2 experiment, a mobile VHF radar was deployed on the island of Antigua to monitor the formation of HF-induced irregularities in the Ba^+ cloud. The radar was sensitive to field-aligned irregularities (FAIs) having a spatial scale of 3 m across the geomagnetic field. In the early time release environment, no HF-induced scatter was detected. It is suggested that ion flow down geomagnetic field lines initially suppressed thermally-driven instabilities responsible for the formation of short-scale field-aligned irregularities. At later times (131-341 s after the Ba release), HF-induced field-aligned irregularities were detected in the Ba^+ cloud. The appearance of moderate enhancements at the downshifted plasma line coincided with the arrival of HF-induced FAIs. At this point, the enhanced plasma line/ion line spectra began to more closely resemble a parametric decay spectrum. As the FAIs intensified, the amplitudes of the upshifted and downshifted plasma lines equalized, and the power asymmetry

disappeared. At most, only weak ion-line enhancements were evident at this point, but the corresponding plasma line spectra were indicative of the parametric decay instability. Overall, once HF-induced FAIs formed in the Ba^+ plasma, the instability physics appeared to be similar to that encountered in the natural F region after FAIs form.

The data presented here are restricted to observations made during continuous wave (CW) transmissions with the Arecibo HF facility. In this mode of operation, the wideband (~100 kHz) spectral signatures of strong turbulence seen in the natural ionosphere at Arecibo [DuBois *et al.*, 1990; Fejer *et al.*, 1991; Cheung *et al.*, 1992; DuBois *et al.*, 1993; Sulzer and Fejer, 1993] are absent. Additional AA-2 studies are planned that focus on the temporal development of Langmuir oscillations and ion waves in the Ba^+ plasma. Special attention will be paid to short (tens of ms) time scales following the transmission of an HF pulse. In previous experiments, data acquired within ~50 ms of HF turn-on has yielded the best evidence for strong turbulence in the Arecibo F region.

Acknowledgments. Two of the authors (F.T.D. and J.H.E.) acknowledge support from NASA under contracts NAS8-39075 and from the Phillips Laboratory, Hanscom Air Force Base under contracts F19628-92-C-0168 and NAS8-39238. The efforts of K.M.G. were supported by the Air Force Office of Scientific Research under task 2310BP. We gratefully acknowledge the outstanding efforts of K. L. Williams and C. L. Younger (Geospace Research, Inc.), and J. W. Brosnahan (LaSalle Research Corporation) in the deployment and operation of the VHF radar on Antigua. We thank P. A. Bernhardt for making optical measurements in support of the AA-2 experiment and for helpful discussions concerning the results. L. M. Duncan, J. F. Vickrey, and C. J. Heinselman provided much needed organizational and logistical assistance in support of the AA-2 launch operation. We are especially grateful for the help of A. Crespo, H. Monroig, V. Iguina, and E. Castro in maintaining the Arecibo HF facility and the 430 MHz radar at a high performance level throughout the *El Coqui* rocket campaign. The Arecibo Observatory is part of the National Astronomy and Ionosphere Center, which is operated by Cornell University under cooperative agreement with the National Science Foundation.

REFERENCES

Bernhardt, P. A., Probing the magnetosphere using chemical releases from the Combined Release and Radiation Effects Satellite, *Phys. Fluids*, *4*, 2249, 1992.

Bernhardt, P. A., P. Rodriguez, C. L. Siefring, and C. S. Lin, Field-aligned dynamics of chemically induced perturbations to the ionosphere, *J. Geophys. Res.*, *96*, 13887, 1991.

Bernhardt, P. A., J. D. Huba, M. B. Pongratz, D. J. Simons, and J. H. Wolcott, Plasma irregularities caused by cycloid bunching of the CRRES G-2 Barium release, *J. Geophys. Res.*, *98*, 1613, 1993.

Carlson, H. C., V. B. Wickwar, and G. P. Mantas, The plasma line revisited as an aeronomical diagnostic: Suprathermal electrons, solar EUV, electron-gas thermal balance, *Geophys. Res. Lett.*, *4*, 565, 1977.

Carlson, H. C., V. B. Wickwar, and G. P. Mantas, Observations of fluxes of suprathermal electrons accelerated by HF excited instabilities, *J. Atmos. Terr. Phys.*, *44*, 1089, 1982.

Carlsten, J. L., Photoionization of barium via the ^3D metastable levels, *Planet. Space Sci.*, *23*, 53, 1975.

Cheung, P. Y., D. F. DuBois, T. Fukuchi, K. Kawan, H. A. Rose, D. Russell, T. Tanikawa, and A. Y. Wong, Investigation of strong Langmuir turbulence in ionospheric modification, *J. Geophys. Res.*, *97*, 10575, 1992.

Coster, A. J., F. T. Djuth, R. J. Jost, and W. E. Gordon, The temporal evolution of 3-m striations in the modified ionsphere, *J. Geophys. Res.*, *90*, 2807, 1985.

Das, A. C., and J. A. Fejer, Resonance instability of small-scale field aligned irregularities, *J. Geophys. Res.*, *84*, 6701, 1979.

Djuth, F. T., HF-induced plasma waves in ionospheric sporadic E, Ph.D. thesis, Rice Univ., Houston, Texas, 1979.

Djuth, F. T., HF-enhanced plasma lines in the lower ionosphere, *Radio Sci., 19*, 383, 1984.

Djuth, F. T., and C. A. Gonzales, Temporal evolution of the HF-enhanced plasma line in Sporadic E, *J. Geosphys. Res., 93*, 196, 1988.

Djuth, F. T., C. A. Gonzales, and H. M. Ierkic, Temporal evolution of the HF-enhanced plasma line in the Arecibo *F* region, *J. Geophys. Res., 91*, 12089, 1986.

Djuth, F. T., M. P. Sulzer, and J. H. Elder, High resolution observations of HF-induced plasma waves in the ionosphere, *Geosphys. Res. Lett., 17*, 1893, 1990.

Djuth, F. T., M. P. Sulzer, and J. H. Elder, Application of the coded long-pulse technique to plasma line studies of the ionosphere, *Geophys. Res. Lett.*, in press, 1994.

DuBois, D. F., H. A. Rose, and D. Russell, Excitation of strong Langmuir turbulence in plasmas near critical density: Application to HF heating of the ionosphere, *J. Geosphys. Res., 95*, 21221, 1990.

DuBois, D. F., H. A. Rose, and D. Russell, Coexistence of parametric decay cascades and caviton collapse at subcritical densities, *Phys. Rev. Lett., 66*, 1970, 1991.

DuBois, D. F., A. Hanssen, H. A. Rose, and D. Russell, Space and time distribution of HF excited Langmuir turbulence in the ionosphere: Comparison of theory and experiment, *J. Geophys. Res., 98*, 17543, 1993.

Fejer, J. A., Ionospheric modification and parametric instabilities, *Rev. Geophys. Space Phys., 17*, 135, 1979.

Fejer, J. A., and E. Leer, Purely growing parametric instability in an inhomogeneous plasma, *J. Geophys. Res., 77*, 700, 1972.

Fejer, J. A., M. P. Sulzer, and F. T. Djuth, Height dependence of the observed spectrum of radar backscatter from HF-induced ionospheric Langmuir turbulence, *J. Geosphys. Res., 96*, 15,985, 1991.

Grach, S. M., A. N. Karashtin, N. A. Mityakov, V. O. Rapoport, and V. Yu. Trakhtengerts, Parametric interaction between electromagnetic radiation and ionospheric plasma, *Radiophys. Quantum Electron.*, Engl. Transl., *20*, 1254, 1977.

Gordon, W. E., and H. C. Carlson, The excitation of plasma lines in blanketing sporadic *E*, *J. Geophys. Res.*, *81*, 4016, 1976.

Gordon, W. E., and J. A. Dobelman, Comparison of measured and calculated antenna patterns for the Islote heater, Rice University Report, Houston, Texas, 13 July 1982.

Hanssen, A., E. Mjolhus, D. F. DuBois, and H. A. Rose, Numerical test of the weak turbulence approximation to ionospheric Langmuir turbulence, *J. Geophys. Res.*, *97*, 12073, 1992.

Ma, T.-Z., and R. W. Schunk, Plasma cloud expansion in the ionosphere: Three-dimensional simulation, *J. Geophys. Res.*, *96*, 5793, 1991.

Morales, G. J., and Y. C. Lee, Generation of density cavities and localized electric fields in a nonuniform plasma, *Phys. Fluids*, *20*, 1135, 1977.

Muldrew, D. B., The role of field-aligned ionization irregularities in the generation of the HF-induced plasma line at Arecibo, *J. Geophys. Res.*, *83*, 2552, 1978a.

Muldrew, D. B., Langmuir wave propagation and the enhanced plasma line in sporadic *E*, *J. Geophys. Res.*, *83*, 5207, 1978b.

Noble, S. T., and F. T. Djuth, Simultaneous measurements of HF-enhanced plasma waves and artificial field-aligned irregularities at Arecibo, *J. Geophys. Res.*, *95*, 15195, 1990.

Perkins, F. W., and J. Flick, Parametric instabilities in inhomogeneous plasmas, *Phys. Fluids*, *14*, 2012, 1971.

Perkins, F. W., C. Oberman, and E. J. Valeo, Parametric instabilities and ionospheric modification, *J. Geophys. Res.*, *79*, 1478, 1974.

Schlegel, K., M. Rietveld, and A Maul, A modification event of the auroral *E* region as studied with EISCAT and other diagnostics, *Radio Sci.*, *22*, 1063, 1987.

Schunk, R. W., and E. P. Szuszczewicz, Early time plasma expansion characteristic of ionized clouds in the ionosphere, *J. Geophys. Res.*, *93*, 12901, 1988.

Schunk, R. W., and E. P. Szuszczewicz, Plasma expansion characteristics of ionized clouds in the ionosphere: Macroscopic formulation, *J. Geophys. Res.*, *96*, 1337, 1991.

Showen, R. L., and D. M. Kim, Time variations of HF-induced plasma waves, *J. Geophys. Res.*, *83*, 623, 1978.

Sultan, P. J., M. Mendillo, and W. L. Oliver, Detection of artificially created negative ion clouds with incoherent scatter radar, *J. Geophys. Res.*, *97*, 4085, 1992.

Sulzer, M. P., A radar technique for high range resolution incoherent scatter autocorrelation function measurements utilizing the full average power of klystron radars, *Radio Sci.*, *21*, 10330, 1986.

Sulzer, M. P., and J. A. Fejer, Radar spectral observations of HF-induced ionospheric Langmuir turbulence with improved range and time resolution, *J. Geophys. Res.*, in press, 1994.

FIGURE CAPTIONS

Figure 1. Overview of the AA-2 release geometry. The locations of Arecibo Observatory (AO), the Arecibo HF facility (HF), a digisonde/optical observing site at Ramey (RA), and the launch site at Tortuguero, Puerto Rico (TO) are shown in the figure. For the *El Coqui* campaign the Arecibo HF beam was tilted 12° from vertical in the direction of geographic north. The 3-dB contour of the HF beam at 250 km altitude is shown as a dotted ellipse. A distance scale along the geomagnetic meridian crossing Arecibo Observatory is provided as a reference.

Figure 2. Electron density versus altitude and time beginning 100 s after launch of AA-2. Prior to the release at 152 s, the F-region peak in the background ionosphere was at 345 km altitude. An upward tilted streak seen just before the release is the rocket body as viewed through a high order sidelobe of the radar. Preceding the rocket echo, small, faint pink dots are evident near 272 km; this is enhanced scatter from HF-excited ion waves. The short-lived transient signals visible near 100 km are echoes from the "heads" of meteor ionization trails. The position of the radar beam was stationary until 228 s; thereafter the beam was moved across the Ba^+ cloud revealing spatial structure.

Figure 3. Horizontal location of 430 MHz radar beam at 240 km altitude relative to Arecibo Observatory (AO). The locations designated by (+) are referenced to time (in seconds) after launch. The release location at 253 km is displayed at bottom right. For the first 228 s after launch the beam is stationary; thereafter positions are shown at 12-s intervals. Also illustrated are the estimated -3 dB and -10 dB contours of the HF beam based on studies conducted by Gordon and Dobelman [1982].

Figure 4. Forty consecutive electron density profiles are shown beginning with the launch of the AA-2 rocket. Each profile is integrated for 12 s; the integration intervals are centered on times corresponding to the "+" locations in Figure 3. The time of each profile is shown at the top. Times in seconds are read top to bottom. For presentation purposes, each profile

is displaced from the preceding one by 0.4 x 10^6 cm^{-3}. Error bars for electron concentrations are ~5% of the values shown. Enhanced ion lines are evident near 272 km altitude prior to the release at 152 s. Immediately before the release, an echo from the rocket is visible at ~250 km.

Figure 5. Upshifted plasma line power expressed as the ratio of signal-to-noise (SNR) versus altitude and time after launch. The noise value includes contributions from the sky noise and radar-receiver noise. Wideband spectra obtained with the coded long-pulse technique were processed to produce this plot. Power spectra were calculated at 150-m intervals and then integrated over the frequency interval 430 MHz + f_{HF} + 1 kHz through 430 MHz + f_{HF} - 45 kHz to yield signal power versus altitude. The bands of "noise" are artifacts of the coded long-pulse technique. The mean clutter power has been subtracted from each altitude profile, but random fluctuations in the residual give rise to "noise" bands. Stronger signals create more clutter, resulting in greater "noise" levels.

Figure 6. Barker power profiles (600 m range resolution) versus time after launch. Data obtained on the bottomside of the Ba^+ cloud is greatly expanded in altitude to highlight the induced ion line enhancements (pink outline near the perimeter of cloud). These enhancements are generally confined to a single 600-m cell. The altitude descent of the enhanced ion line closely matches that of the enhanced plasma line (Figure 5). The vertical streak at left is caused by backscatter from the rocket.

Figure 7. A) Critical altitude deduced from the upshifted plasma line data of Figure 5 (dots) and ion line data of Figure 6 (continuous line). B) Vertical velocity (negative velocity = motion downwards) of the critical layer in the Ba^+ cloud as determined from the measurements of A). Data are plotted only during periods when the radar beam is stationary. Velocity deduced from ion line observations are shown as (+); the error bar at left denotes $\pm 1\sigma$ errors for these measurements. The continuous line is a least-squares fit to the upshifted plasma line data. In this case, the $\pm 1\sigma$ fitting errors are approximately equal to the width of the line displayed, and no error bars are plotted. C) Scale length determined at the critical altitude using ion line measurements of electron

concentration. The scale length is ~40 km in the background F-region prior to the release, but ranges between 4 and 6 km in the Ba^+ plasma. The measurements of scale length have one-sigma error bars of approximately ±390 m.

Figure 8. Total, altitude-integrated, power received at the upshifted and downshifted plasma lines versus time after launch. Signal strength is expressed as a signal-to-noise ratio (SNR). The noise power received through the 2-MHz bandpass at the downshifted plasma line is used as the noise reference. Power measurements made at the upshifted plasma line have been corrected for the narrower (1-MHz) bandpass employed for these observations and for differences in the gain of the 430 MHz line feed at the upshifted and downshifted plasma lines. The schedule of HF transmissions during the AA-2 release is depicted at the bottom. These include continuous wave (CW) operations, high duty cycle pulsing (HD), and low duty cycle pulsing (LD). See text for details.

Figure 9. Typical enhanced backscatter spectrum observed in the Ba^+ cloud during periods of strong excitation at the upshifted plasma line. Observations are made simultaneously across all bands using the coded long-pulse technique. Measurements are shown for a single 150-m range gate containing maximum scatter. The signal at the upshifted plasma line exhibits a pedestal near 20 dB signal-to-noise ratio; this is the combined effect of the spectral windowing function and wideband clutter from signals at other ranges. The elevated baseline at the ion line is also caused by clutter. An average of 40 consecutive radar pulses is employed for the weaker signals near 430 MHz - f_{HF} and 430 MHz, but an average of only ten pulses is used for the measurement at 430 MHz + f_{HF}. Error bars are 16% of the mean values shown at the downshifted plasma line and ion line, and 32% of the values at the upshifted plasma line.

Figure 10. Power spectra simultaneously measured at the downshifted and upshifted plasma lines and ion line (columns) versus altitude (rows) at 188.5 s after launch. The altitude of each row is listed in the upper right hand corner of the ion line spectrum. Measurements from ten consecutive radar pulses (300-ms time interval) were integrated for this display. The downshifted

plasma line and ion line observations are plotted on a linear ordinate scale; the upshifted plasma line data are shown on a logarithmic scale because of their larger amplitudes. The signal-to-noise ratio (S/N) of the strongest spectral peak in each column is listed at the top of the column. The mean noise level is determined by sky plus radar-receiver noise and does not include contributions from clutter. The baseline levels at the ion line and upshifted plasma line are primarily the result of clutter from signals at other ranges; the baseline at the downshifted plasma line is mostly caused by noise from the sky and receiver. Error bars are 32% of the averaged values shown.

Figure 11. Ion line power spectra versus altitude at 188.5 s after launch. Altitudes are listed in the upper right hand corner of the spectral boxes. Measurements from 100 consecutive radar pulses (3-s time interval) were integrated for this display. The integration period is centered on the time of the observations of Figure 10. The maximum signal-to-noise ratio (after clutter subtraction) is 6.4 at 242.34 km altitude. During the 3-s period of integration, the height of the enhanced ion line descended from 242.49 to 242.19 km altitude. The weak echoes centered near 0 kHz in the lowest and highest altitude cells are incoherent scatter returns from the Ba^+ cloud. Error bars are 10% of the averaged values shown.

Figure 12. Power spectra simultaneously measured at the downshifted and upshifted plasma lines and ion line (columns) versus altitude (rows) at 285.0 s after launch. The altitude of each row is listed in the upper right hand corner of the ion line spectrum. Measurements from 100 consecutive radar pulses (3-s time interval) were integrated for this display. The display format is similar to that of Figure 10, except that the upshifted plasma line is now shown on a linear scale. Error bars are 10% of the mean values shown.

Figure 13a. Power spectra at the downshifted plasma line measured 340.8 s after launch. Altitudes are listed above each spectral box. Measurements from 100 consecutive radar pulses (3-s time interval) were integrated for this display. The signal-to-noise ratio (S/N) of the strongest spectral peak in the panel is listed at top. Error bars are 10% of the mean values shown.

Figure 13b. Power spectra at the ion line measured 340.8 s after launch. The data format is identical to that of Figure 13a.

Figure 13c. Power spectra at the upshifted plasma line measured 340.8 s after launch. The data format is identical to that of Figure 13a.

Figure 14. Frequency locations of HF-enhanced spectral peaks versus time after launch. Simultaneous measurements at the upshifted plasma line, the ion line, and the downshifted plasma line are shown in the top three panels. The continuous line in the uppermost panel is a theoretical curve discussed in the text. For reference, the altitude of the strongest spectral peak at the upshifted plasma line is displayed at the bottom. The temporal resolution of the measurements is 300 ms.

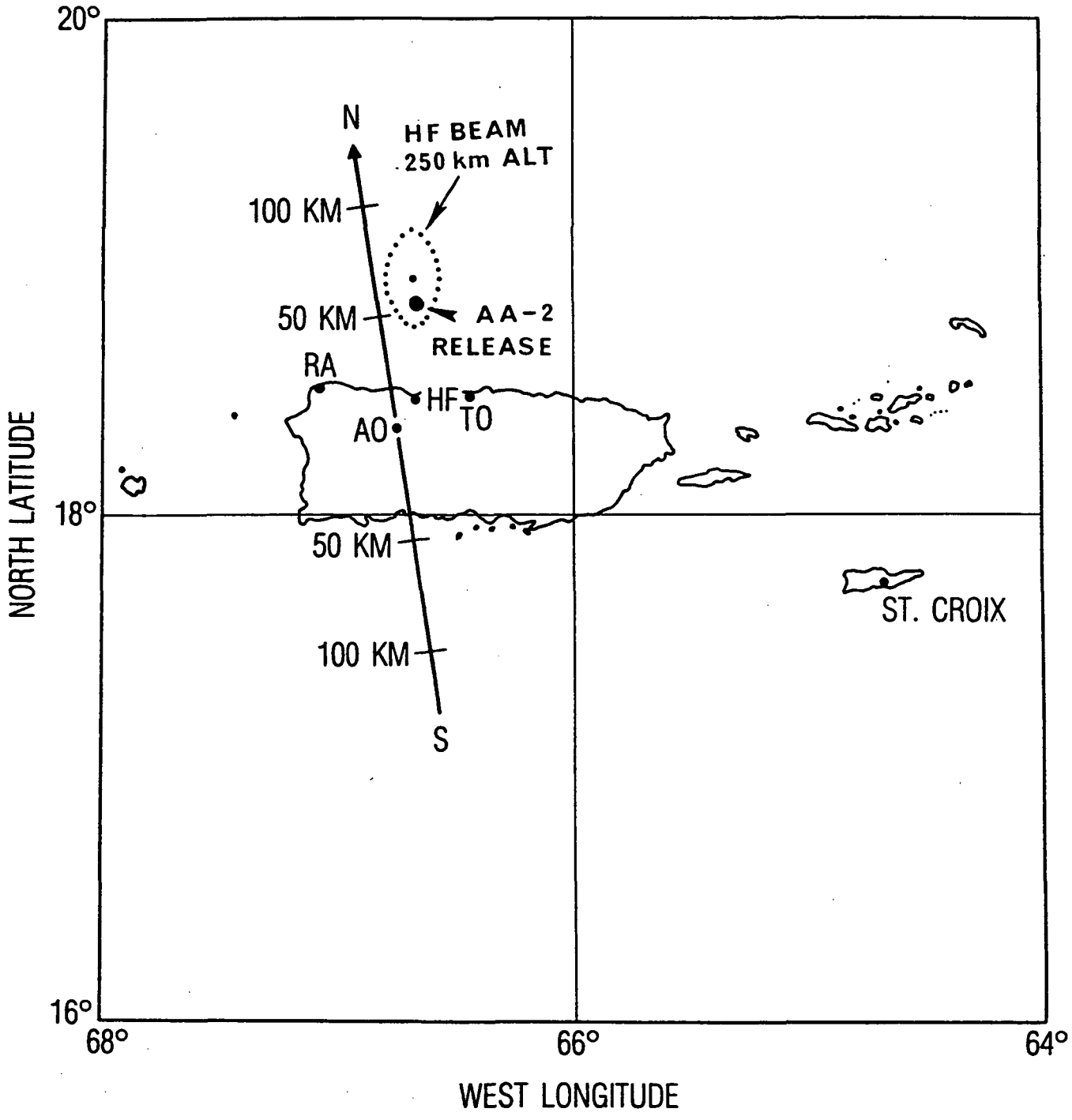
20°
18°
16°
68°
66°
64°
NORTH LATITUDE
WEST LONGITUDE
N
S
HF BEAM
250 km ALT
100 KM
50 KM
AA-2
RELEASE
RA
HF
TO
AO
50 KM
100 KM
ST. CROIX

Figure 1

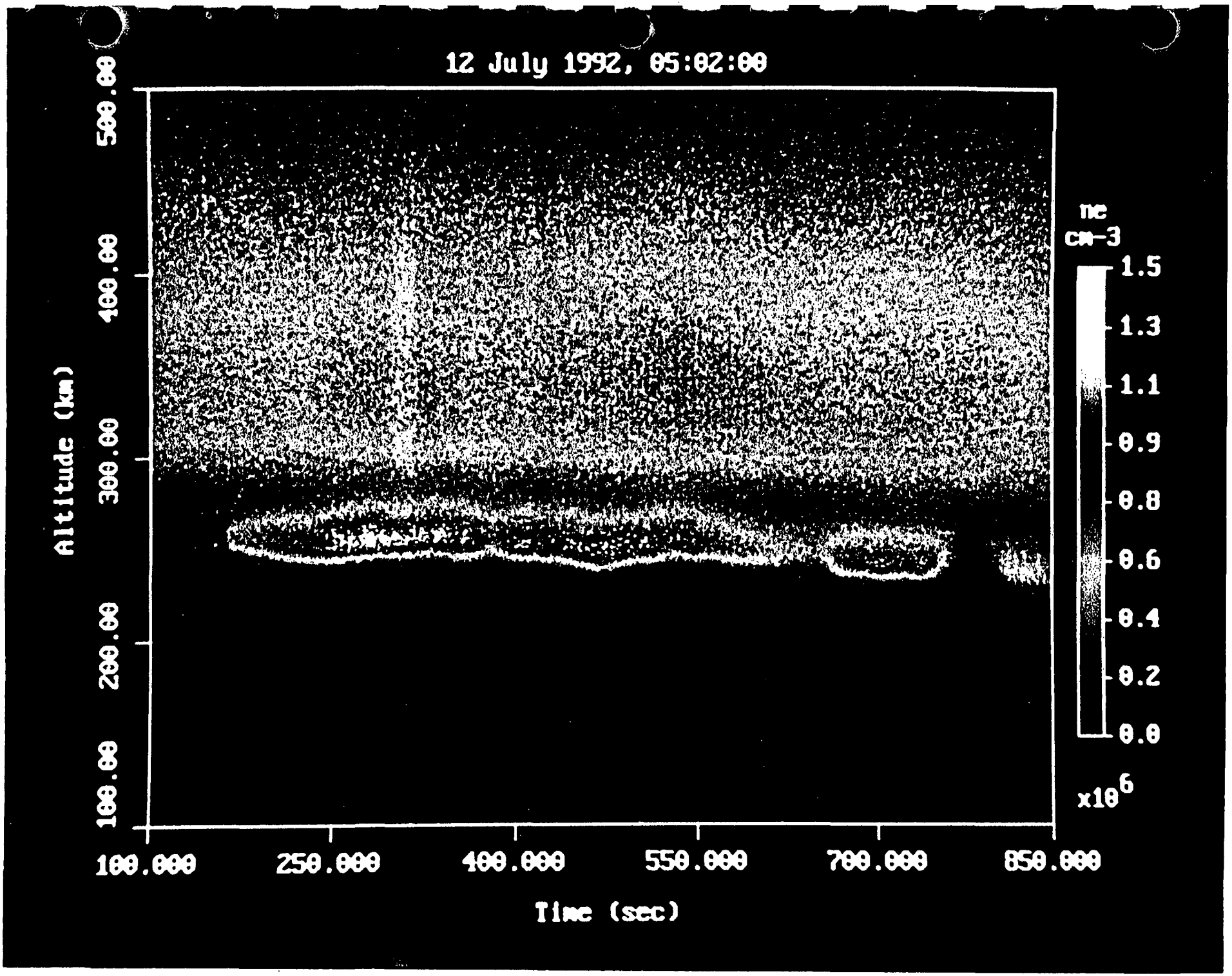
12 July 1992, 05:02:00
Altitude (km)
500.00
400.00
300.00
200.00
100.00
100.000
250.000
400.000
550.000
700.000
850.000
Time (sec)
ne
cm-3
1.5
1.3
1.1
0.9
0.8
0.6
0.4
0.2
0.0
x10^6

Figure 2

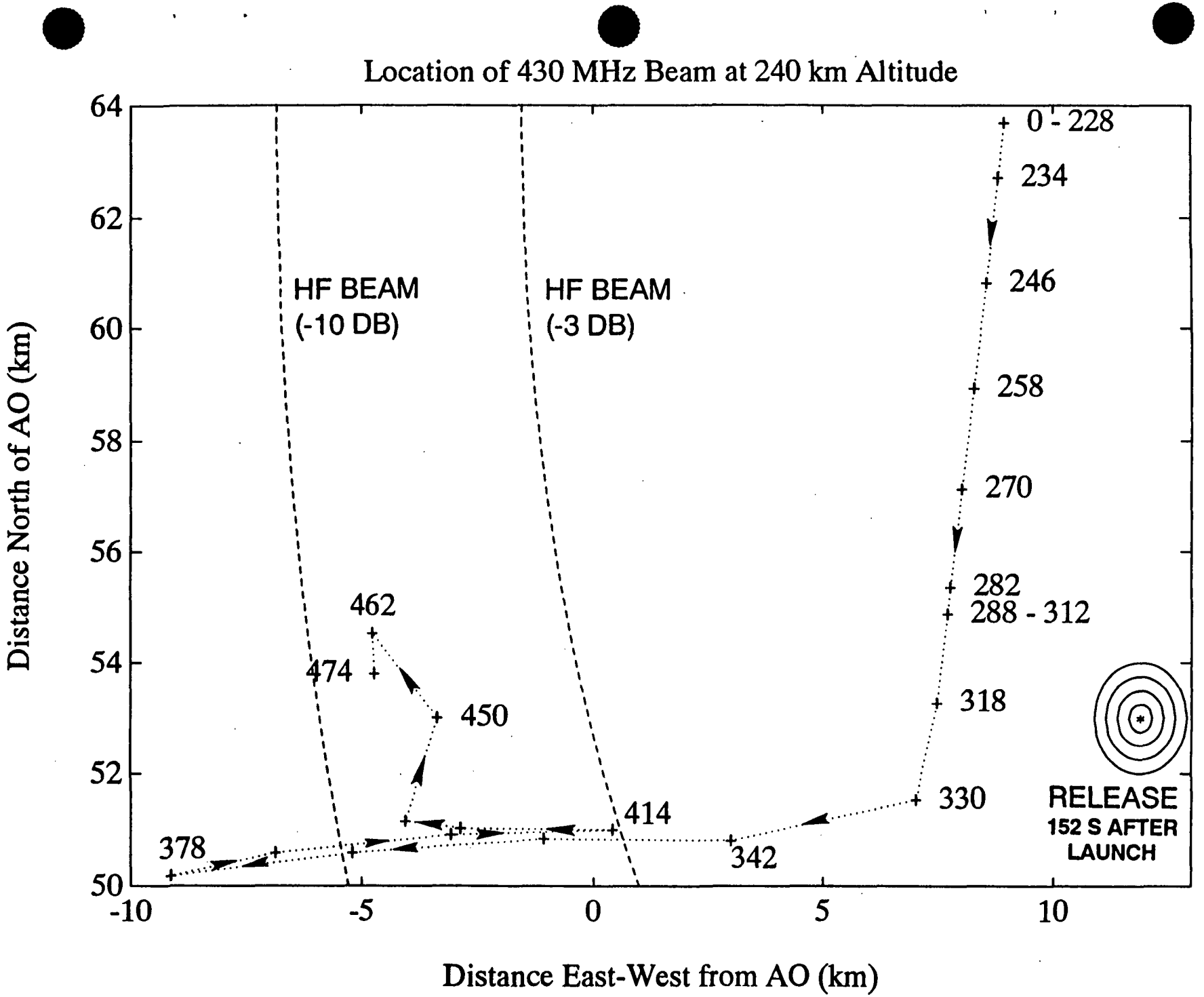
Location of 430 MHz Beam at 240 km Altitude
Distance North of AO (km)
Distance East-West from AO (km)
64
62
60
58
56
54
52
50
-10
-5
0
5
10
HF BEAM
(-10 DB)
HF BEAM
(-3 DB)
0 - 228
234
246
258
270
282
288 - 312
318
330
462
474
450
414
378
342
RELEASE
152 S AFTER
LAUNCH

Figure 3

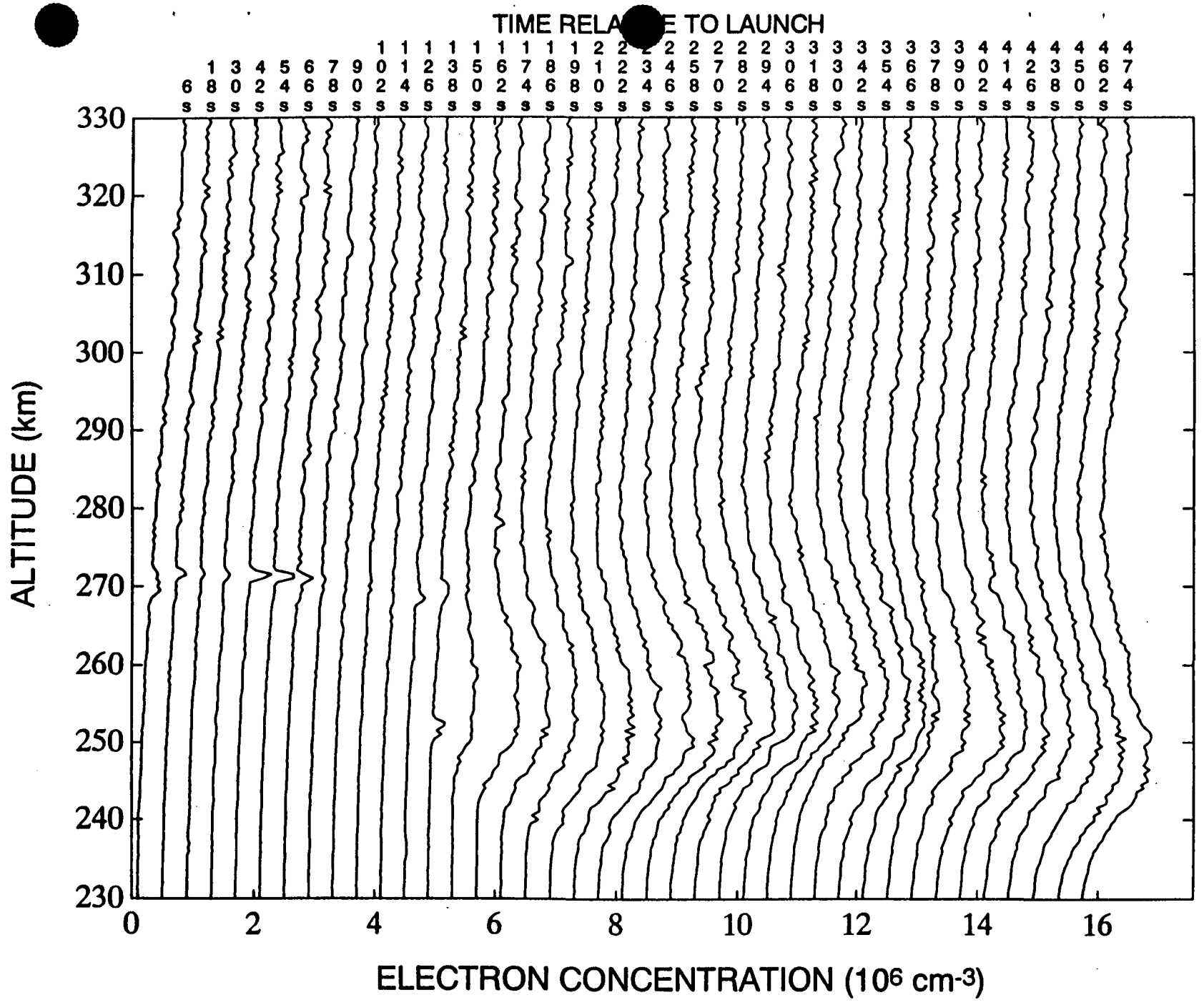
TIME RELATIVE TO LAUNCH
ALTITUDE (km)
330
320
310
300
290
280
270
260
250
240
230
0
2
4
6
8
10
12
14
16
ELECTRON CONCENTRATION (10⁶ cm⁻³)

Figure 4

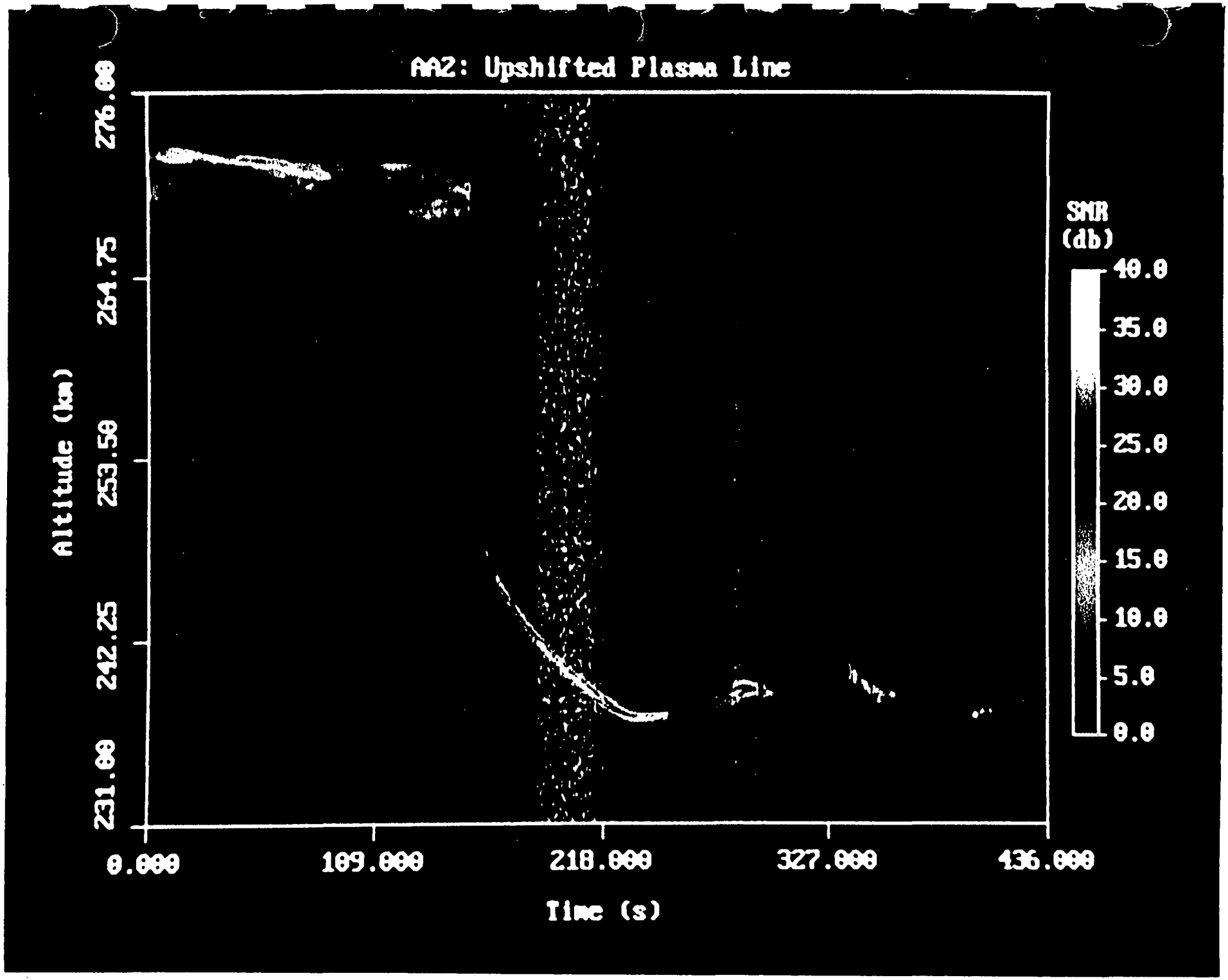
AA2: Upshifted Plasma Line
Altitude (km)
276.00
264.75
253.50
242.25
231.00
0.000
109.000
218.000
327.000
436.000
Time (s)
SNR
(db)
40.0
35.0
30.0
25.0
20.0
15.0
10.0
5.0
0.0

Figure 5

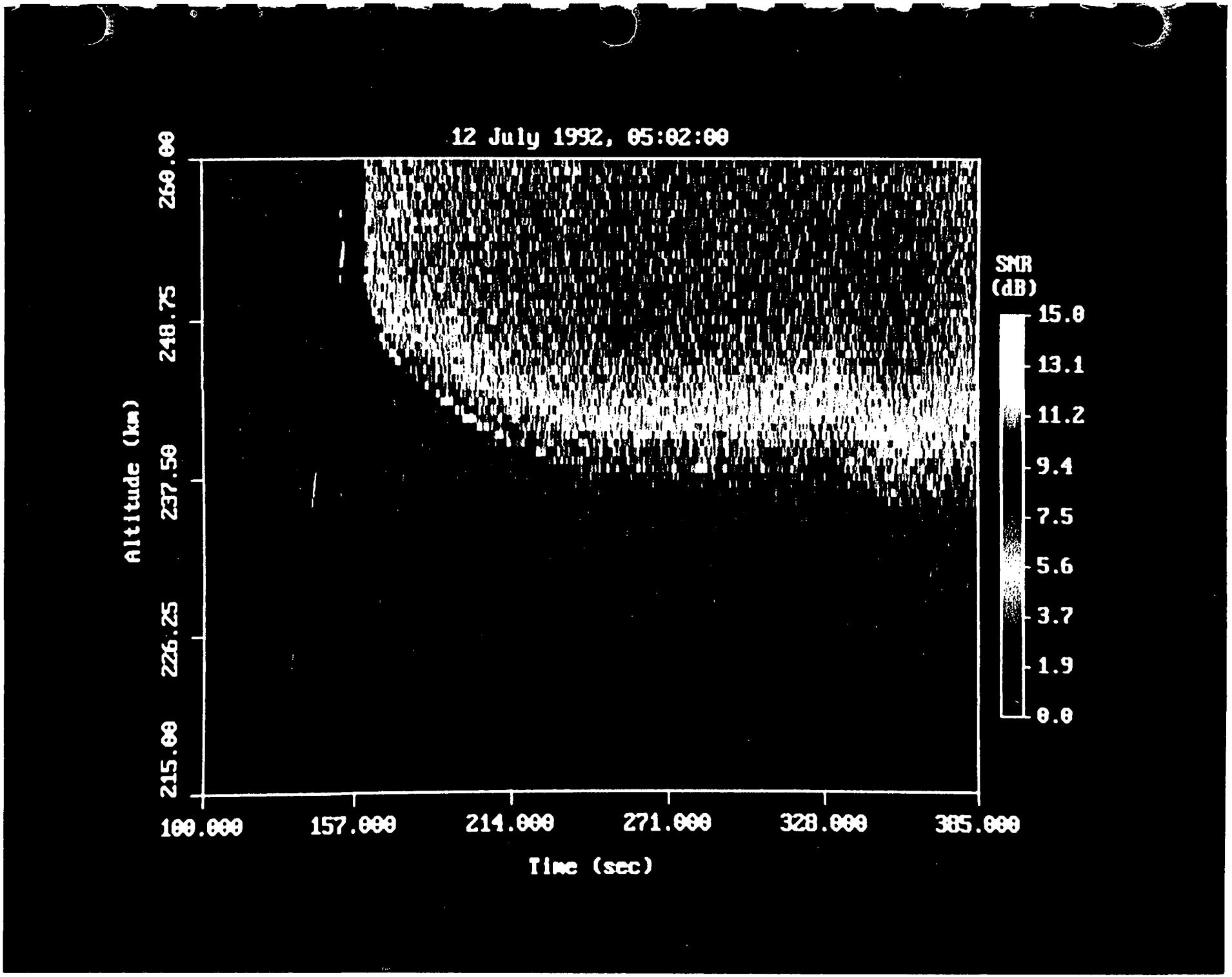
12 July 1992, 05:02:00
Altitude (km)
260.00
248.75
237.50
226.25
215.00
100.000
157.000
214.000
271.000
328.000
385.000
Time (sec)
SNR
(dB)
15.0
13.1
11.2
9.4
7.5
5.6
3.7
1.9
0.0

Figure 6

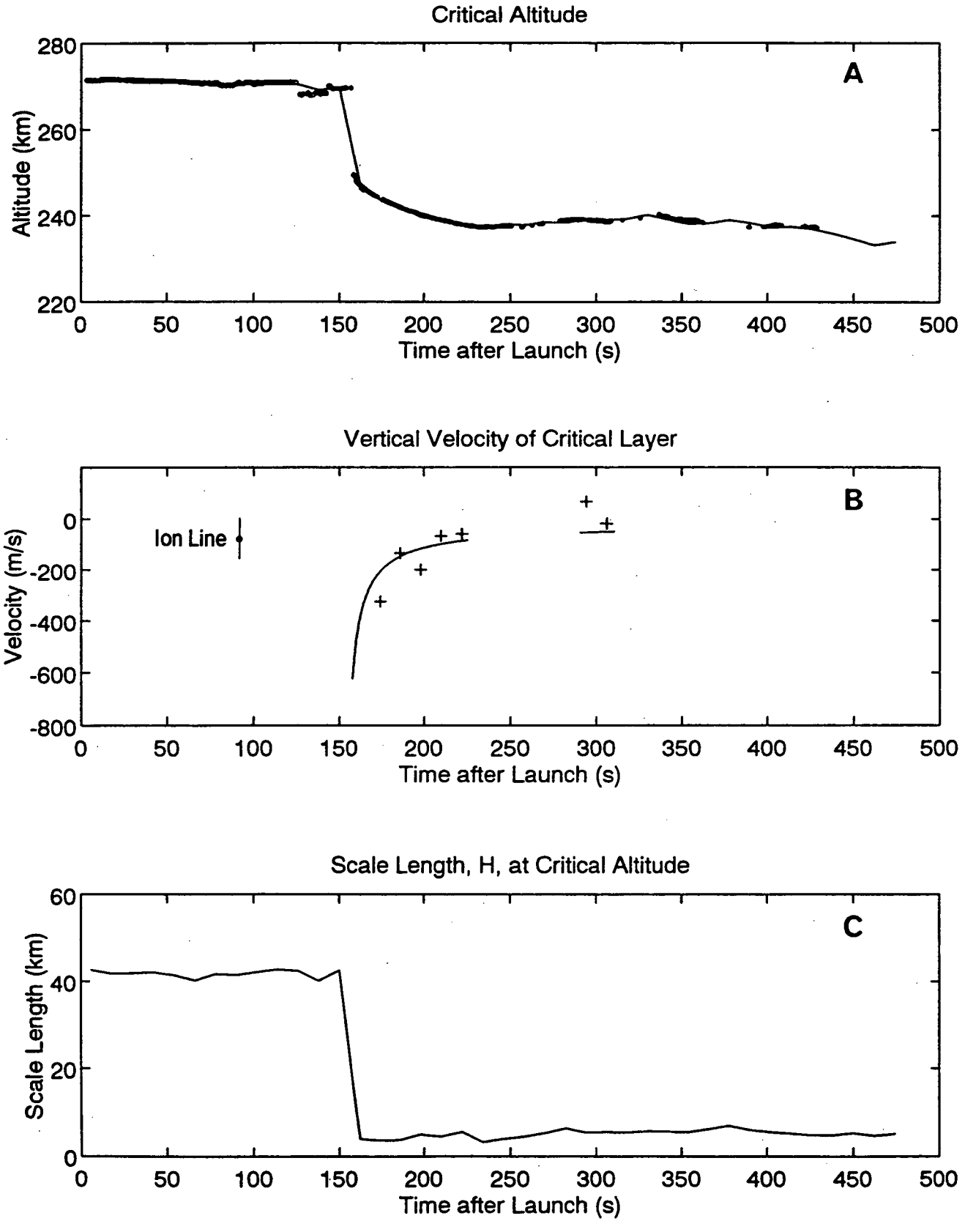
Critical Altitude
A
Altitude (km)
280
260
240
220
0
50
100
150
200
250
300
350
400
450
500
Time after Launch (s)
Vertical Velocity of Critical Layer
B
Ion Line
Velocity (m/s)
0
-200
-400
-600
-800
Time after Launch (s)
Scale Length, H, at Critical Altitude
C
Scale Length (km)
60
40
20
0
Time after Launch (s)

Figure 7

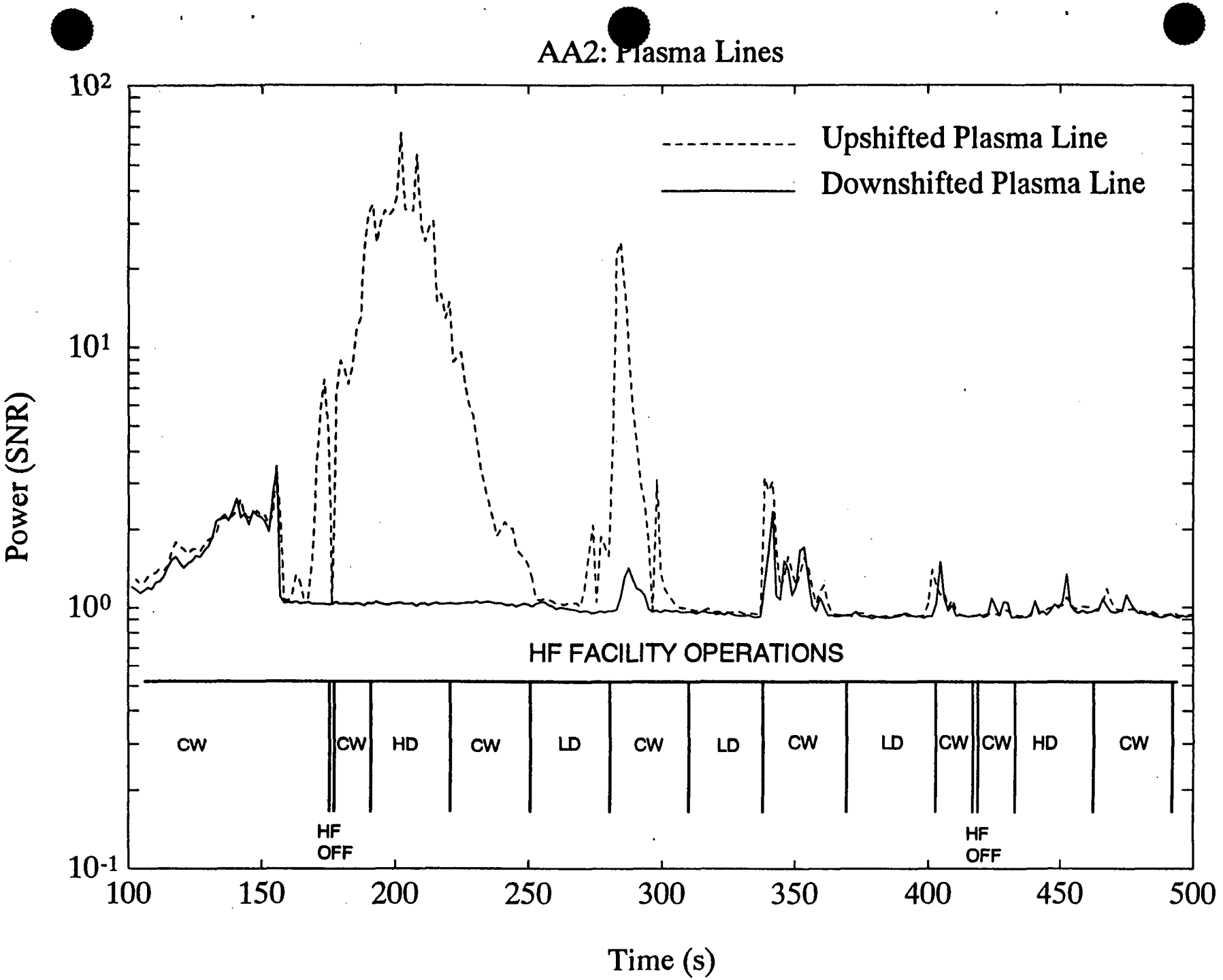
AA2: Plasma Lines
Upshifted Plasma Line
Downshifted Plasma Line
Power (SNR)
10^2
10^1
10^0
10^{-1}
HF FACILITY OPERATIONS
CW
CW
HD
CW
LD
CW
LD
CW
LD
CW
CW
HD
CW
HF OFF
HF OFF
100
150
200
250
300
350
400
450
500
Time (s)

Figure 8

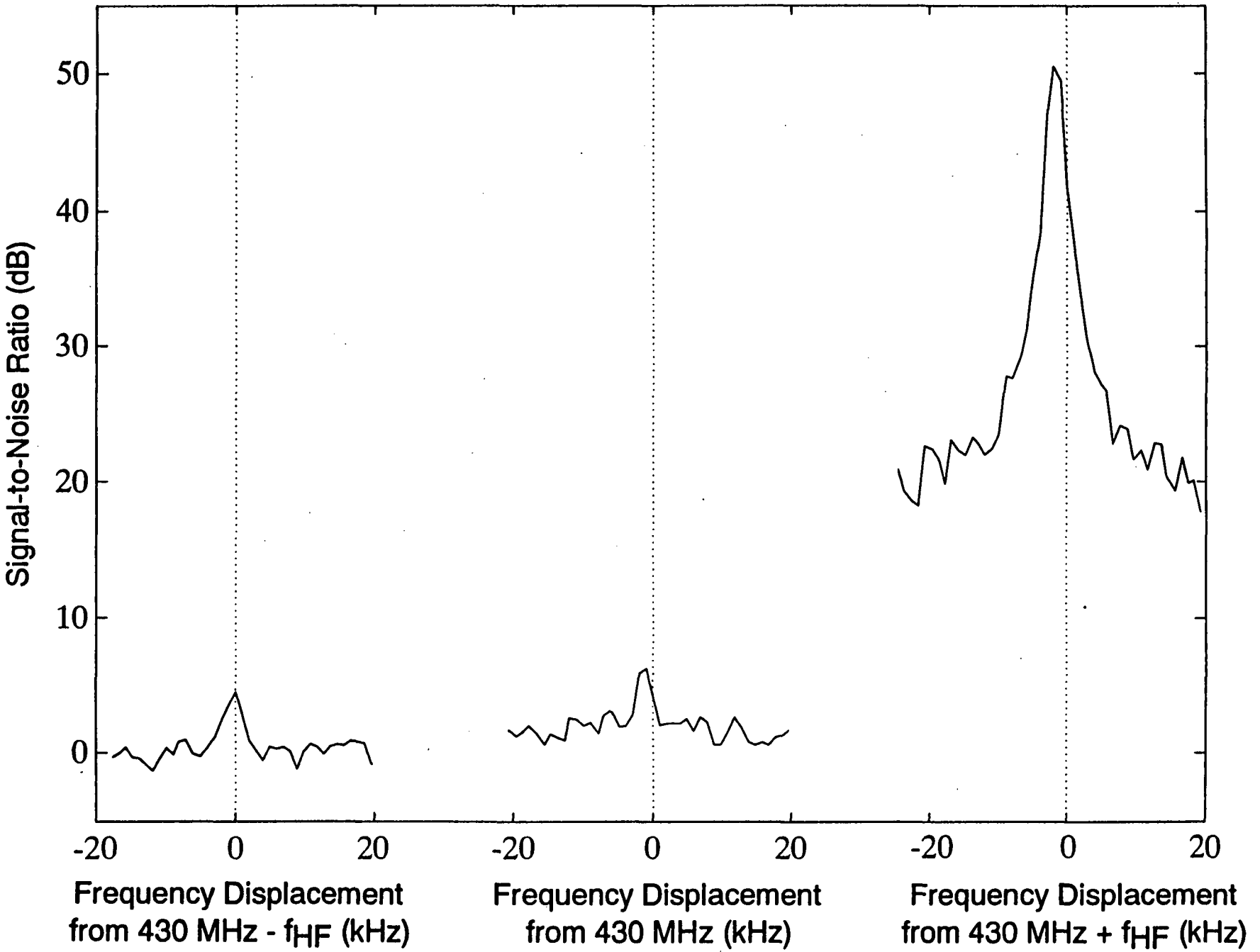
Signal-to-Noise Ratio (dB)
50
40
30
20
10
0
-20
0
20
Frequency Displacement
from 430 MHz - fHF (kHz)
Frequency Displacement
from 430 MHz (kHz)
Frequency Displacement
from 430 MHz + fHF (kHz)

Figure 9

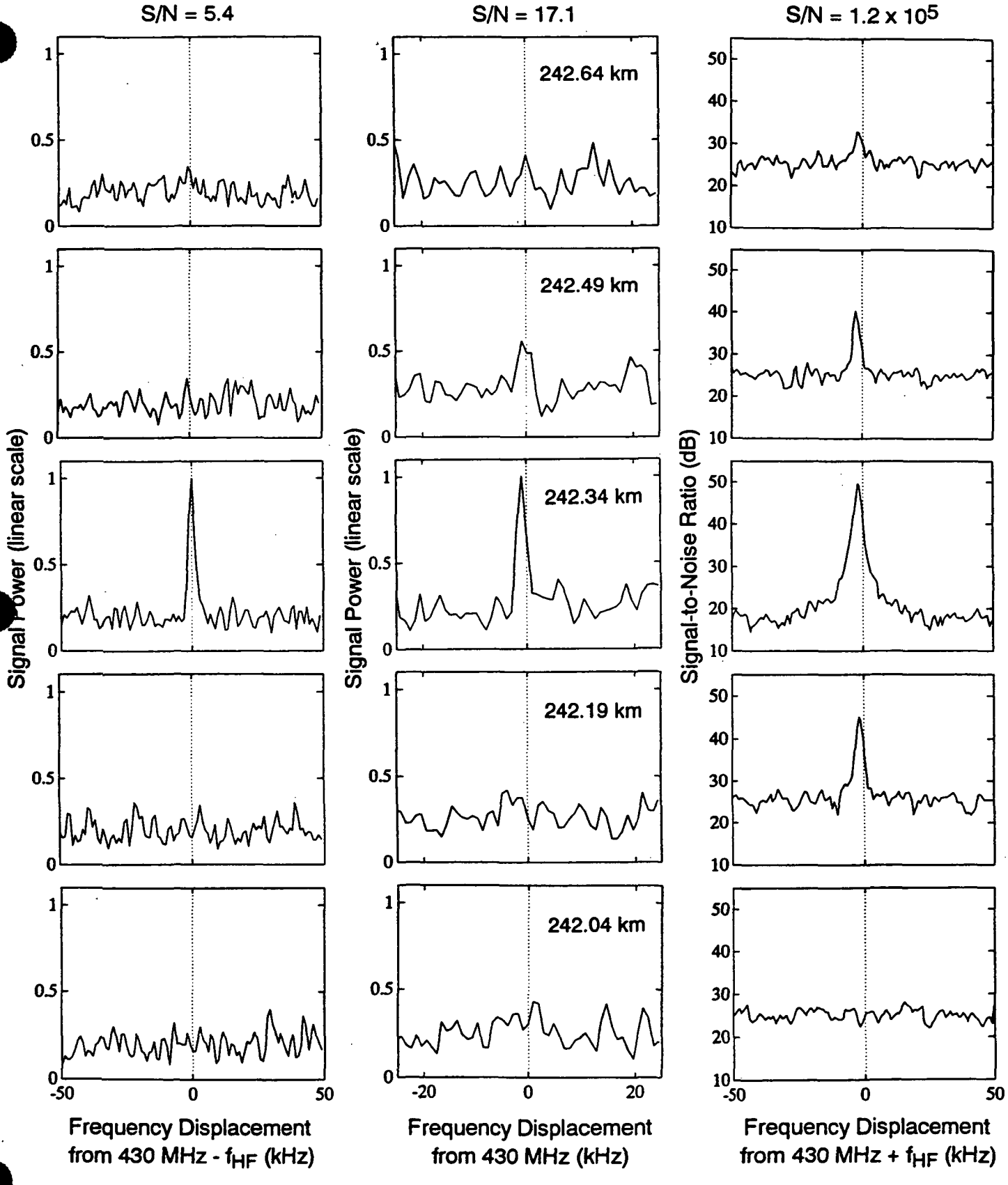
S/N = 5.4
S/N = 17.1
S/N = 1.2 x 10^5
242.64 km
242.49 km
242.34 km
242.19 km
242.04 km
Signal Power (linear scale)
Signal Power (linear scale)
Signal-to-Noise Ratio (dB)
Frequency Displacement from 430 MHz - f_HF (kHz)
Frequency Displacement from 430 MHz (kHz)
Frequency Displacement from 430 MHz + f_HF (kHz)

Figure 10

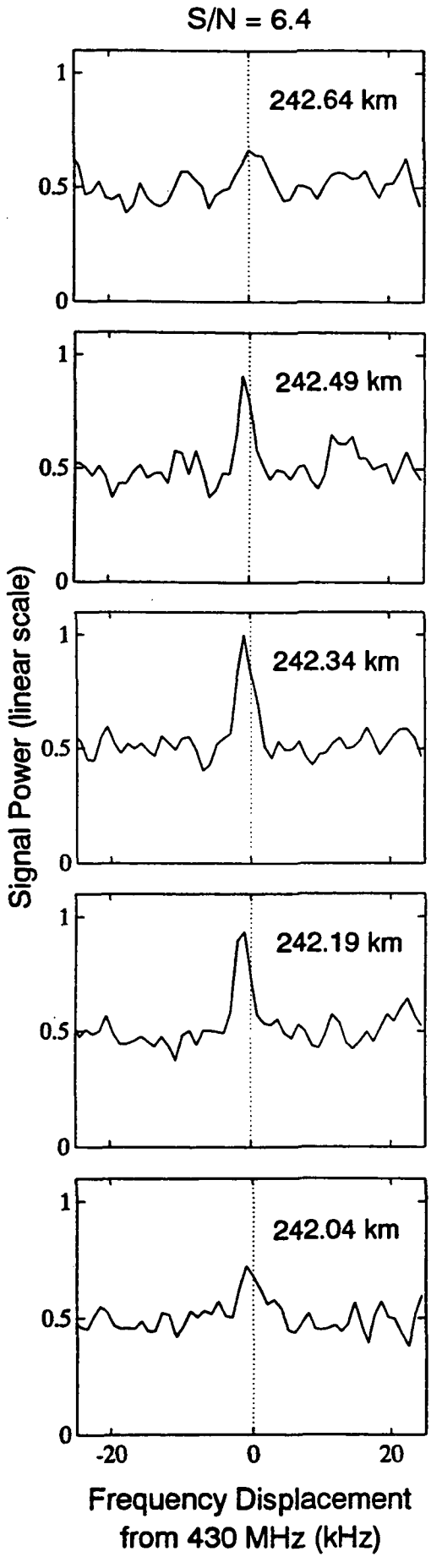
S/N = 6.4
242.64 km
242.49 km
242.34 km
242.19 km
242.04 km
Signal Power (linear scale)
Frequency Displacement
from 430 MHz (kHz)

Figure 11

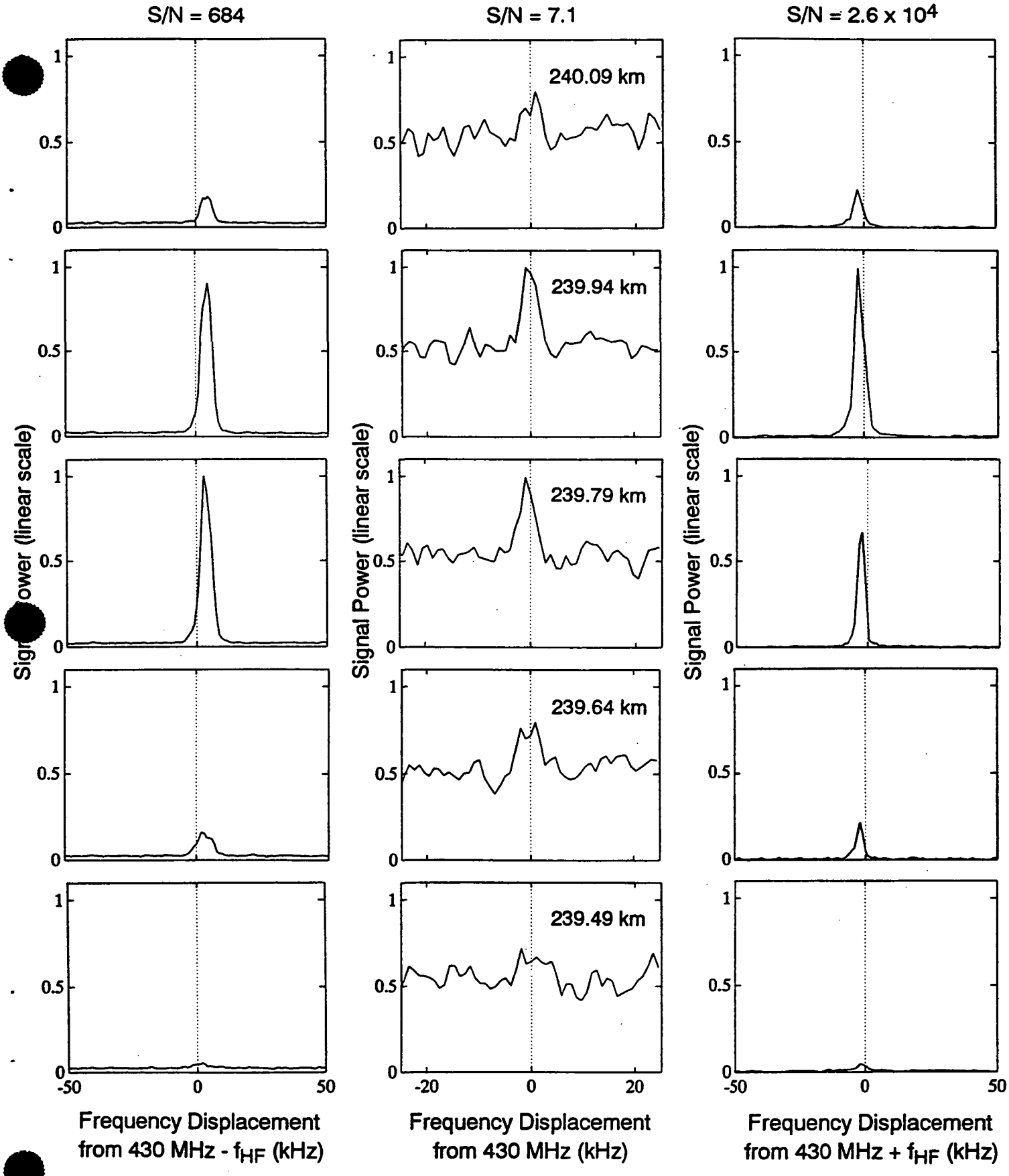
S/N = 684
S/N = 7.1
S/N = 2.6 x 10^4
240.09 km
239.94 km
239.79 km
239.64 km
239.49 km
Signal Power (linear scale)
Frequency Displacement from 430 MHz - f_HF (kHz)
Frequency Displacement from 430 MHz (kHz)
Frequency Displacement from 430 MHz + f_HF (kHz)

Figure 12

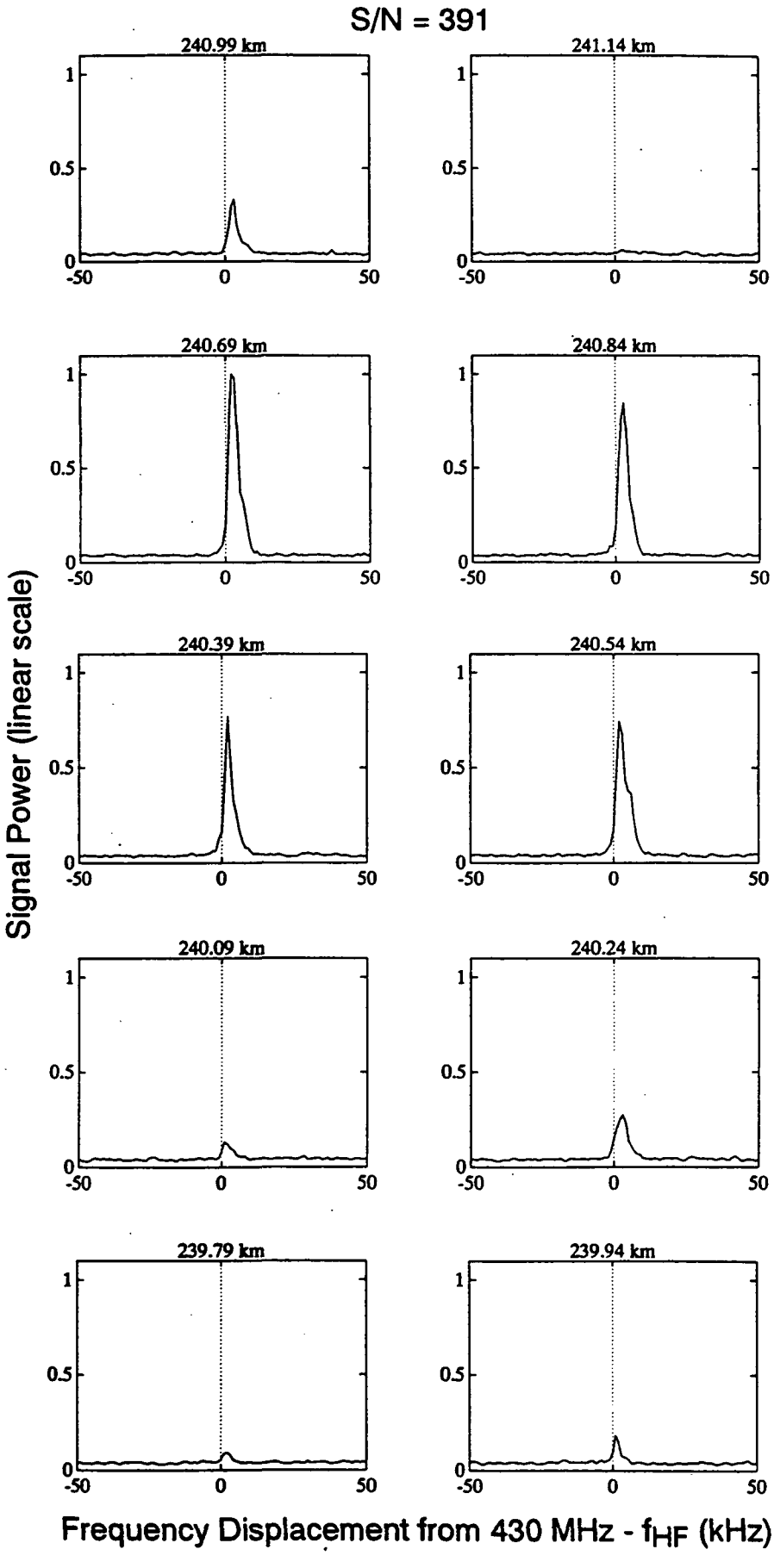
S/N = 391
240.99 km
241.14 km
240.69 km
240.84 km
240.39 km
240.54 km
240.09 km
240.24 km
239.79 km
239.94 km
Signal Power (linear scale)
Frequency Displacement from 430 MHz - f_{HF} (kHz)

Figure 13a

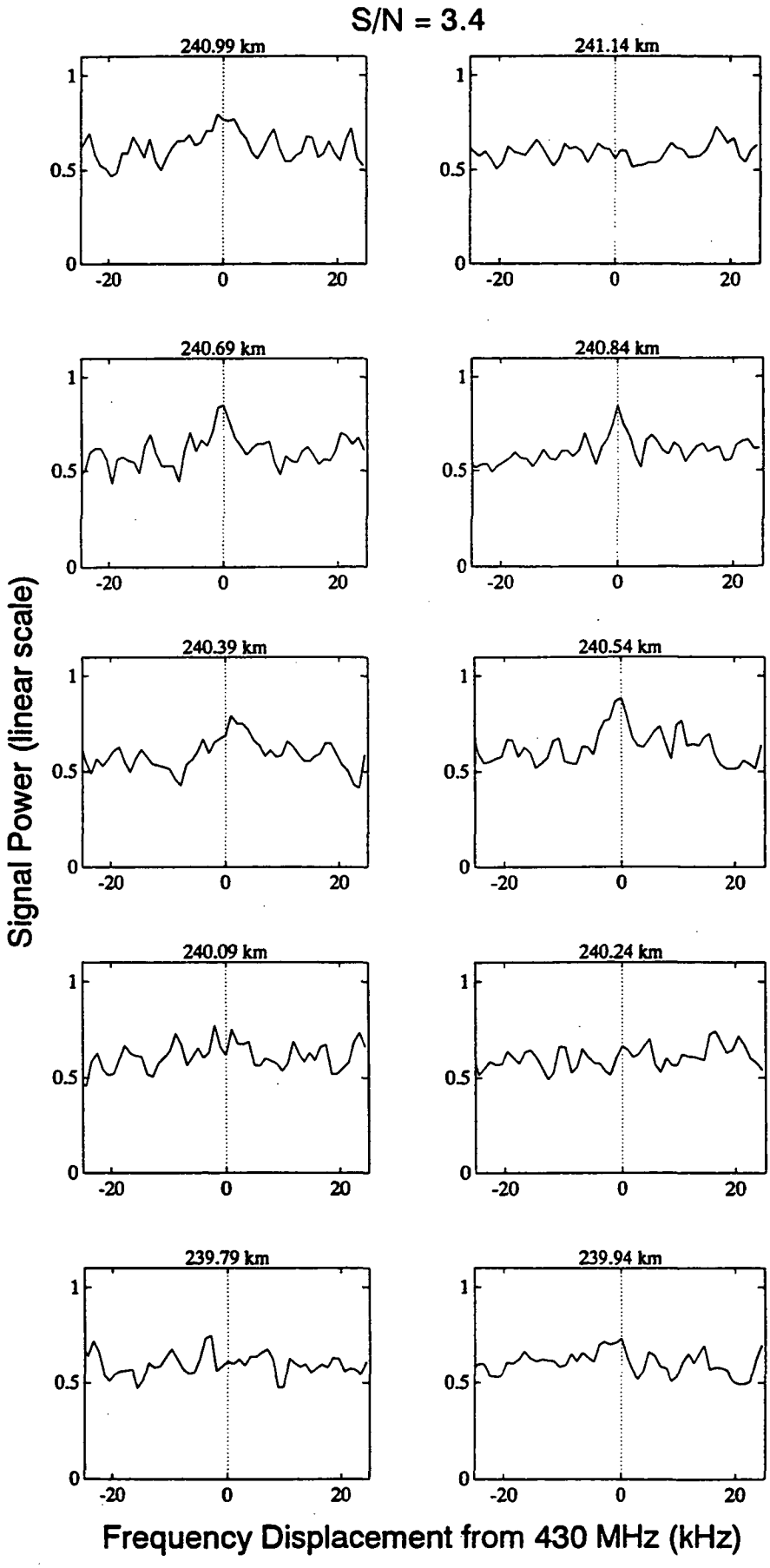
S/N = 3.4
240.99 km
241.14 km
240.69 km
240.84 km
240.39 km
240.54 km
240.09 km
240.24 km
239.79 km
239.94 km
Signal Power (linear scale)
Frequency Displacement from 430 MHz (kHz)

Figure 13b

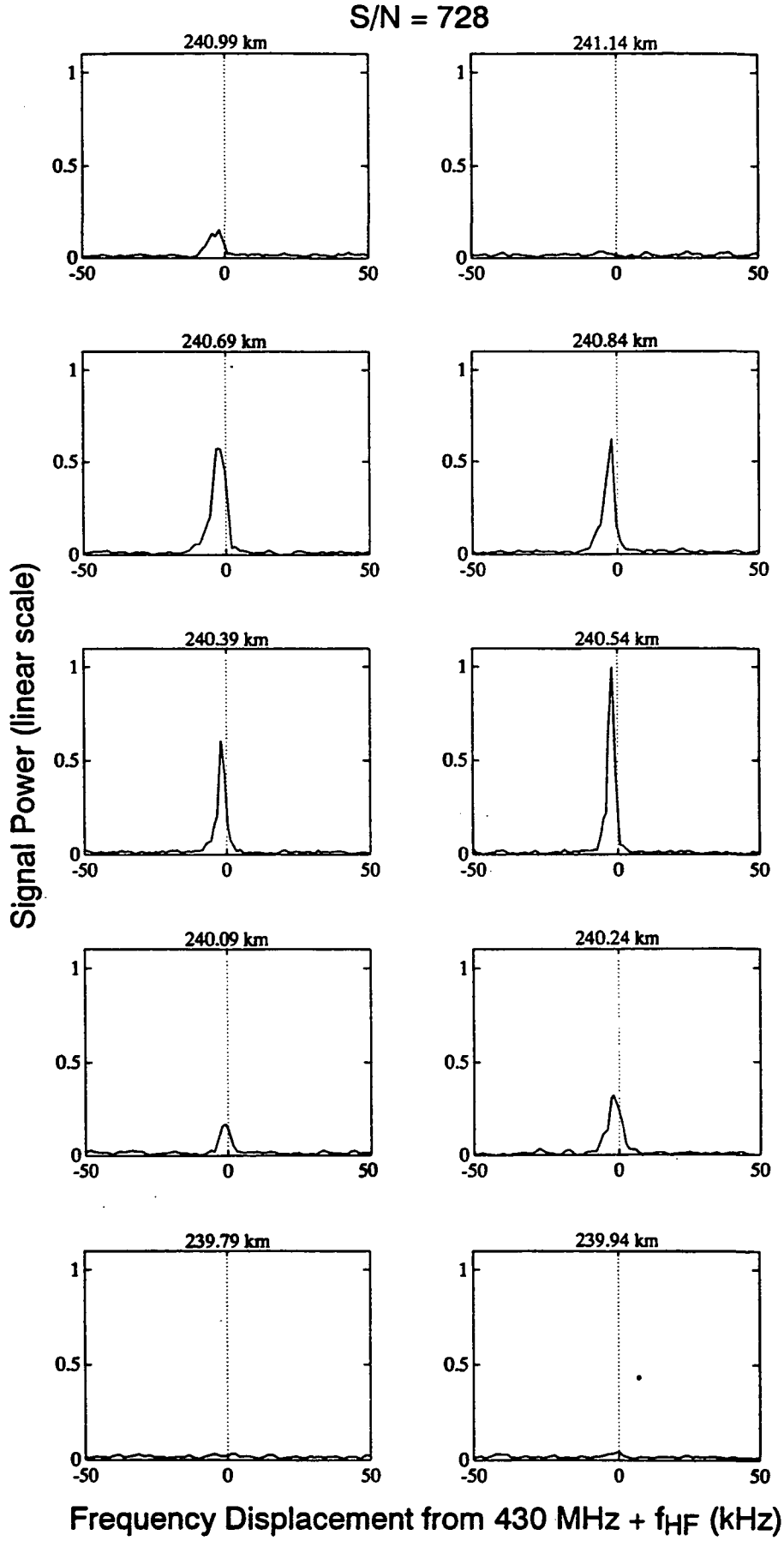
S/N = 728
240.99 km
241.14 km
240.69 km
240.84 km
240.39 km
240.54 km
240.09 km
240.24 km
239.79 km
239.94 km
Signal Power (linear scale)
Frequency Displacement from 430 MHz + f_{HF} (kHz)

Figure 13c

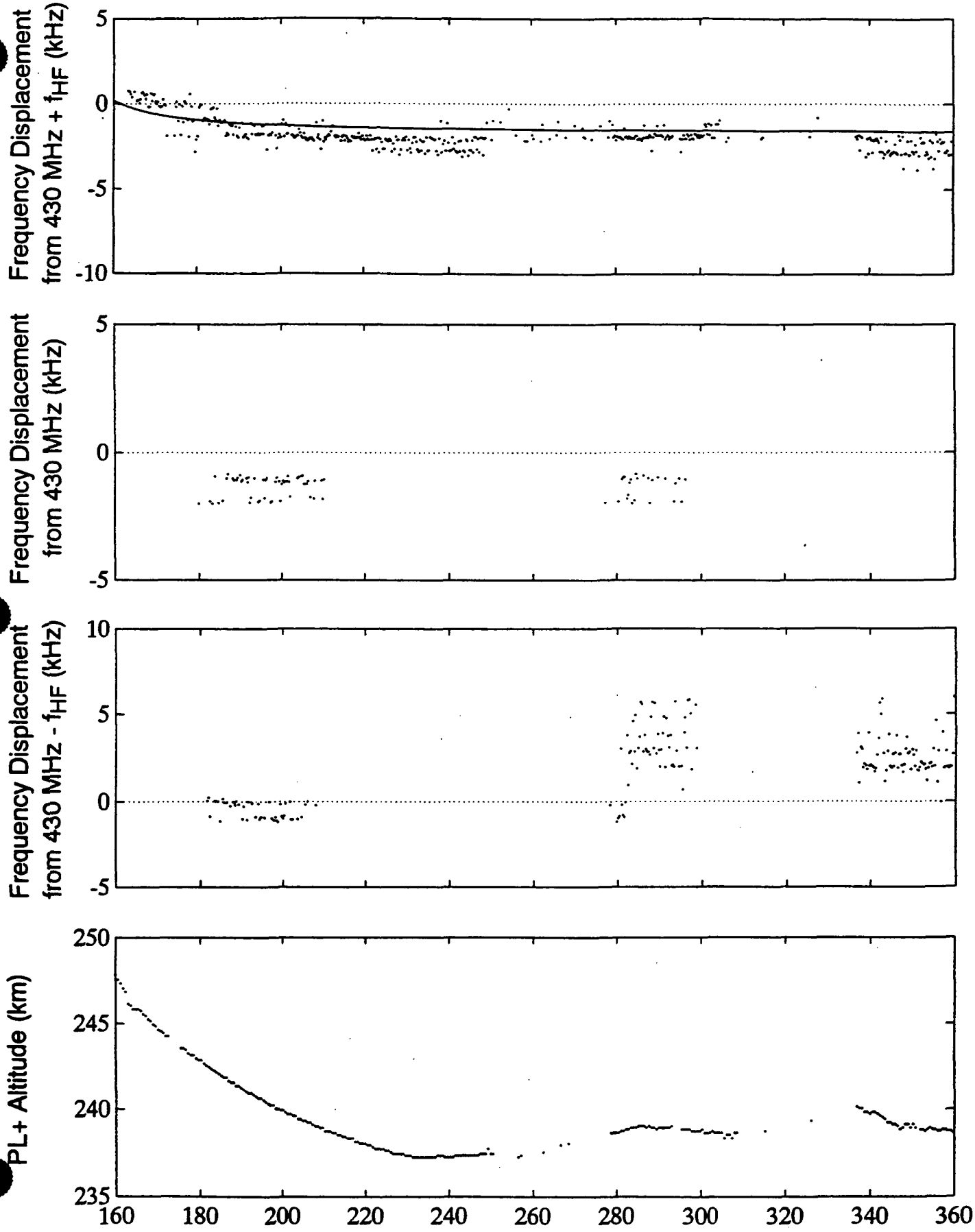
Frequency Displacement from 430 MHz + f_{HF} (kHz)
5
0
-5
-10
Frequency Displacement from 430 MHz (kHz)
5
0
-5
Frequency Displacement from 430 MHz - f_{HF} (kHz)
10
5
0
-5
PL+ Altitude (km)
250
245
240
235
160
180
200
220
240
260
280
300
320
340
360
Time (s)

Figure 14

3. AA-4: The Ionospheric Focussed Heating (IFH) Experiment

The AA-4 experiment involved a collaborative effort between F. T. Djuth of Geospace Research, Inc. (GRI) and P. A. Bernhardt (and others) of the Naval Research Laboratory (NRL). GRI's principal contributions involved the acquisition of the Arecibo incoherent scatter radar data, detailed analyses of the experimental results, and an interpretive study conducted in collaboration with investigators from NRL. This resulted in the scientific publication presented below, which is currently in press in the *Journal of Geophysical Research.*

The Ionospheric Focussed Heating (IFH) Experiment

P. A. Bernhardt, C. L. Siefring, P. Rodriguez, D. G. Haas, M. M. Baumback,
H. A. Romero, D. A. Sollin
Plasma Physics Division, Naval Research Laboratory, Washington, DC 20375

F. T. Djuth
Geospace Research, Inc. El Segundo, CA 90245

L. M. Duncan
University of Tulsa, Tulsa, OK 74104

D. E. Hunton
Phillips Laboratory, GPID, Hanscom Air Force Base, MA 01731

C. J. Pollock
NASA/Marshall Space Flight Center Code ES53, Huntsville, AL 35812

M. P. Sulzer and C. A. Tepley
Arecibo Observatory, Arecibo, PR 00613

L. S. Wagner and J. A. Goldstein
Information Technology Division, Naval Research Laboratory, Washington, DC 20375

ABSTRACT

The Ionospheric Focussed Heating (IFH) rocket was launched on 30 May 1992. The sounding rocket carried an instrument and chemical payload along a trajectory that crossed the intersection of the beams from the 430 MHz incoherent scatter radar and the 5.1 MHz high-power radio-wave facility near Arecibo. The release of 30 kg of CF_3Br into the F-region at 285 km altitude produced an ionospheric hole that acted like a convergent lens to focus the HF transmissions. The power density inside the radio beam was raised by 12 dB immediately after the release. A wide range of new processes were recorded by in situ and ground based instruments. Measurements by instruments flying through the modified ionosphere show

small-scale micro-cavities (< 1 meter) and downshifted electron-plasma (Langmuir) waves inside the artificial cavity, electron density spikes at the edge of the cavity, and Langmuir waves coincident with ion-gyro-radius (4 meter) cavities near the radio wave reflection altitude. The Arecibo incoherent scatter radar showed 20 dB or greater enhancements ion acoustic and Langmuir wave turbulence after the 5.1 MHz radio beam was focussed by the artificial lens. Enhancements in airglow from chemical reactions and, possibly, electron acceleration were recorded with optical instruments. The Ionospheric Focussed Heating experiment verified some of the preflight predictions and demonstrated the value of active experiments that combine high power radio waves with chemical releases.

I. Introduction

The Ionospheric Focussed Heating (IFH) experiment was designed to demonstrate the use of chemical releases to enhance the effective radiated power of high-power HF facilities and to measure in situ the turbulence in the heated and chemically modified plasma. The rocket payload for the IFH experiment consisted of a chemical canister and a set of diagnostic instruments. The IFH payload was launched on 30 May 1992 during the Combined Release and Radiation Effects Satellite (CRRES) program. All of the CRRES Caribbean rockets took off from the north coast of Puerto Rico. The CRRES rocket campaign, called "El Coqui" was organized to take advantage of the ionospheric heating facility, incoherent scatter radar, and other ground support diagnostics located near the Arecibo Observatory in Puerto Rico [Djuth, 1993; Kelley et al., 1994; Djuth et al., 1994].

The term "Ionospheric Heating" refers to ionospheric modification by high power radio waves. The transmitted high frequency (HF)

electromagnetic wave is called the pump. The effective radiated power (ERP) of the pump is calculated as the product of the transmitter power and the antenna gain for the facility. The ERP of the Arecibo HF facility was about 50 MW at the 5.1 MHz frequency used during the El Coqui campaign. The ERP was about 10 MW lower than usual because of reduced transmitter antenna gain resulting from tilting the normally vertical beam. The HF beam was tilted 12 degrees to the north to allow penetration by the rockets without endangering populated areas.

The Arecibo incoherent scatter radar (ISR) is a primary diagnostic for the heated plasma. The transmitted wave (f_T = 430 MHz) from the radar is scattered from plasma waves (f_p) yielding scattered electromagnetic waves (f_s) that are received with the 305 meter dish antenna located at Arecibo. The scattering conditions require that the scattering wavelength is equal to one-half the transmitted wavelength ($\lambda = c/f_T = 0.698$ m) of the radar.

When the powerful HF transmitter is turned on, enhanced ion lines may be produced by scatter from HF induced ion acoustic waves [Showen and Kim, 1978]. All ion line spectra reside within a 20 kHz band centered on the radar frequency. Plasma line spectra are produced by electron plasma waves scattering the radar signal. The frequencies of these lines fall near $f_T \pm f_{HF}$ where f_{HF} is the pump frequency.

The electromagnetic pump may be scattered by plasma waves to yield stimulated electromagnetic emissions (SEE) [Thide et al., 1989]. SEE is often characterized by a downshifted maximum (DM) located about 15 kHz below the pump frequency. During the IFH experiment, SEE observations were conducted with a radio frequency spectrum analyzer connected to a broad band receiving antenna.

The process for conversion of high power radio waves into plasma waves has been explained in terms of parametric instabilities [Fejer, 1979] or Langmuir turbulence [Dubois et al. [1990]. The pump electromagnetic wave can decay into two plasma waves, an electron plasma wave and an ion acoustic wave propagating in opposite directions. The frequency of the electron plasma waves is offset from the pump frequency by the frequency of the ion acoustic wave.

High power radio waves simultaneously produce large scale (>10 km) cavities, ion gyro radius structures (~ 10 m), medium scale irregularities (~ 1 km), and small scale Langmuir turbulence (~ 1 m). Often, these irregularities are located in the same region of heated plasma. At Arecibo, during special conditions found at winter and solar minimum, large scale cavities produced by thermal expansion of the plasma have been observed near the reflection point of the HF beam [Duncan et al., 1988; Hansen et al., 1990]. Inside these cavities the ISR often detects enhanced ion lines from ion acoustic waves [Duncan et al., 1988; Bernhardt et al., 1989].

The effects of electron acceleration are seen as airglow clouds attached by magnetic field lines to the HF wave reflection region [Bernhardt et al., 1988, 1989, 1991b]. Suprathermal electrons produced by electron plasma waves acting on the thermal population in the F-layer stream down magnetic field lines to collide with and excite atomic oxygen in the neutral atmosphere. Fluxes of energetic electrons can excite the red-line (630.0 nm) and green-line (557.7 nm) emissions from atomic oxygen in the upper atmosphere. The electron energies required to excite measurable intensities for the two lines are 3.5 and 6.0 eV, respectively. The intensities of 630.0 and 557.7 emissions have been analyzed to yield

estimates of the suprathermal electron energy spectra [Bernhardt et al., 1989].

All of the phenomena mention above (i.e., enhanced ion-lines, SEE, parametric instabilities, electron acceleration, enhanced airglow) occur if the power density from the HF pump wave exceeds a threshold. One way of exceeding existing thresholds is to focus the beam with an artificial ionospheric lens. The purpose of the IFH experiment was to (1) use a chemical release to form an artificial lens that focuses the radio beam of the Arecibo HF facility and (2) measure the effects of the resulting increase in ERP on the ionospheric heating processes. This paper presents an overview of the observations that were affected by the focussing. The next section describes the rocket payload that formed the artificial lens and measured the effects of the chemical release in situ. Section III outlines the observations made by the Langmuir probe, plasma wave receiver and electric field instruments on the rocket. The data from the Arecibo incoherent scatter radar are described in Section IV. Airglow enhancements following the chemical release are discussed in Section V. Conclusions regarding the IFH experiment are given in Section VI.

II. Experiment Concept - Chemically Produced Cavity

At Arecibo, large-scale cavities and enhanced ion-acoustic waves have been found to be coincident with electron acceleration that produces airglow [Bernhardt et al, 1989]. Self action of the HF wave generates the large-scale density structures that "self-focus" the HF wave [Hansen et al., 1990; Hansen, Morales, and Maggs, 1992]. The processes that couple the HF-induced cavities to enhanced ion-acoustic waves are not understood so an experiment was devised to control the cavity formation and then see

the response of the enhanced ion lines and the optical emissions. The active experiment used a chemical to form a large electron scale cavity in the HF beam. The effects of the artificial cavity on the heated ionosphere were recorded with in situ and ground based instruments. This experiment was called "Ionospheric Focussed Heating" (IFH) because it was thought that the chemically produced cavity would focus the HF yielding substantially larger field strengths for the HF waves [Bernhardt and Duncan, 1987].

The ionospheric hole produced by the release of CF_3Br removed electrons by dissociative attachment. The effectiveness of this chemical was demonstrated in the F-region during the NASA-sponsored NICARE 1 experiment [Bernhardt et al., 1991]. The dissociative attachment reaction is

$$CF_3Br + e^- \rightarrow Br^- + CF_3 \quad \text{rate coefficient: } k_1 \sim 10^{-7} \text{ cm}^3/\text{s}. \quad (1)$$

With a 30 kg release of this material, the electron population was depleted within 10 km of the release point [Bernhardt et al., 1991]. The negative and positive ions are mutually neutralized by the reaction

$$Br^- + O^+ \rightarrow Br^* + O^* \quad \text{rate coefficient: } k_2 \sim 10^{-8} \text{ cm}^3/\text{s}. \quad (2)$$

Care must be taken to distinguish between airglow from O^* excited by surprathermal electron fluxes and by chemical reactions in the negative ion plasma.

The plasma waves measured in situ during the IFH experiment were expected to be strongly influenced by the presence of the negative ions. During the NICARE 1 and 2 experiments, new wave modes were excited inside

the negative ion cloud even without the presence of a high power radio wave [Ganguli et al., 1993]. Enhanced electric field fluctuations come from lower hybrid waves, ion plasma waves, and ion cyclotron waves excited by the presence of Br^- and O^+ in the chemically modified plasma [Scales et al., 1993]. With the IFH experiment, the addition of an electromagnetic pump field added to the complexity of the plasma wave structures in the negative ion cloud.

The magnitude of the focussing by the chemically produced cavity was estimated to be 20 dB in the theoretical paper by Bernhardt and Duncan [1987]. The heating at the focus yielded channeling of the HF beam.

The IFH experiment was designated as the CRRES AA-4 rocket in March of 1988. In situ instruments were delivered by Naval Research Laboratory, Phillips Lab, and Marshall Space Flight Center for integration into the payload in 1990. The launch of AA-4 occurred on 30 May 1992 at 0411 Atlantic Standard Time (0811 Universal Time) from the launcher located near Vega Baja in Puerto Rico. The chemical payload consisted of 30 kg of CF_3Br inside a pressurized tank heated to 340 K. The release occurred at 08:13:49.3 UT within 5 km of the center of the Arecibo HF beam. The radar track of the IFH rocket trajectory established the release location was 18.97 ^oN latitude, 66.60 ^oW longitude, and 283 km altitude. Using real time trajectory information, the chemical tank valve was opened with a command signal so that the release was deposited 20 km below the reflection altitude of the 5.1 MHz HF transmissions. The gas expansion and inertial motion caused the electron depletion to pass through the reflection altitude.

Figure 1 illustrates the locations of the flight trajectory, heater beam, and ISR scan projected onto the ground plane containing the island of

Puerto Rico. The CF_3Br release occurred slightly to the east of the HF beam center. Data at 630.0 nm from the Arecibo Fabry-Perot interferometer were analyzed to yield a thermospheric wind velocity of 40 m/s westward. The ionospheric hole created by the release drifted with this velocity into the center of the heater beam. By using post launch extrapolations for the rocket trajectory and commanded release, the ISR beam was positioned at the release point. After the ionospheric hole was well developed, the ISR was scanned in azimuth to keep track of the westward convection of the ionospheric hole.

The IFH rocket was fully instrumented to measure the plasma densities, electric fields, plasma waves, and suprathermal electrons expected to be detected in the modified plasma (Table I). The placement of the sensors is shown in Figure 2. All of the booms were located 1 meter or more ahead of the two chemical release valves. Upon release the instruments were surrounded by the CF_3Br cloud. The cloud initially expanded with a mean thermal speed $(2kT/m)^{1/2}$ = 200 m/s keeping the rocket payload as its center of mass. After electron attachment, the negative ions became tied by gyro orbits to the magnetic field lines and the rocket passed through the top edge of the electron depletion.

Both electron and ion densities were measured using probes on the IFH rocket. The Naval Research Laboratory provided a double Langmuir probe that was biased at a fixed voltage (+6 V) to collect electrons. The separation between the two probes was 1.26 meters. Two disk probes biased to collect positive ions were mounted on the payload skin just aft of the E-Field Booms. The disk probes, one small (1.5") and one large (3"), were provided by the Phillips Laboratory.

Multiple electric field and plasma wave receivers were provided by

the Naval Research Laboratory covering the 0 to 12 MHz frequency range. The electric fields were detected with booms deployed from the payload after launch. The spacings between sensors on the booms varied from 0.3 to 3.4 meters. Plasma waves near the HF pump frequency of 5.1 MHz were detected with two radio frequency sensors with spacings of 5.5 and 11 cm. The radio frequencies are downconverted to a 150 kHz band and digitized with 12-bit words. Details of the downconverter are given by Haas et al. [1993].

The energy spectrum of suprathermal electrons between 0.5 and 50 eV was to be detected with the Thermal Electron Capped Hemispherical Spectrometer (TECHS) instrument provided by Marshall Space Flight Center. The TECHS was mounted on the opposite side of the EF-5 and EF-6 booms. Unfortunately, after launch the voltage sweep was lost on the instrument and the energies of the detected electrons have not been determined.

III. In Situ Measurements

The data from the flight instruments can be divided into 5 phases (Figure 3). In Phase 0, before the release, the electron density measurements showed both 3.4 s spin modulation and fine scale irregularities (Figure 3a). At this time, the 5.1 MHz reflection altitude was 305 km. The irregularities were probably generated by the heater because their amplitude grew as the rocket moved closer to the HF reflection height. The normalized fluctuations ($\Delta n/n$) increased from 3% at 270 km altitude to 7% to 283 km just before release. The low frequency electric field data also show enhanced fluctuations during this period. These fluctuations may provide evidence for field aligned irregularities extending down from the reflection altitude. These irregularities could

be the result of the constant ionospheric heating for more than one hour prior to launch. The $\Delta n/n$ fluctuation level was less than 1% on the downleg of trajectory in the same altitude range when the rocket was well away from the heated volume. During another launch from Puerto Rico, Kelley et al. [1994] reported in situ measurements of small scale irregularities down to 18 km below the 5.1 MHz reflection altitude.

Before the rocket could cross the ambient reflection level for the 5.1 MHz HF waves, the electron attachment chemical was expelled from a heated tank. For the first 9 seconds (Phase 1) after the CF_3Br release, the depressed electron plasma is pitted with narrow micro cavities with sizes of less than 1 meter (see Figure 3b) where size is assumed to be the rocket velocity times the measurement time. Since the rocket was moving at an oblique angle (123 degrees) with respect to the magnetic field, the sizes of stationary, field aligned structures would be smaller by a factor of $\mathrm{Sin}(123^{o}) = 0.839$ than the scales given in Figure 3 and 4. A high resolution sample of this data is plotted versus distance along the trajectory in Figure 4a. The micro cavities were recorded by both Langmuir probes. Usually the features smaller than the distance between the two probes were detected only at one of the probes. The micro cavities larger than the 2 meter probe separation were usually measured with both probes simultaneously. Strong electric fields saturated the E-field instrument during this early time.

During Phase 2, the IFH payload entered the negative-ion cloud boundary layer where the electron density was 1 to 10 % of ambient (Figures 3b and c). The density fluctuations ($\Delta n/n \sim 17\%$) were dominated by spikes with widths of about seven meters. A detailed spatial sample of these micro spikes is illustrated in Figure 4b. In situ measurements showed

electric field reversals simultaneous with the micro spikes and cavities.

The transition between electron micro-cavities in phase 1 to electron micro-spikes in phase 2 has been explained by Scales et al.[1994a and b] using electrostatic simulations of the three component plasma. A shear in the electron velocity at the negative-ion/electron boundary layer seems to drive the instability that produces the irregularities. At early times in the center of the electron depletion, the negative ions form density spikes that are neutralized by electron density cavities. The background positive ion plasma remains relatively uniform. At later times, in the boundary layer, the electron spikes form as the negative-ion and positive-ion plasma evolves into density cavities. Unfortunately, the frequency response of the positive-ion disk probe measurements was too low to verify the computed variations in positive ion density.

The amplitude of density fluctuations was at a minimum ($\Delta n/n \leq 7\%$) when the payload was between the negative ion boundary layer and the HF wave reflection altitude. During Phase 3 the rocket payload approached the new 5.1 MHz reflection region (between 311 and 316 km altitude at times 21 through 30 seconds after release). As with phase 0, the irregularity fluctuation level increased as the rocket approached the critical density of 3.23×10^5 cm^{-3}. High resolution spatial plots of selected data are illustrated in Figure 4. The time, rocket speed, and altitude for the start of each data sample is given. The deepest cavities between 197 and 198 seconds in Figure 3d show internal structures in greater detail in Figure 4c where the distance along the trajectory is used as the horizontal axis. The two 40% cavities near 1.1 km distance (317.4 km altitude) at the right side of Figure 4d have radii of about 4 meters.

The chemical release at 283 km expanded over the altitude (290 km)

where the HF wave reflected before the release. Consequently, any irregularities at that level are overwhelmed by the dissociative attachment of electrons. When the rocket passed through the new reflection level at the top of the electron density hole, the observed irregularities must have been newly formed because the HF wave did not penetrate to this level before the release - ten seconds earlier. The average radius of the cavities in this region were on the order of an O^+ ion cyclotron radius (4 meters). Irregularities of this size have been detected with radio backscatter by [Minkoff et al., 1974; Belenov et al., 1977; Coster et al., 1985]. In situ measurements of similar size structures have been reported by M.C. Kelley et al. [1994] during a rocket flight through the Arecibo heater beam on 9 June 1992.

After passing through the reflection level, the rocket entered the unheated plasma labeled phase 4 in figure 3d. Here, the electron density fluctuations decreased to values of $\Delta n/n$ less than one-percent.

The chemical release and subsequent electron depletion modified the HF wave electric field. Figure 5 shows the changes in the 5.1 MHz electric field measured in situ between 169.0 and 169.5 seconds after launch. At this time the rocket velocity was 1411 m/s with an angle of 17^o with the vertical. The electric field measurements shows successive minima as the rocket passes through the nulls in the standing wave (or Airy) pattern of the reflected 5.1 MHz transmission. The minimum distance between the nulls is expected to be $\lambda_1/2$ where $\lambda_1=c/(n_1 f_1)$, c is the speed of light, n_1 is the refractive index in the magneto-plasma, and f_1 = 5.1 MHz is the transmitter frequency. The plasma density just below release is $n_e = 2.6 \times 10^{11}$ m^{-3}, the gyro frequency in the ionosphere over Arecibo is f_{ce} = 1.07 MHz, and the propagation angle between a vertical wave vector and the

magnetic field is $\Theta = 40^{o}$. With these parameters, the refractive index for the 5.1 MHz wave is $n_1 = 0.530$ and the wavelength in the plasma is $\lambda_1 = 111$ meter. Dividing $\lambda_1/2$ by the rocket velocity gives the scale length shown in Figure 5a. During the upleg of the flight, the nulls in the 5.1 MHz wave measurements are greater than $\lambda_1/2$ (Figure 5a,b, and c).

After the release at 169.29 seconds, the free electrons vanish and a horizontally-stratified standing-wave would have nulls spaced by $\lambda_0/2$ where $\lambda_0 = c/f_1 = 58.82$ meters in free space. Also, the electric field amplitude should drop by a factor of $(n_1)^{1/2} = 0.73$ to maintain that same power density as the in the unmodified plasma. This effect is illustrated by the one-dimensional computation of the standing wave at 5.1 MHz reflecting above an electron density depletion in a horizontally stratified layer (Figure 6). The ionospheric profile represents a vertical cut through the ionosphere 3 seconds after the CF_3Br release. The one-dimensional calculations for these fields do not account for the limited horizontal extent of the ionospheric hole and the bending of the HF wave fronts.

The <u>in situ</u> measurements of the electric fields for the 5.1 MHz wave (Figure 5) differ from the calculated fields (Figure 6) in several ways. The electric field amplitude increases by a factor of 3 after the release and the nulls have spacings both greater and less than $\lambda_0/2$. The power density immediately after release increases by a factor of 16 or 12 dB. This enhancement is attributed to focussing by the ionospheric hole. The erratic variations in the wave nulls result from the rocket passing through a time-varying interference pattern established in the electron density cavity. A multi-dimensional model of these fields is being constructed to study these fields.

The frequency spectrum from the 5.1 MHz downconverter on the IFH

rocket is shown in Figure 7. While the rocket payload was inside the ionospheric hole, the 5.1 MHz pump was broadened into a downshifted spectrum with a width of 1.3 kHz. This broadening started at the time of the release (169.3 seconds after launch). The intensities of the downshifted waves were greater than 10 dB above the prerelease level. The source of the broadening may have been scatter of electromagnetic waves by the small scale irregularities at the edge of the negative ion cloud [Scales et al., 1994a and b].

The width and intensity of the waves returned to the prerelease level 26 seconds after release when the rocket had passed through the Phase 2 irregularities. A localized burst of broad band HF noise ($\Delta f \leq 8$ kHz) was next recorded when the payload transited the critical region of the ionosphere during Phase 3. Accurate determination of the HF reflection point is not possible from the electron density data because of modulation from the spin and precession of the payload. Based on the disappearance of the 5.1 MHz signals from the plasma wave receiver (Figure 8), the critical level was penetrated between 199 and 200 seconds after launch.

A plot of the electron density irregularities, the spectral deviations from 5.1 MHz, and low frequency electric fields show evidence of Langmuir and ion acoustic waves coincident with the density cavities near the reflection level (Figure 8). These data are consistent with formation of field aligned irregularities that guide Langmuir generated by parametric decay of the pump electromagnetic wave. The measured irregularities seem to be field-aligned ducts described by Muldrew [1978 and 1988] that guide Langmuir waves.

The width of the high frequency spectral broadening near the reflection level is about 2 kHz. As will be shown later in Figure 12, the

broaden in Langmuir wave scatter of the 430 MHz radar is on the order of 10 or 20 kHz. The apparently narrow in situ spectral measurements may be due to the presence of negative ions at the top of the ionospheric hole. The narrowness of the spectrum is not due to instrument instrumental which had a ± 75 kHz bandwidth capability (Table I). A more detailed discussion of the in situ wave measurements near the HF reflection region are given by Rodriguez et al. [1994].

IV. Incoherent Scatter Radar Measurements

Even though the 5.1 MHz HF transmitter was in operation continuously, no enhanced ion lines were recorded up to 450 seconds after the launch of the IFH rocket. The trajectory of the rocket was measured by the sidelobes of the Arecibo radar. Backscatter by the thermal ion line showed the reduction in electron density following the chemical release. Both of these effects are shown by the left half of Figure 9. The azimuth of the radar was fixed at 13 degrees until 300 seconds after launch. During this period, no enhanced scatter from ion-acoustic waves was measured even though strong low-frequency electric fields were measured in situ (Figure 8). This may have been because the Arecibo radar beam was not aligned with the turbulent area inside the rapidly evolving ionospheric hole. After this time, the azimuth was scanned from one edge of the ionospheric hole to the other.

The right half of Figure 9 shows the effects of focussing through the artificial hole. Because of a 40 m/s westward drift, the hole center moved to an azimuth of -5 degrees, 500 seconds after release. Around this time, a strongly enhanced ion line (EIL) was observed where the HF wave reflected at the critical density region. This region occurred where the pump

frequency equaled the electron plasma frequency across the top of the artificial hole. The intensity of this EIL was the largest recorded during the May-July period of the El Coqui rocket campaign. This unusual intensification of the EIL was most likely the result of focussing by the chemically-produced hole in the F-region.

The radar downshifted plasma line (PL) went through a number a changes during the IFH experiment (Figure 10). Before the chemical release, a weak PL was recorded near the HF reflection height of 290 km in the F-region. During the first ten seconds following the release, the plasma line was recorded at multiple altitudes between 285 and 300 km. The intensity increased by 10 dB in a path aligned with the rocket trajectory between 295 and 300 km. After this initial enhancement, the PL vanished only to reappear at the top of the chemically-produced cavity with an intensity comparable to the prerelease value. the absence of plasma-lines when the instruments on the rocket were recording strong Langmuir waves (Figure 8) is again attributed to the misalignment of the radar beam inside the active region of the ionospheric hole.

The strongest enhancements in the PL occurred between 280 and 430 seconds after release. The 10 km range spread at this time (Figure 10) may be the result of sidelobe smearing associated with the coded radar pulse. The actual range in altitude is probably similar to the 2 km spread shown from the strongest enhanced ion line in Figure 9. At 480 seconds after launch (310 seconds after release) the azimuth scan reversed directions. Both the plasma line and enhanced ion line show spatial symmetry around this time. This indicates that turbulence was excited at the HF reflection layer by focussing through a long-lived ionospheric lens.

The plasma line ten seconds after release was enhanced by 10 dB

(Figure 11). After release at 169.3 seconds, the HF reflection layer splits into a region along the rocket trajectory near 300 km altitude and a region near the original 290 km level. The large plasma line enhancement at 300 km altitude is coincident with the strong downshifted Langmuir waves recorded on the rocket (Figure 7). The transient disturbance displayed in Figure 11 may be associated with turbulence in the boundary layer of the negative ion cloud [Scales et al., 1994].

The spectra of the plasma lines and enhanced ion lines were obtained during the data gaps shown as white vertical bars in Figure 10. A sample of the spectra during the period of strong enhancements 335 seconds after release (504 seconds after launch) is illustrated in Figure 12. The plasma line spectrum in Figure 12a shows all of the characteristic features (i.e., decay line, cascade bump) of an un-focussed plasma line at Arecibo. The enhanced ion line is easily distinguishable from the background (thermal) ion line (Figure 12b). A typical feature of enhanced ion lines is that the upshifted and downshifted components are nearly symmetrical. This is the case for the focussed enhanced ion line (Figure 12b). The only unusual features of the observed plasma or ion lines were their large intensities.

Besides electromagnetic wave focussing, processes such as linear mode conversion [Mjølhus, 1990] could be responsible for enhanced coupling to Langmuir waves. If linear mode coupling were the source of the enhanced ion lines, one would expect assymetries in the plasma line and ion line spectra. This because the upgoing electromagnetic wave would be expected to mode convert into an upgoing Z-mode which reflects and become a downgoing Langmuir wave [Mjølhus, 1990]. With a downgoing Langmuir wave, the downshifted plasma line and the enhanced ion lines should be absent. We have also ruled direct mode coupling because the wave normals of the of

the rays do not have the critical angle required for linear conversion.

Based on raytracing through a model ionosphere, the source of the enhanced turbulence has been attributed to focussing by the chemically produced cavity. Without the chemical release, the pump beam reflects near 300 km independent of ray launch angle (Figure 13a). In the early phase of the release, the strong electron density gradients form a focal point inside the ionospheric hole. Using an electron density model that matches the ISR electron density profile 10 seconds after the CF_3Br release, the focus is 8 km from the center of the hole whereas the upper reflection boundary of the hole is 15 km from the center (Figure 13b). The hole evolves by the action of chemistry and plasma transport. At some point in the evolution, the HF focal point and the reflection boundary coalesce yielding a region of large electric fields. This condition occurs at about 300 seconds after release. The large electric fields responsible for the enhanced radar backscatter occur because (1) the HF waves are focussed onto a reflection contour of the electron density and (2) the group velocity goes to zero at the reflection level causing an accumulation of the wave energy. The focussing processes are limited by diffraction [Bernhardt and Duncan, 1987] and by irregularities that may scatter the electromagnetic waves. Figure 13c shows a tube of rays focussed on the upper boundary of the ionospheric hole 293 seconds after release. This is the time period when the unusual enhancements of ion acoustic and electron plasma waves were observed in the ISR data.

V. Ground-Based Optical and Radio Observations

A number optical instruments were operated at the Arecibo Observatory during the IFH experiment. Photometers with 5 degree fields of view were

pointed at the release location and recorded the 557.7 and 630.0 nm emissions. A low-light-level CCD camera with a 60 degree field of view recorded 630 nm emissions from the release and HF focussing regions. A description of these instruments is given by Bernhardt et al. [1988].

An enhancement of airglow during the IFH experiment occurred immediately after the CF_3Br release. Figure 14 illustrates the 20 Rayleigh increase in 557.7 nm (green-line) and the 4 Rayleigh increase in the 630.0 nm (red-line) of atomic oxygen. These enhancements probably come from the excited atomic oxygen that was a product of mutual neutralization reaction (2). Bernhardt [1987] predicted that $O(^1D)$ should be the primary excited oxygen state from Br^- and O^+ mutual neutralization. Based on the observations that the 557.7 nm intensities were five times larger than the 630.0 nm intensities, we conclude that $O(^1S)$ was the primary product of the reaction

$$Br^- + O^+ \rightarrow Br(^2P^o) + O(^1S) + 6.065\ eV \qquad (3)$$

and that green-line and red-line emissions came from

$$O(^1S) \rightarrow O(^1D) + h\nu(557.7\ nm) \qquad \tau_1 = 0.71\ s \qquad (4)$$

$$O(^1D) \rightarrow O(^3P) + h\nu(630.0,\ 636.4\ nm) \qquad \tau_2 = 147\ s \qquad (5)$$

where τ_1 and τ_2 are the radiative lifetimes of the states.

The process described by (3), (4), and (5) is consistent with the observations. The red-line emission peaked 80 seconds after the maximum green-line emission. Also, the red-line intensity was 20% of the green-

line intensity. Both of these effects can be attributed to the relatively long lifetime of the $O(^1D)$ state which is formed by electronic transition from the shorter-lived $O(^1S)$ state. The integrated volume emission rate was reduced by diffusion of the $O(^1D)$ atoms and by collisional quenching before radiation [Bernhardt, Tepley, and Duncan, 1989].

At the time of the strongly enhanced ion line, between 450 and 570 seconds after launch, a small 1 Rayleigh enhancement is observed in the 630.0 nm (red-line) channel of the photometer. This peak is coincident with the enhanced ion lines produced by focussing of the HF radio waves. Its magnitude is surprisingly small. Since HF-induced perturbations in the green-line are typically 5% of the red-line values [Bernhardt et al., 1989], a corresponding peak would be too weak to be detectable in the 557.7 nm channel (Figure 14a). The low-light-level CCD camera did not show any enhancements in red-line airglow.

Previous experiments at Arecibo have indicated that extremely strong enhanced ion lines are accompanied by larger (~ 50 Rayleigh) increases in red-line airglow [Bernhardt et al., 1988; 1989]. This was not the case for the IFH experiment. We are currently investigating a number of explanations for the apparent weakness of heater induced airglow. These include the effects of residual negative ions in the plasma and tilting of the HF beam from vertical.

Using ground-based spectrum analyzers attached to wide band HF antennas, observations of stimulated electromagnetic emissions (SEE) were attempted at Arecibo, PR and Providenciales, Caicos. No SEE was detected during the entire El Coqui campaign. This is not totally unexpected because previous experiments have demonstrated that SEE is more often observed at higher latitude heating facilities [Thide et al, 1989].

Los Alamos and NRL set up bistatic HF propagation links between Dominica and Providenciales, Caicos during the IFH release and other CRRES rocket experiments. Propagation frequencies were chosen to reflect near the release points for chemicals. The CF_3Br release produced a large Doppler shift in the HF wave passing through the disturbed regions. A manuscripts describing the results of these experiments are in preparation [P.E. Argo, private communication, 1994].

VI. Conclusions

The IFH chemical release produced a large (> 30 km diameter) hole in the F-layer centered within 6 km of the 5.1 MHz HF beam. The reactions between CF_3Br and the ambient electrons yielded a turbulent negative-ion plasma. The action of the high power radio wave on the negative-ions, positive-ions, and electrons produced micro-cavities with diameters of less than 1 meter and factors of 10 or greater reductions in the already depressed plasma density. In the boundary layer between the negative ion and electron dominated regions, electron density spikes were recorded with the in situ Langmuir probes. These spikes may result from cavities in the negative ions that are filled by electrons to maintain charge neutrality. The negative-ion, positive-ion and electron simulation models of Scales, Bernhardt, and Ganguli [1993, 1994] and Scales et al. [1994] are being used to study this process.

The in situ measurements of the electron density near the HF reflection region at the top of the ionospheric hole show electron plasma waves trapped or guided by cavities the size of the positive ion gyro-radius. The frequency spread of these Langmuir waves is 8 kHz or less. The structure observed at the reflection region may be associated with

field aligned cavities guiding Langmuir waves generated by the parametric decay instability (PDI) as described by Muldrew [1978, 1988]. Processes that can generate field aligned irregularities by the thermal parametric instability have been summarized by Mjølhus [1993]. Horizontal structures may be formed by the ponderomotive force in the peaks in the standing wave of the HF pump [Leyser and Thidé, 1988].

From the in situ and ground based observations, we deduce that the artificial ionospheric hole yielded 10 to 20 dB enhancements in the pump wave intensity by focussing. This degree of focussing is consistent with the predictions by Bernhardt and Duncan [1987]. The strongest focussing lasted for 150 seconds after the ionospheric hole had evolved so that the focal point was located on the reflection level at the top of the hole. The amplitudes of the ion acoustic waves and electron plasma oscillations were increased by more than 20 dB during the period of the strongest focussing. The weakness of the red-line airglow enhancements during this time is difficult to explain. Airglow induced by RF heating usually comes from surprathermal electrons colliding with ambient atomic oxygen. The negative ions trapped on the magnetic field lines below the HF reflection level may have scattered the suprathermal electrons before they could excite the oxygen.

An experiment complementary to IFH used a barium release from a sounding rocket. This experiment (CRRES AA-2) produced an electron density enhancement in the powerful radio beam from Arecibo HF facility [Djuth et al., 1994]. It is instructive to compare the results of the IFH and AA-2 radar measurements. Following the barium release of the AA-2 experiment, the intensity of the upshifted plasma line increased by about 12 dB and the downshifted plasma line vanished below the noise floor of the radar

receiver. The downshifted and upshifted enhanced ion lines showed corresponding assymmetries. The measured assymmetric plasma lines may have been the result of ion cloud expansion or steep density gradients. Because an electron density enhancement defocuses an HF beam, focussing does not explain the AA-2 results. The source of the assymmetric radar spectra is not understood and should be a subject for future research [Djuth et al., 1994].

Both the IFH and AA-2 experiments yielded large enhancements in HF induced Langmuir turbulence. The IFH experiment produced the largest increase in plasma line strength (20 dB) but AA-2 yielded the largest absolute plasma line intensity. A quantitative comparison of the two techniques is difficult because the intensity of the plasma line before the IFH release was much less than the intensity before the AA-2 release. It is a open question whether ionospheric holes or electron enhancements produce the largest effect on ionospheric heating.

The IFH experiment has demonstrated that the release of an electron-attachment chemical will form an artificial lens in the F-region that may be used to increase the power density of any HF facility. The effective radiated power of these facilities can be increased by about 20 dB for periods of time longer than 2 minutes. Similar IFH experiments should be attempted in the future to give a temporary boost in the power levels available for ionospheric heating. This boost may yield phenomena that are not produced with current heating facilities.

Acknowledgments

The authors gratefully acknowledge the support of the staff of Arecibo Observatory, and graduate students from the Department of Physics and Astronomy, Clemson University and the Department of Electrical Engineering, Cornell University. The Arecibo Observatory is part of the National Astronomy and Ionosphere Center, operated by Cornell University under contract with the National Science Foundation. The research at NRL was supported by the National Aeronautics and Space Administration and the Office of Naval Research. One of the authors (F.T.D) acknowledges support from NASA under contract NAS8-39075 and from the Phillips Laboratory, Hanscom Air Force Base under contract F19628-92-C-0168.

REFERENCES

Belenov, A.f., et al., Parameters of artificial small-scale ionospheric irregularities, Radiophys. Quantum electron. Engl. Transl., 20, 1805-1813, 1977.

Bernhardt, P.A. and L.M. Duncan, "Ionospheric focussed heating - a hybrid modification experiment," J. Atmos. Terr. Phys., 49, 1107, 1987.

Bernhardt, P.A., L.M. Duncan, and C.A. Tepley, "Artificial Airglow Excited by High-Power Radio Waves," Science, Volume 242, pp 1022-1027, 18 November 1988.

Bernhardt, P. A., C. A. Tepley, and L. M. Duncan, "Airglow enhancements associated with plasma cavities formed during ionospheric heating experiments", J. Geophys. Res., 94, 9071-9092, 1989.

Bernhardt, P.A., P. Rodriguez, C.L. Siefring, and C.S. Lin, Field-aligned dynamics of chemically induced perturbations to the ionosphere, J. Geophys. Res., 96, 13887-13900, 1991a.

Bernhardt, P.A., W.A. Scales, S.M. Grach, A.N. Karashtin, D.S. Kotik, S.V. Polyakov, Excitation of artificial airglow by high power radio waves from the "SURA" ionospheric heating facility, Geophys. Res. Lett., 18, 1477-1480, 1991.

Bernhardt, P.A. Field-aligned dynamics of chemically induced perturbations to the ionosphere, J. Geophys. Res., 96, 13887-13900, 1991.

Coster, A.J., F.T. Djuth, R.J. Jost, and W.E. Gorden, The temporal evolution of 3-m striations in the modified ionosphere, J. Geophys. Res., 90A, 2807-2818, 1985

Derblom, H., B. Thide, T.B. Leyser, J.A. Nordling, A. Hedberg, P. Stubbe, H. Kopka, and M. Rietveld, Tromsø Heating Experiments: Stimulated Emission at HF Pump Harmonic and Subharmonic Frequencies, J. Geophys. Res., 94, 10111-10120, 1989.

Djuth, F.T., El Coqui Active Experiment Explore the Ionosphere, Soundings, 2, 1-3, Winter 1993.

Djuth, F.T., M.P. Sulzer, J.H. Elder, and K.M. Groves, The CRRES AA-2 release: HF wave-plasma interactions in a dense Ba^+ cloud, submitted to J. Geophys. Res., 1994.

Dubois, D.F., H.A. Rose, and D. Russell, Excitation of strong Langmuir turbulence in plasmas near critical density: Application to HF heating of the ionosphere, J. Geophys. Res., 94, 10111-10120, 1990.

Duncan, L.M., S.P. Sheerin, and R.A. Behnke, Observations of ionospheric cavities generated by high-power radio waves, Phys. Rev. Lett., 61, 239-242, 1988.

Fejer, J.A., Ionospheric modification and parametric instability, Rev. Geophys. space Phys., 17, 135-157,1979.

Ganguli, G., P.A., Bernhardt, W.A. Scales, P. Rodriguez, C.L. Siefring, H.A. Romero, Physics of Negative Ion Plasmas Created by Chemical Releases in Space, SPI Conference Proceedings and Reprint Series, T. Chang Ed., Scientific Publishers, Cambridge, Mass., 1993.

Hansen, J.D., G.J. Morales, L.M. Duncan, J.E. Maggs, and G. Dimonte, Large-scale ionospheric modifications produced by nonlinear refraction of an HF wave, Phys. Rev. Lett., 65, 3285-3288, 1990.

Hansen, J.D., G.J. Morales, and J.E. Maggs, Large-scale HF-induced ionospheric modifications: Theory and modeling, J. Geophys. Res., 97, 17019-17032, 1992.

Haas, D.G., C.L. Siefring, M.M. Baumback, P. Rodriguez, D.P. Mcnutt, Rocket-borne downconverter for measuring space plasma turbulence, submitted to Rev. Sci. Ins., 1993.

Kelley, M.C., T. Arce, J. Saloway, T. Armstrong, M.P. Sulzer, and L.M. Duncan, "Density depletions at the ion gyro radius scale induced by the Arecibo heater", submitted to J. Geophys. Res., 1994.

Leyser, T.B., and B. Thidé, Effects of pump-induced density depletions on the spectrum of stimulated electromagnetic emissions, J. Geophys. Res., 93, 8681-8688, 1988.

Minkoff, J., P. Kugelmenn, and I. Wiessman, Radio frequency scattering from a heated ionospheric volume, 1, VHF/UHF field-aligned and plasma-line backscatter measurements, Radio Science, 9, 941-955, 1974.

Mjølhus, E., On linear conversion in a magnetized plasma, Radio Science, 25, 1312-1339, 1990.

Mjølhus, E., On the small scale striation effect in ionospheric radio modification experiments near harmonics of the electron gyro frequency, J. Atm. Terr. Phys., 55, 907-918, 1993.

Muldrew, D.B., The role of field-aligned ionization irregularities in the generation of HF-induced plasma line at Arecibo, J. Geophys. Res., 83, 2552-2560, 1978.

Muldrew, D.B., Duct model explanation of the plasma line overshoot observed at Arecibo, J. Geophys. Res., 93, 7598-7604, 1988.

Scales, W.A., P.A. Bernhardt, and G. Ganguli, Simulations of Negative Ion Clouds and Electron Density Depletions Produced During Electron Attachment Chemical Release Experiments, SPI Conference Proceedings and Reprint Series, T. Chang Ed., Scientific Publishers, Cambridge, Mass., 1993.

Scales, W.A., P.A. Bernhardt, G. Ganguli, C.L. Siefring, and P. Rodriguez, Small-scale plasma irregularities produced during electron attachment chemical releases, Geo. Res. Lett., 21, 605-608, 1994.

Scales, W.A., P.A. Bernhardt, and G. Ganguli, Early time evolution of a chemically produced electron depletion, submitted to J. Geophys. Res., 1994.

Showen, R.L., and D.M. Kim, Time Variations of HF-Induced Plasma Waves, J. Geophys. Res., 83, 623-628, 1978.

Thide, B., A. Hedberg, J. A. Fejer, and M.P. Sulzer, First Observations of Stimulated Electromagnetic Emission At Arecibo, Geophys. Res. Lett., 16, 369-372, 1989.

Figures

Figure 1. Ground projection of the IFH rocket trajectory relative to the island of Puerto Rico. The location of the 5.1 MHz HF heater and the 430 MHz UHF radar beams are also indicated. The CF_3Br release occurred along the trajectory slightly to the east of the center of the HF beam.

Figure 2. Sensors and instruments on the IFH rocket. The chemical canister was located between the instrument section and the rocket motor.

Figure 3. Electron density measured by the IFH rocket in four ten second periods. The values are derived assuming that electron density is proportional to the measured current from the NRL Langmuir probe LP2. In regions of very low density, such as phase 1 and the early part of phase 2, the negative ions may provide a substantial portion of the Langmuir probe current. Density fluctuations are evidence of (a) rocket spin, (b) micro cavities, (c) spikes, and (d) heater induced cavities. The rocket speed and altitude at the beginning and end of each period is indicated along with the range of times after launch.

Figure 4. Electron density details along several portions of the IFH rocket trajectory. The time, speed, and altitude for the start each segment is given along the top of each data sample. The discrete density steps in the data are due to the finite length for the digital word from the logarithmic amplifiers of the Langmuir probe.

Figure 5. In situ measurements of the electric fields (V/m) near the 5.1 MHz pump wave. A large increase in wave amplitude follows the CF_3Br release.

Figure 6. Computed standing wave in a horizontally stratified ionosphere with a localized electron depletion.

Figure 7. Spectrogram of the pump fields and associated Langmuir waves. The spectra is naturally divided into (1) a prerelease narrow line, (2) downshifted broadening after release, (3) a burst when passing through the HF reflection level 196 to 199 second after launch, and (4) a disappearance of the pump thereafter.

Figure 8. Detail of the electron density, Langmuir waves around 5.1 MHz, and low frequency ion acoustic waves near the HF reflection level. The Langmuir waves and ion acoustic waves seem to be trapped or guided by the density cavities. Spectra of low frequency electric fields is measured between sensors EF1 and EF4 of Figure 2.

Figure 9. Incoherent scatter ion line obtained by the Arecibo radar during the IFH experiment. The radar backscatter is affected by (1) reduction of electron density in the F-layer, (2) side-lobe scatter from the rocket body, and (3) enhanced ion acoustic waves at the top of the F-layer hole. The radar was operated in a spectral mode during the times of data gaps in the figure.

Figure 10. Incoherent scatter measurement of the plasma line at 430 - 5.1 MHz. The plasma line shows (1) the HF reflection layer before the release, (2) a brief focussing after release, (3) a new reflection height at the top of the ionospheric hole, and (4) 20 dB increase in the plasma line after focussing occurs.

Figure 11. Plasma line splitting during the ten seconds after the release of CF_3Br. The strongest backscatter from Langmuir waves is 10 dB stronger than the prerelease plasma line. The downshifted Langmuir waves illustrated by the in situ observations of Figure 6 may be the source of the scattered radar signal.

Figure 12. Spectrum of the downshifted plasma line (a) and the enhanced ion line (b) during the time of intense HF focussing.

Figure 13. Rays from the 5.1 MHz HF transmitters propagating through (a) the unmodified F-layer, (b) the ionospheric hole 10 seconds after release, and (c) the hole at a later time when the focal point is at the HF reflection level. The electron density contours are derived from a spherical release model adjusted to fit density measurements obtained from the ISR radar.

Figure 14. Green-line (557.7 nm) and red-line (630.0 nm) enhancements following the CF_3Br release during the IFH experiment. The bulk of these enhancements can be explained by excitation of atomic oxygen after mutual neutralization of O^+ and Br^- in the chemically modified plasma. A small red-line increase is observed during the "focussing" period of strong enhanced ion and plasma lines shown in Figures 9 and 10.

Table I

INSTRUMENTATION FOR THE IFH ROCKET

Experiment	Group	Sensor	Parameter	Specifications	Sample Rate
Langmuir Probes					
LP1	NRL	20 cm Probe	Electron	26 to $4x10^6$ cm^{-3}	5.556 ksamp/s
LP2	NRL	20 cm Probe	Density	3 to $4x10^5$ cm^{-3}	5.556 ksamp/s
($\delta n/n$)1	NRL	20 cm Probe	Relative	0 to 3	11 ksamp/s
($\delta n/n$)2	NRL	20 cm Probe	Density	0 to 3	11 ksamp/s
DP1	PL	3.0" Disk	Ion	10 to 10^6 cm^{-3}	1.4 ksamp/s
DP2	PL	1.5" Disk	Density	10 to 10^6 cm^{-3}	11.2 ksamp/s
Electric Fields					
DC,LF,AC 14	NRL	4.3 m Dipole	DC and	0 to 5.6 kHz	11.2 ksamp/s
DC,LF,AC 12	NRL	0.3 m Dipole	Low Freq.	0 to 5.6 kHz	11.2 ksamp/s
DC,LF,AC 34	NRL	0.3 m Dipole	E-Fields	0 to 5.6 kHz	11.2 ksamp/s
DC,LF,AC 56	NRL	0.3 m Dipole		0 to 5.6 kHz	11.2 ksamp/s
Downconv 1	NRL	1.5 m RF	Langmuir	2.5 to 12 MHz	One 1600 point
Downconv 2	NRL	1.5 m RF	and Pump	2.5 to 12 MHz	spectrum/s
Downconv 3	NRL	5.5 cm RF	Waves	5.050 MHz$\pm$75 kHz	4 Mbit/s
Downconv 4	NRL	11.0 cm RF		5.075 MHz$\pm$75 kHz	4 Mbit/s
Energy Spectra					
TECHS	MSFC	Cylinder	Thermal	.5 to 50 eV (32)	320 msec scan
			Electrons	45^o x 15^o (8)	32x8 spectra

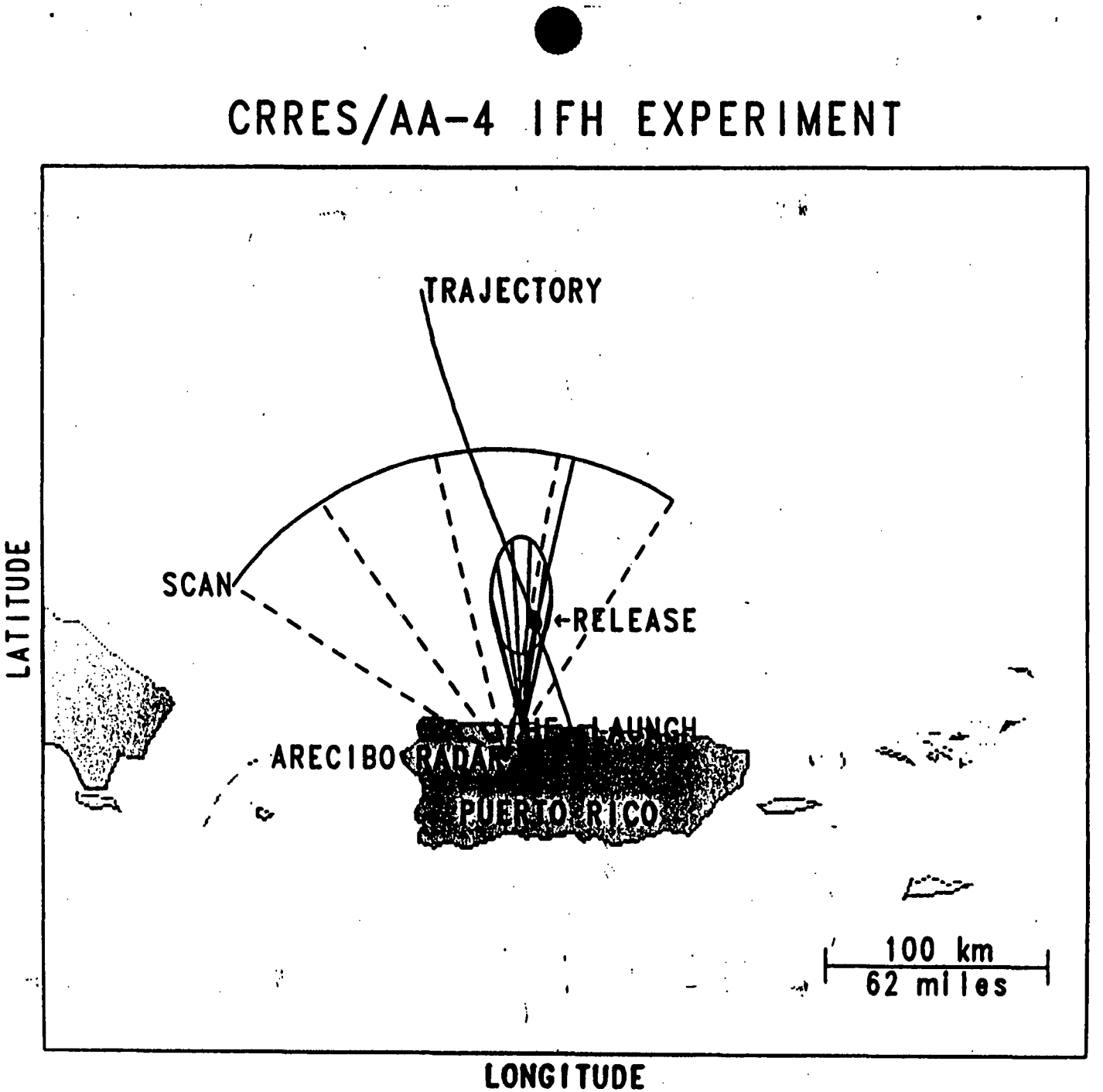
CRRES/AA-4 IFH EXPERIMENT
TRAJECTORY
SCAN
RELEASE
ARECIBO RADAR
PUERTO RICO
100 km
62 miles
LATITUDE
LONGITUDE

Figure 1.

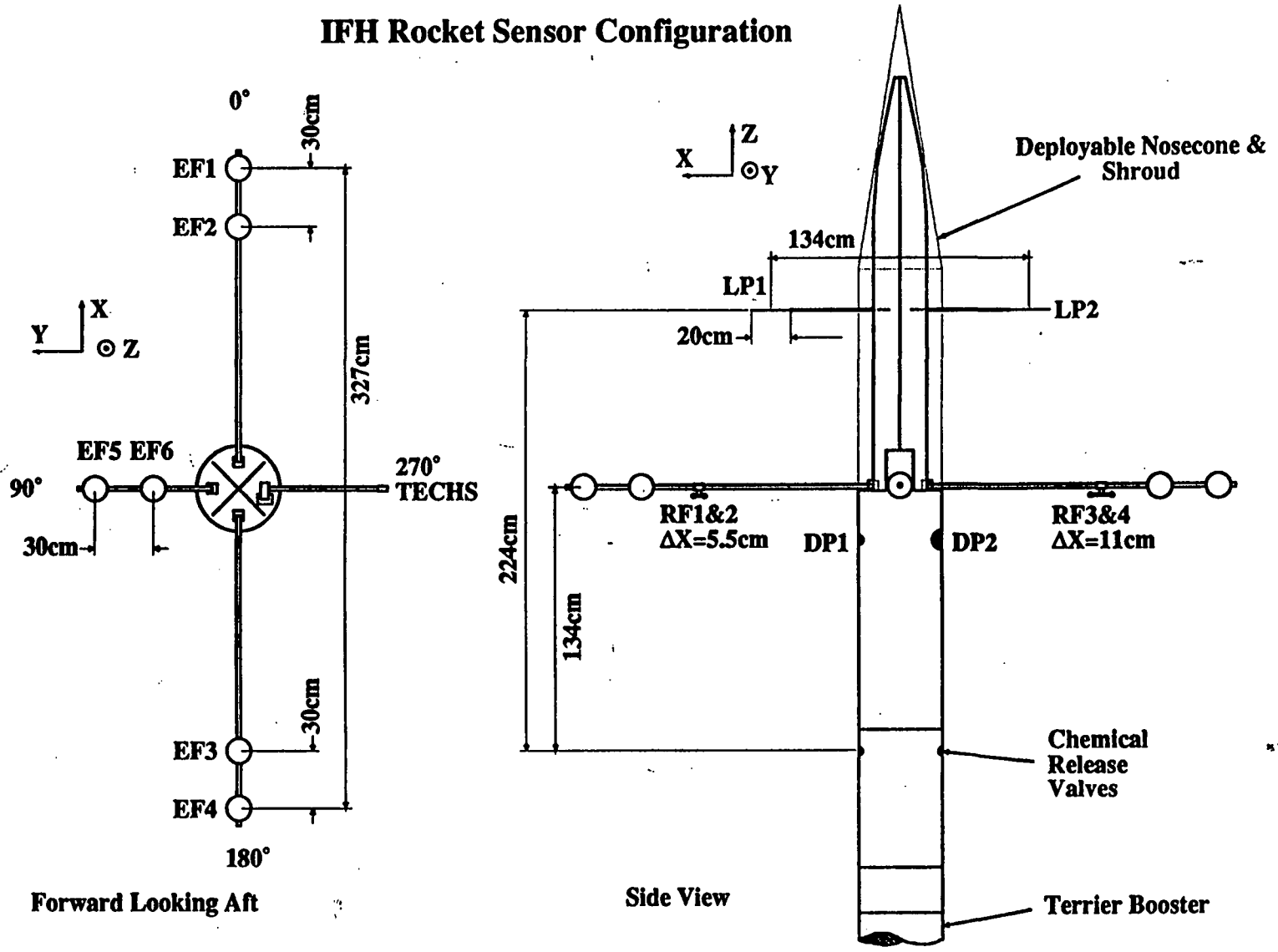
IFH Rocket Sensor Configuration
0°
30cm
EF1
EF2
X
Y
Z
327cm
EF5 EF6
90°
270°
TECHS
30cm
30cm
EF3
EF4
180°
Forward Looking Aft
X
Z
Y
Deployable Nosecone &
Shroud
134cm
LP1
LP2
20cm
224cm
134cm
RF1&2
ΔX=5.5cm
DP1
DP2
RF3&4
ΔX=11cm
Chemical
Release
Valves
Side View
Terrier Booster

Figure 2.

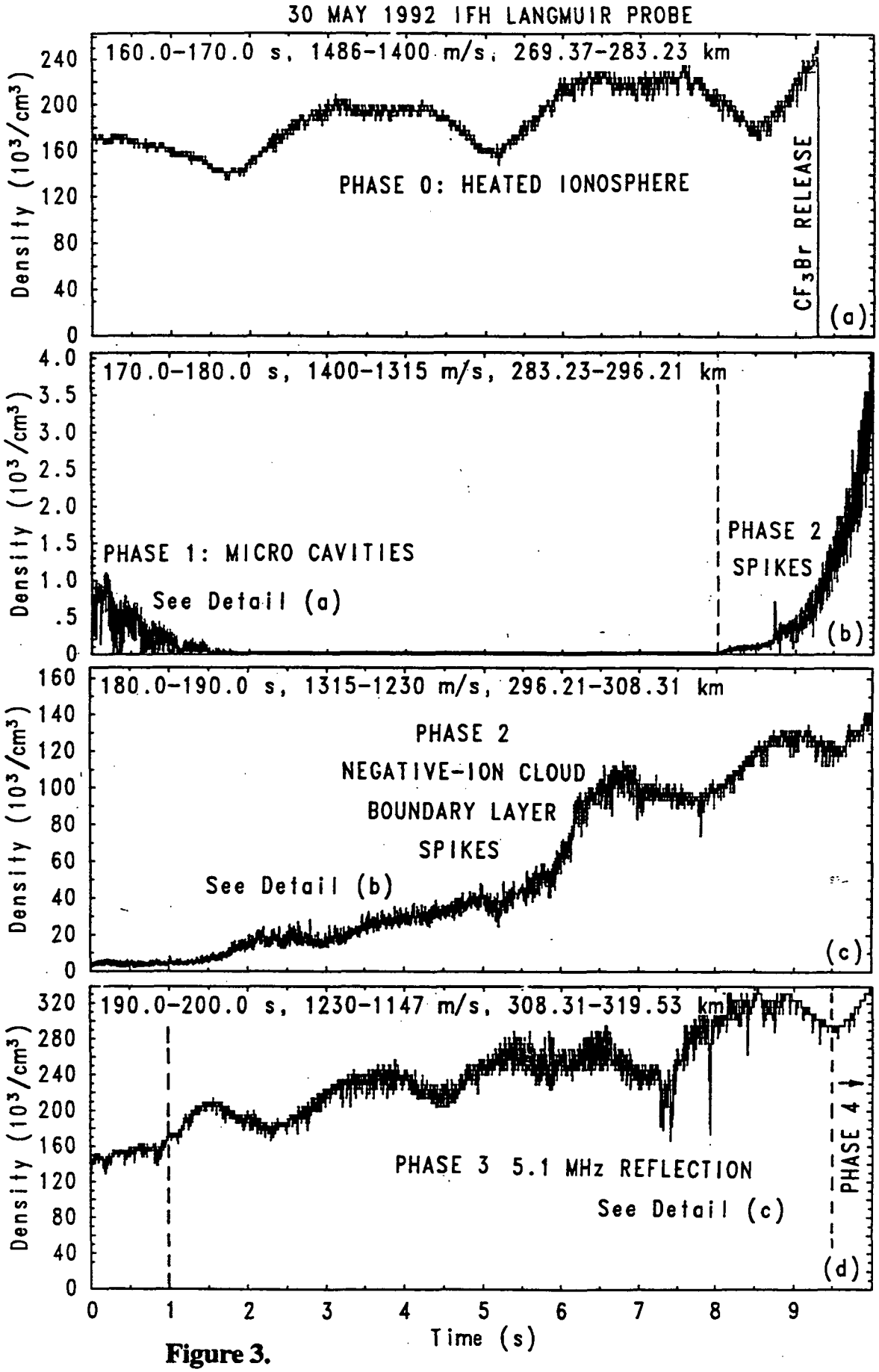
30 MAY 1992 IFH LANGMUIR PROBE
160.0-170.0 s, 1486-1400 m/s, 269.37-283.23 km
PHASE 0: HEATED IONOSPHERE
CF3Br RELEASE
(a)
170.0-180.0 s, 1400-1315 m/s, 283.23-296.21 km
PHASE 1: MICRO CAVITIES
See Detail (a)
PHASE 2
SPIKES
(b)
180.0-190.0 s, 1315-1230 m/s, 296.21-308.31 km
PHASE 2
NEGATIVE-ION CLOUD
BOUNDARY LAYER
SPIKES
See Detail (b)
(c)
190.0-200.0 s, 1230-1147 m/s, 308.31-319.53 km
PHASE 3 5.1 MHz REFLECTION
See Detail (c)
PHASE 4
(d)
Density (10³/cm³)
Time (s)

Figure 3.

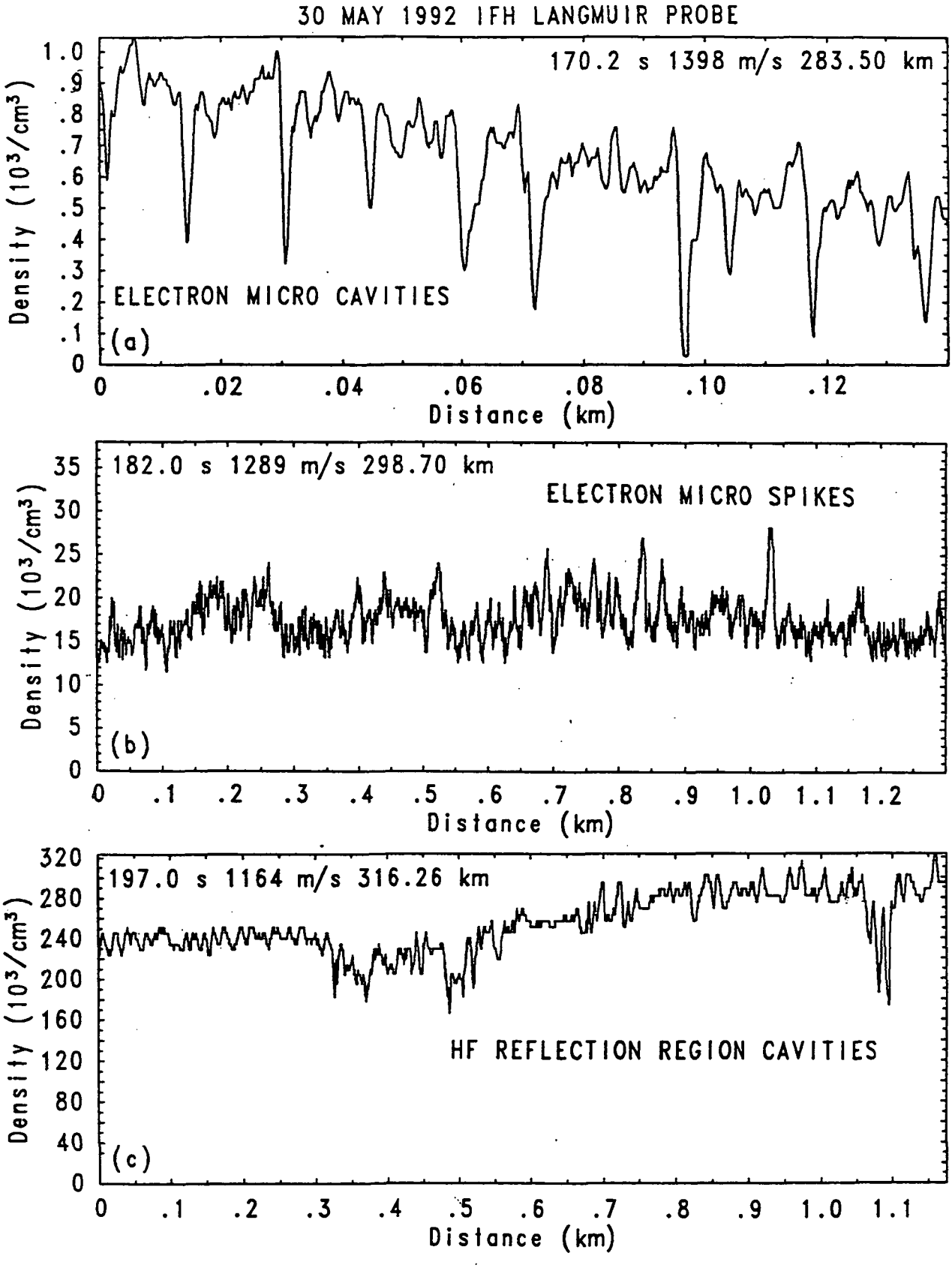
30 MAY 1992 IFH LANGMUIR PROBE
170.2 s 1398 m/s 283.50 km
ELECTRON MICRO CAVITIES
(a)
Density (10^3/cm^3)
Distance (km)
182.0 s 1289 m/s 298.70 km
ELECTRON MICRO SPIKES
(b)
Density (10^3/cm^3)
Distance (km)
197.0 s 1164 m/s 316.26 km
HF REFLECTION REGION CAVITIES
(c)
Density (10^3/cm^3)
Distance (km)

Figure 4.

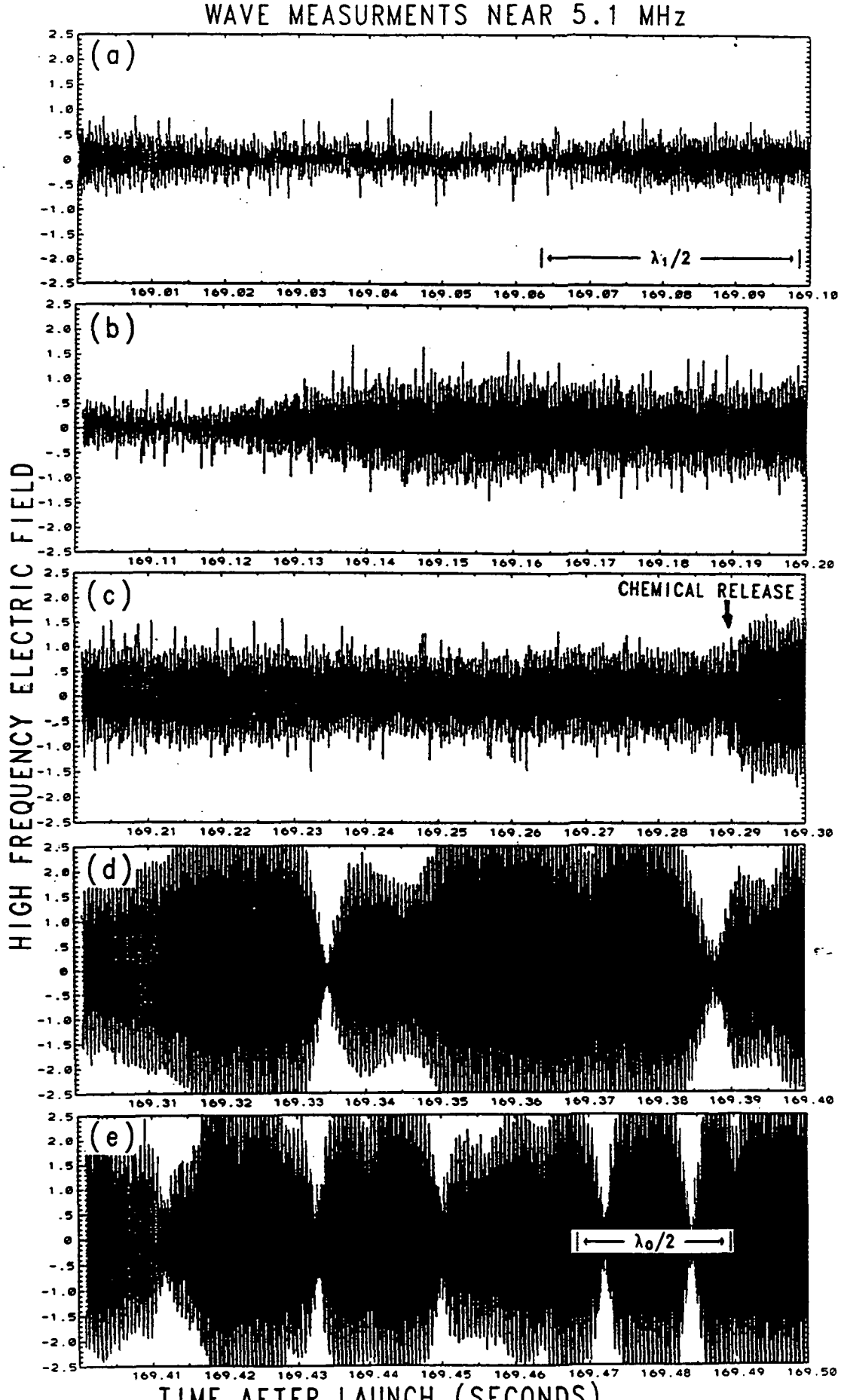
WAVE MEASURMENTS NEAR 5.1 MHz
(a)
(b)
(c)
(d)
(e)
λ1/2
λo/2
CHEMICAL RELEASE
HIGH FREQUENCY ELECTRIC FIELD
TIME AFTER LAUNCH (SECONDS)

Figure 5.

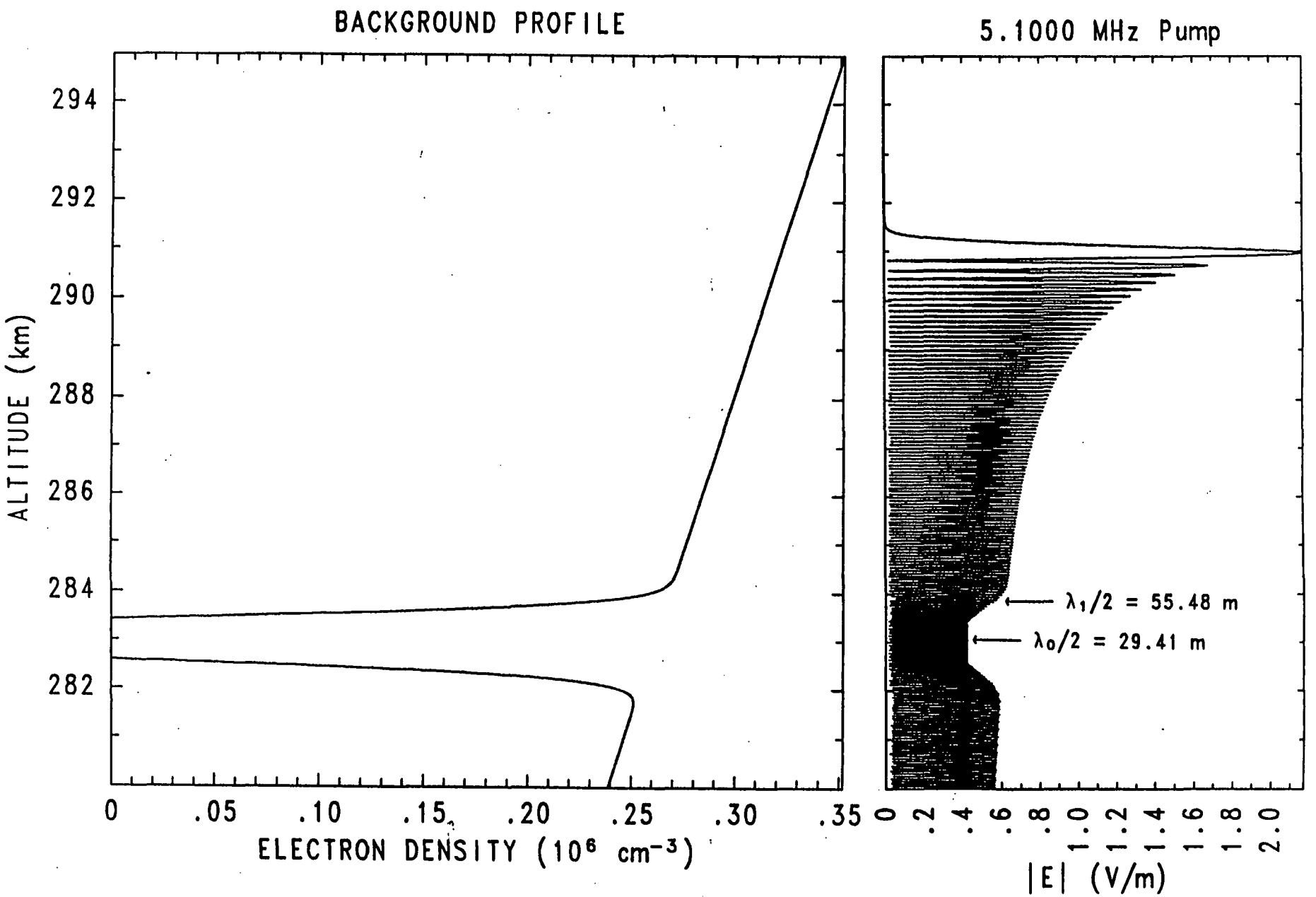
BACKGROUND PROFILE
5.1000 MHz Pump
ALTITUDE (km)
294
292
290
288
286
284
282
0
.05
.10
.15
.20
.25
.30
.35
ELECTRON DENSITY (10⁶ cm⁻³)
λ₁/2 = 55.48 m
λ₀/2 = 29.41 m
0
.2
.4
.6
.8
1.0
1.2
1.4
1.6
1.8
2.0
|E| (V/m)

Figure 6.

5.1 MHz Down Converter

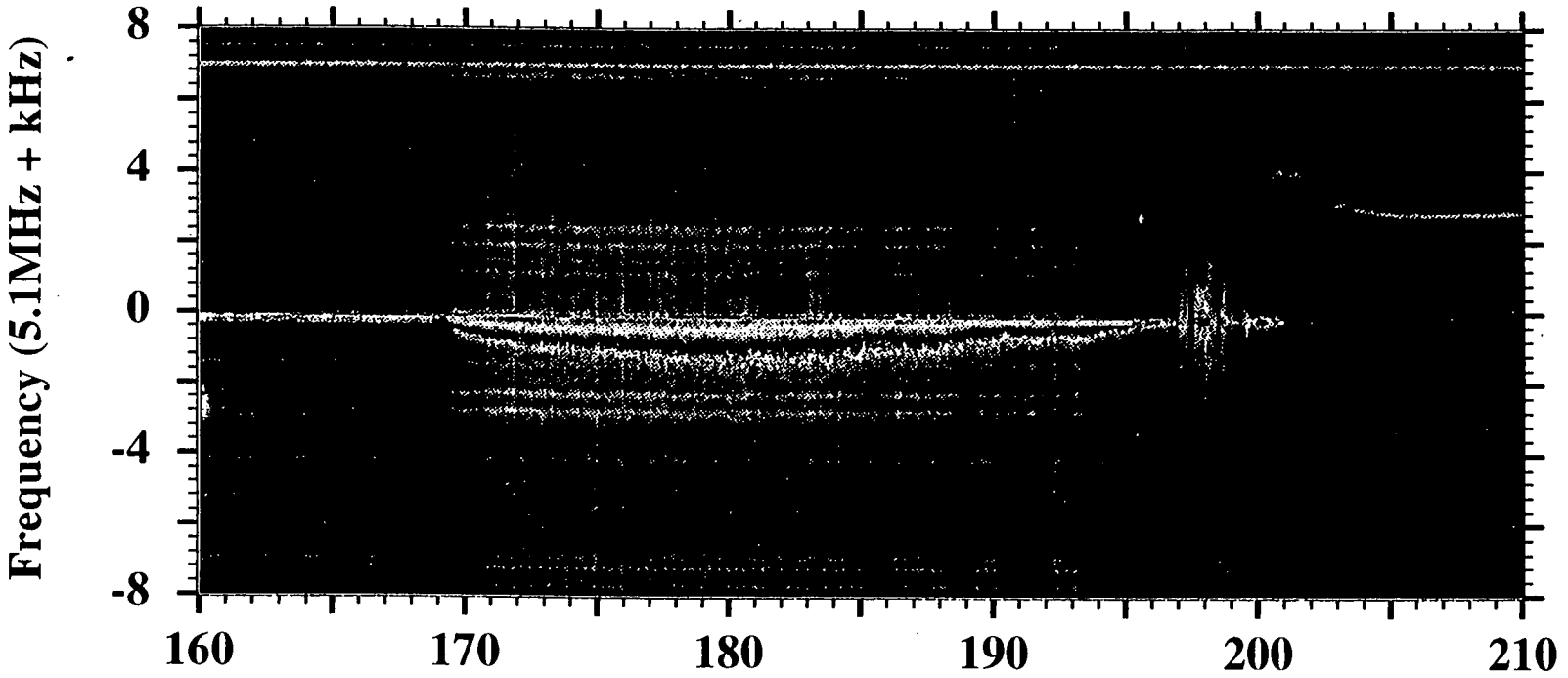

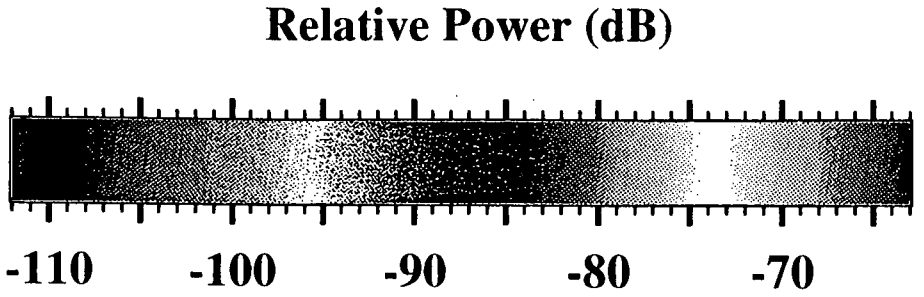

Figure 7

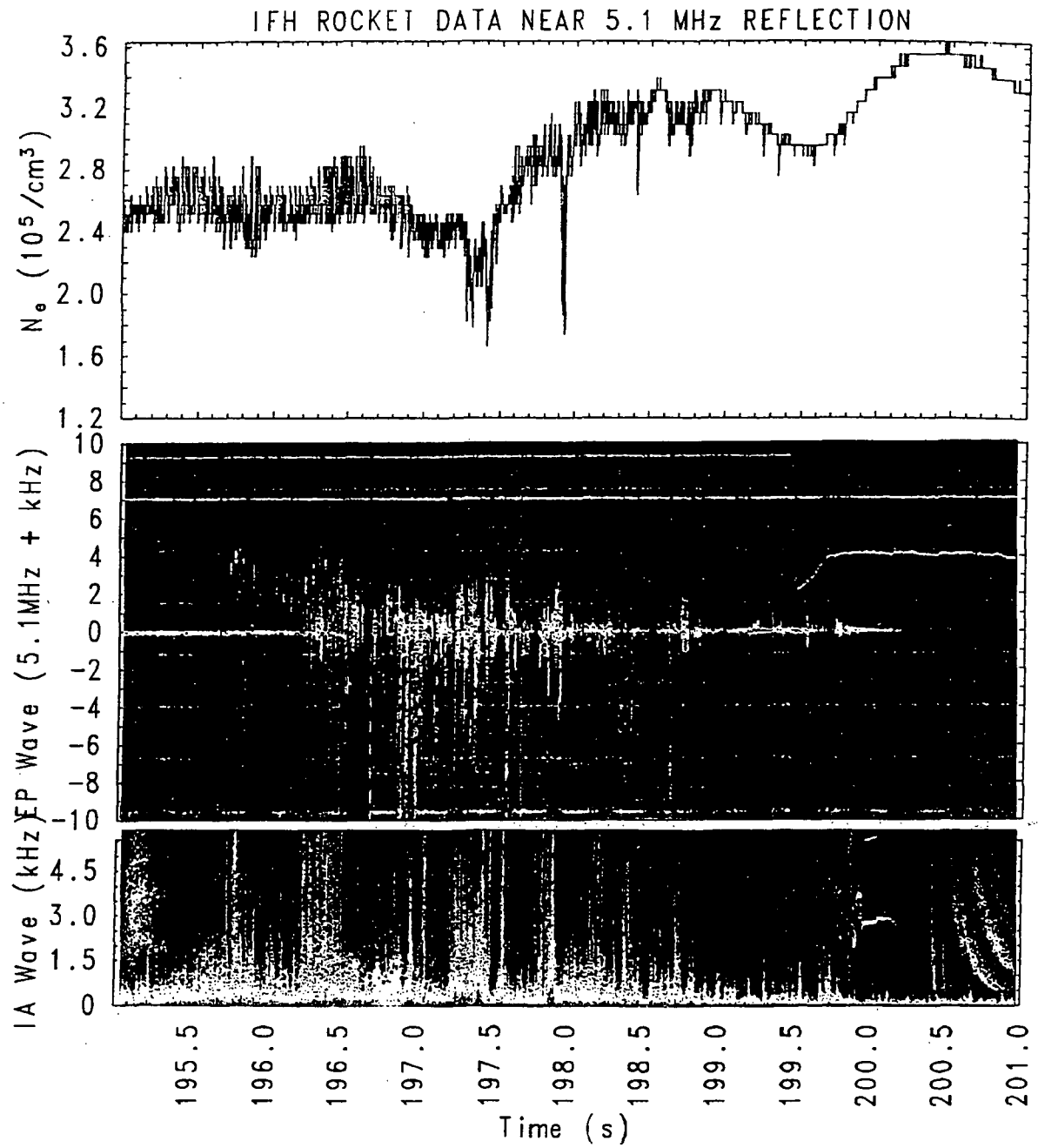
IFH ROCKET DATA NEAR 5.1 MHz REFLECTION
N_e (10^5/cm^3)
3.6
3.2
2.8
2.4
2.0
1.6
1.2
EP Wave (5.1MHz + kHz)
10
8
6
4
2
0
-2
-4
-6
-8
-10
IA Wave (kHz)
4.5
3.0
1.5
0
195.5
196.0
196.5
197.0
197.5
198.0
198.5
199.0
199.5
200.0
200.5
201.0
Time (s)

Figure 8

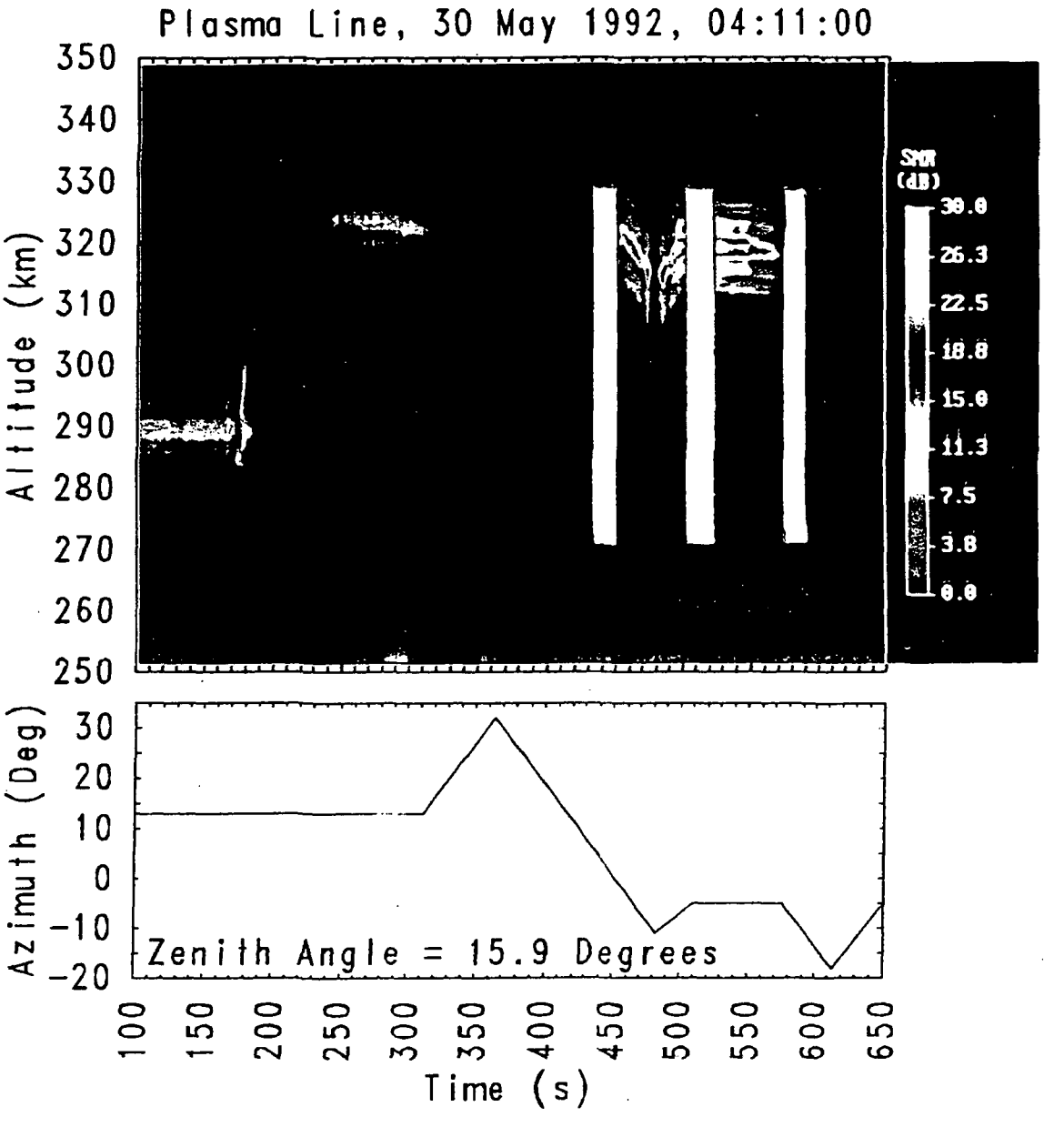
Plasma Line, 30 May 1992, 04:11:00
Altitude (km)
350
340
330
320
310
300
290
280
270
260
250
SNR (dB)
30.0
26.3
22.5
18.8
15.0
11.3
7.5
3.8
0.0
Azimuth (Deg)
30
20
10
0
-10
-20
Zenith Angle = 15.9 Degrees
100
150
200
250
300
350
400
450
500
550
600
650
Time (s)

Figure 9.

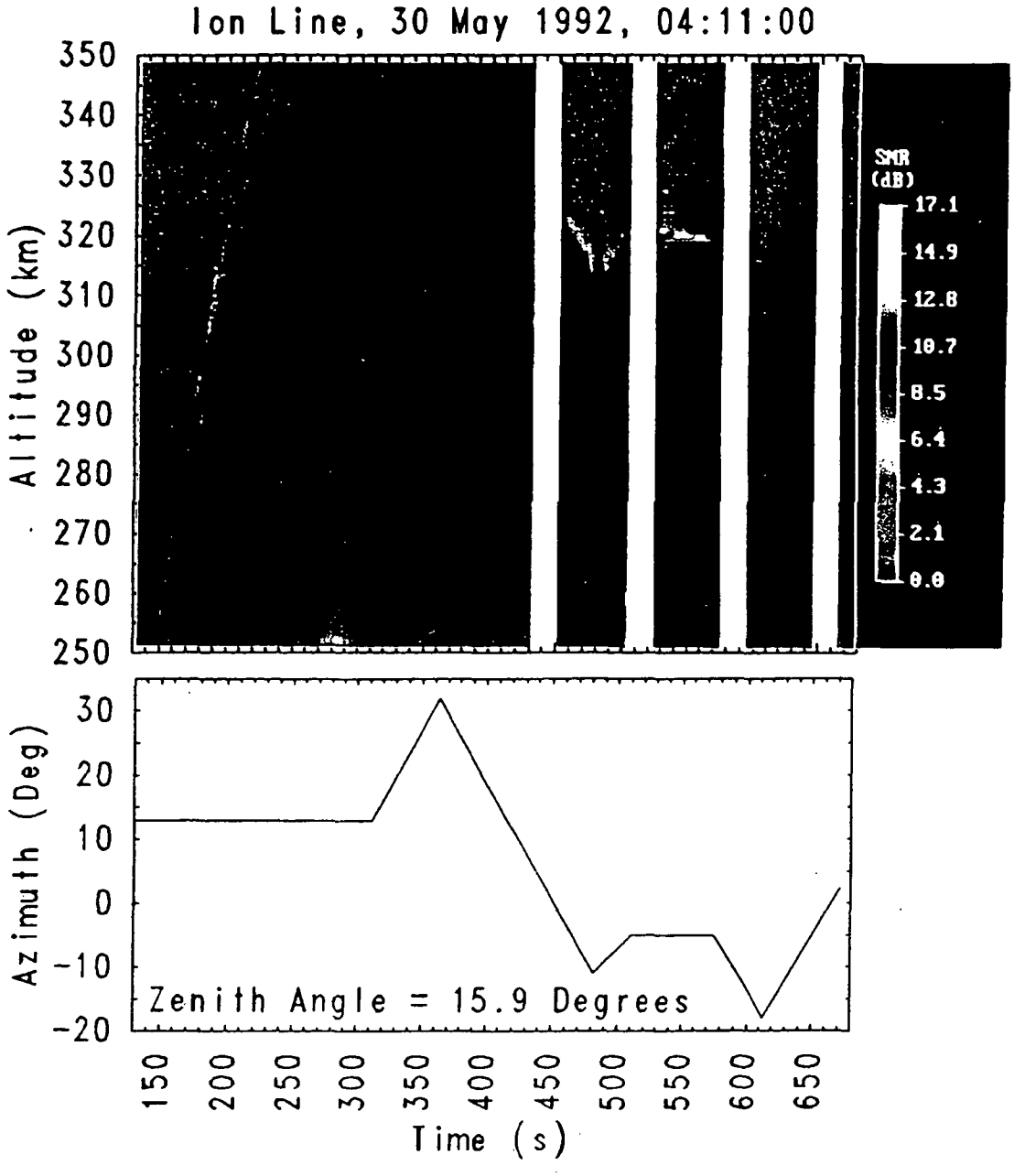
Ion Line, 30 May 1992, 04:11:00
Altitude (km)
350
340
330
320
310
300
290
280
270
260
250
SNR (dB)
17.1
14.9
12.8
10.7
8.5
6.4
4.3
2.1
0.0
Azimuth (Deg)
30
20
10
0
-10
-20
Zenith Angle = 15.9 Degrees
150
200
250
300
350
400
450
500
550
600
650
Time (s)

Figure 10

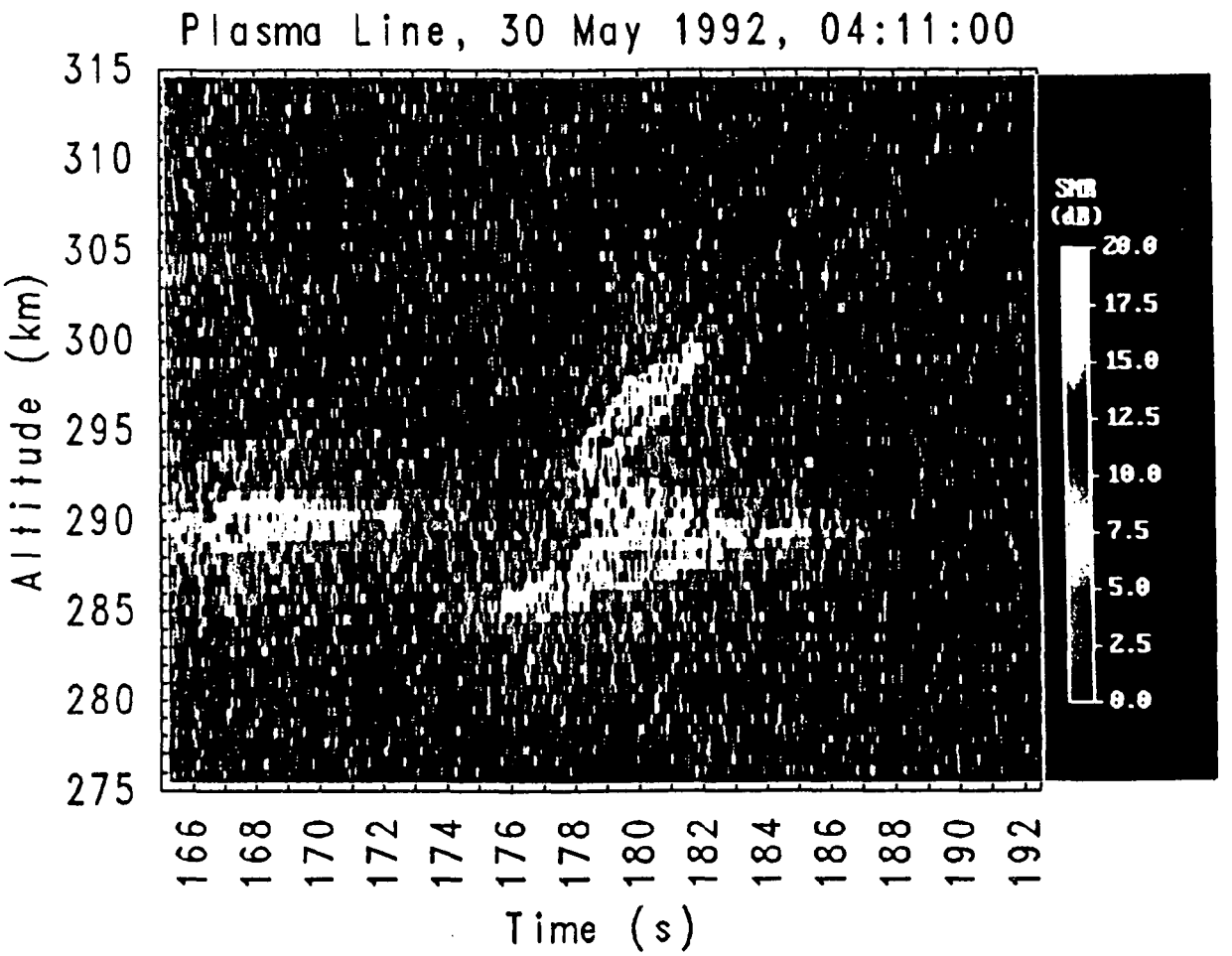
Plasma Line, 30 May 1992, 04:11:00
Altitude (km)
315
310
305
300
295
290
285
280
275
166
168
170
172
174
176
178
180
182
184
186
188
190
192
Time (s)
SNR (dB)
20.0
17.5
15.0
12.5
10.0
7.5
5.0
2.5
0.0

Figure 11

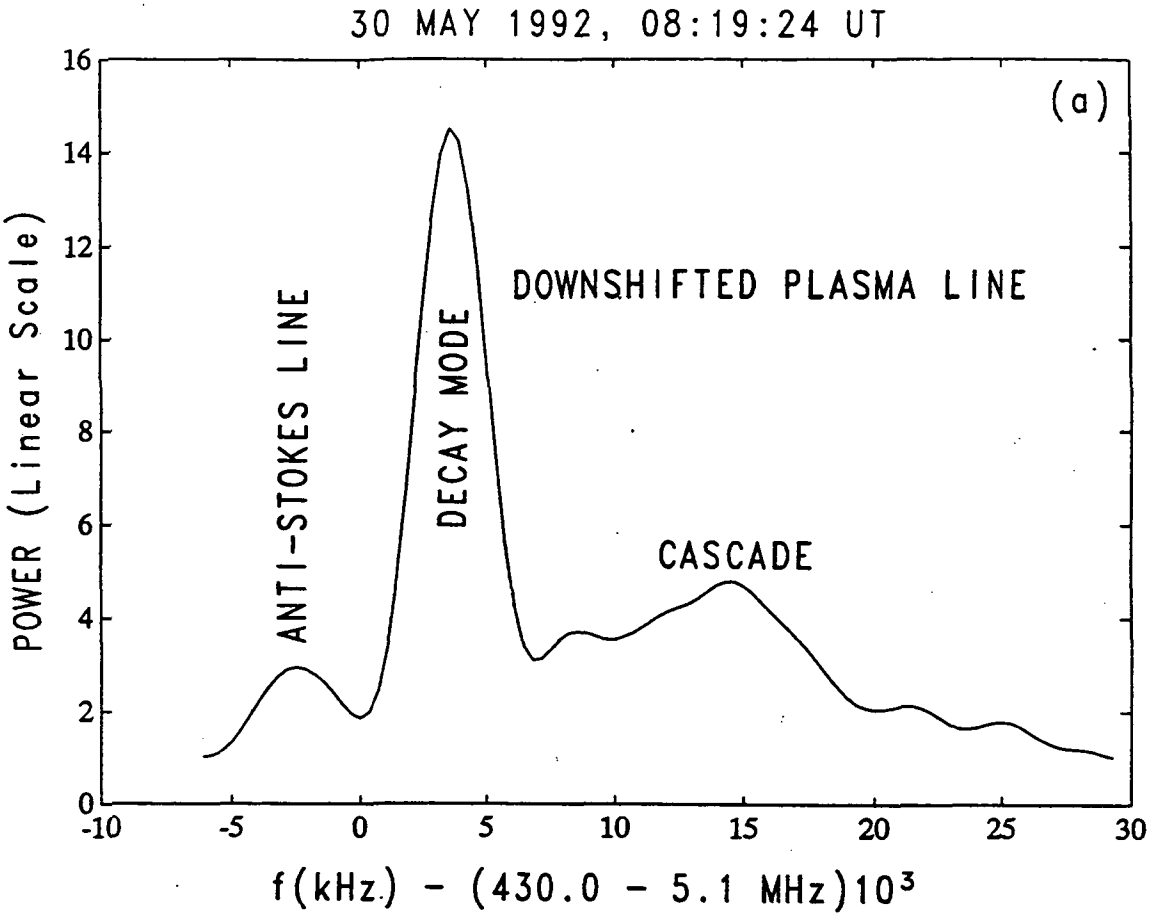
30 MAY 1992, 08:19:24 UT
(a)
POWER (Linear Scale)
ANTI-STOKES LINE
DECAY MODE
DOWNSHIFTED PLASMA LINE
CASCADE
f(kHz.) - (430.0 - 5.1 MHz)10³

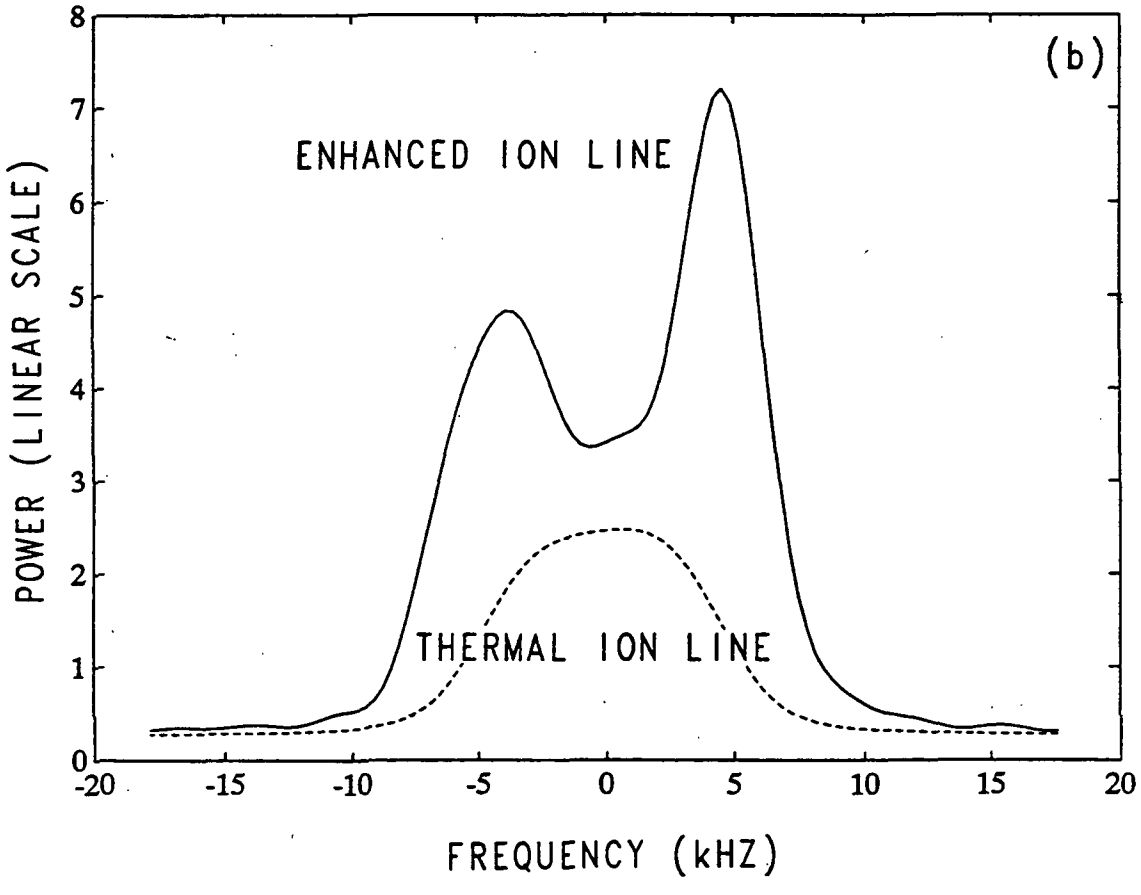
(b)
POWER (LINEAR SCALE)
ENHANCED ION LINE
THERMAL ION LINE
FREQUENCY (kHZ)

Figure 12.

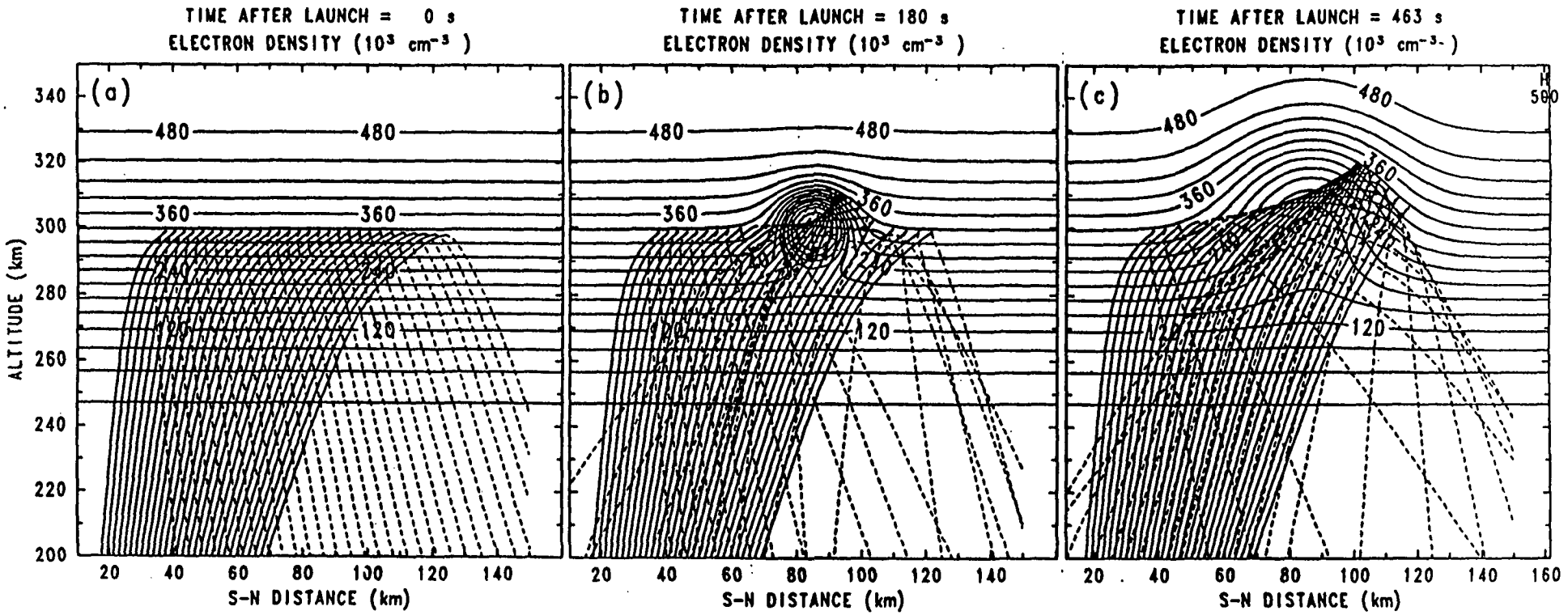
TIME AFTER LAUNCH = 0 s
ELECTRON DENSITY (10^3 cm^{-3})
TIME AFTER LAUNCH = 180 s
ELECTRON DENSITY (10^3 cm^{-3})
TIME AFTER LAUNCH = 463 s
ELECTRON DENSITY (10^3 cm^{-3})
(a)
(b)
(c)
480
360
240
120
ALTITUDE (km)
S-N DISTANCE (km)

Figure 13.

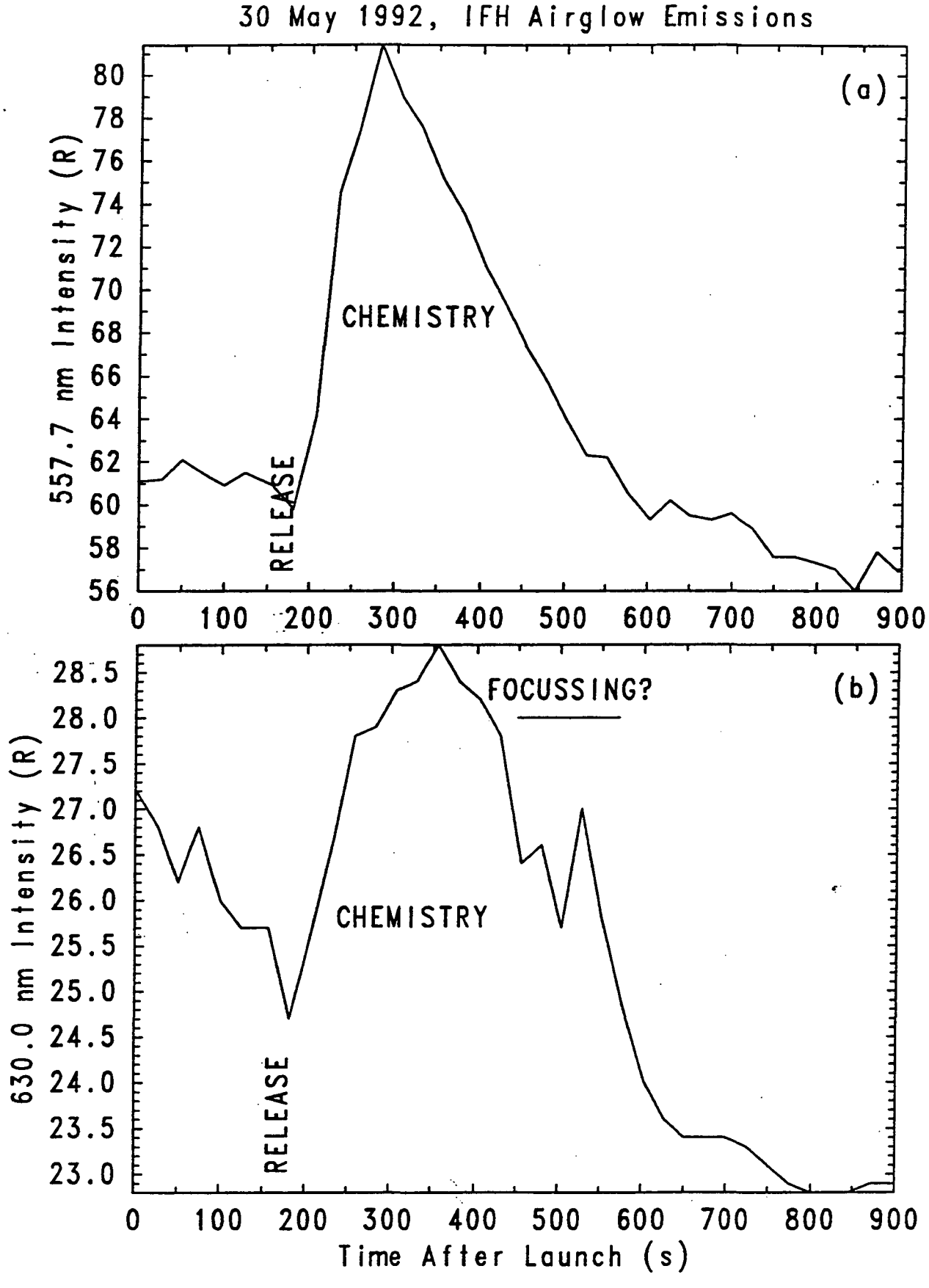
30 May 1992, IFH Airglow Emissions
(a)
557.7 nm Intensity (R)
80
78
76
74
72
70
68
66
64
62
60
58
56
CHEMISTRY
RELEASE
0
100
200
300
400
500
600
700
800
900
(b)
630.0 nm Intensity (R)
28.5
28.0
27.5
27.0
26.5
26.0
25.5
25.0
24.5
24.0
23.5
23.0
FOCUSSING?
CHEMISTRY
RELEASE
Time After Launch (s)

Figure 14.

4. Incoherent Scatter Observations during Releases AA-1/AA-7 and AA-3b

In this section, the primary results of Arecibo 430 MHz observations are presented for the AA-1/AA-7 releases and the AA-3b release. During the AA-1 and AA-7 releases, a 49.92 MHz radar interferometer was also deployed by Geospace Research, Inc. on the island of Antigua . This radar served as a sensitive diagnostic of geomagnetic field-aligned irregularities in the Ba^+ cloud. Indeed, during the AA-2 release (which entailed use of the Arecibo high-power HF facility) this radar system played a key role in establishing the linkage between field-aligned irregularity formation and the nature of Langmuir turbulence excited by the HF beam in the Ba^+ cloud (Section 2). AA-1 and AA-7 involved the release of Ba in the ionosphere near 250 km altitude in the absence of any HF modifications. No echoes from geomagnetic field-aligned irregularities were detected with the VHF radar during either of these releases. This is presumably the result of the high release altitudes employed for the two experiments. However, the explosive Ba release events of AA-1 and AA-7 were detected with the VHF radar system. The echoes observed at the moment of release have relatively large amplitudes; they are caused by specular reflections from the Ba^+ cloud. Initially, plasma frequencies within the cloud exceed the operating frequency of the radar (49.92 MHz). These echoes are transient in nature, lasting only ~2 s, and provide no known data of scientific interest. As a result, they are not discussed in the work presented below.

4.1 Arecibo Radar Measurements in Support of AA-1 and AA-7

The AA-1 and AA-7 releases occurred at altitudes too high to satisfy their original program objectives (which relied on the formation of plasma striations). However, they did produce important data concerning the manner in which the Ba^+ clouds develop in the natural ionosphere. The two most interesting effects involve (1) large increases in electron temperature measured in advance of the expanding Ba^+ cloud, and (2) the generation of a hot plasma column behind the Ba^+ cloud at late times (>30 s) after the release. The hot column is most likely aligned with the geomagnetic field and is depleted in electron density relative to the background plasma.

4.1.1 Description of the AA-1/AA-7 Releases

The AA-1 release took place at 05:03:33 AST on July 2, 1992, approximately 141 s after the launch at 05:01:12 AST. At the time of release the solar depression angle was 12.3°. The rocket payload consisted of 22 kg of Ba and 276 gm of Sr, which was

used as a dopant. These chemicals were carried in six canisters that were simultaneously discharged at 255 km altitude. The thermite consisted of a Ti/B mixture successfully used in other CRRES releases. At the time of release the rocket speed was 1.795 km/s. The westward, northward and vertical components of the rocket velocity were 0.271 km/s, 0.341 km/s, and 1.741 km/s, respectively. A thermite release of this type produces shells of neutral gas that expand radially relative to the rocket velocity. During prior CRRES releases involving the Ba/Ti/B mixture [e.g., Bernhardt *et al.*, 1993], the mean radial expansion speed was found to be ~1.4 km/s with a thermal spread of roughly ± 0.3 km/s relative to the mean. An overview of the release geometry and the locations of several essential ground sites is provided in Figure 1. The AA-1 release point, like many of the *El Coqui* campaign chemical releases, was positioned well inside the viewing limits of the Arecibo 430 MHz radar beam (i.e. within 20° of the zenith). At time of the release the radar beam was stationary and pointed 15° from the zenith. The viewing direction was slightly east (1.8° azimuth) of geographic north. The horizontal separation between the release point and radar beam location at the release height was ~16.4 km.

The AA-7 release took place two days after AA-1 on July 4, 1992. Launch occurred at 04:58:00 AST, and the chemicals were discharged 141 s after launch at 05:00:21 AST. At the moment of release, the solar depression angle was 12.2°. The release payload was identical to that of AA-1. At the time of release the rocket was at 254 km altitude, and its speed was 1.803 km/s. The westward, northward and vertical components of the rocket velocity were 0.351 km/s, 0.432 km/s, and 1.715 km/s, respectively. As in the case of AA-1, the Arecibo radar beam was stationary at the time of release. It was pointed slightly east of geographic north (3.9° azimuth) at a zenith angle of 15°. The horizontal distance between radar beam location at the release altitude and the release point was ~4.7 km, considerably less than in AA-1 (see Figure 1).

The vaporization efficiency is estimated to be ~40%, based on test measurements from rocket-borne Ba/Ti/B releases at Wallops Island, VA. For the AA-1 and AA-7 experiments, the predicted yield is $\sim 4 \times 10^{25}$ atoms of Ba vapor. Under full solar illumination of the cloud at UV wavelengths between 310 and 200 nm, the Ba ionization time constant is 28 s [e.g., Carlsten, 1975]. Because the neutral Ba cloud becomes optically thin within a few seconds of the release, one expects the cloud as a whole to ionize with an e-fold time of about 30 s.

4.1.2 Arecibo Radar Operations

In support of AA-1 and AA-7, special efforts were made to fully exploit the information available with the Arecibo incoherent scatter radar. This involved the deployment of a high-speed radar processor system at Arecibo by Geospace Research, Inc. (GRI). The observing program was designed to provide wideband spectral information without compromising altitude resolution or system sensitivity. Three types of phase-coded radar pulses were employed. These included a 13-baud Barker-coded pulse (BKR) having a baud length of 4 μs; a seven frequency 308-μs long pulse [Sulzer 1986], referred to as a multi-radar autocorrelation function pulse (MRACF); and a 512-baud, pseudo-random phase-coded pulse (1-μs bauds), generically termed a coded long-pulse (CLP). The three pulses were cyclically transmitted within a "frame time" of 30 ms. A frame consisted of three 10 ms interpulse periods (IPPs), one for each type of pulse. Throughout the experiment period, ionospheric backscatter from each radar pulse was simultaneously sampled at the radar center frequency (430 MHz) and across both "plasma line" sidebands (430 MHz $\pm$ f_r), where f_r is the plasma line offset frequency. The plasma line bandpasses were centered near 430 MHz $\pm$ 5.0 MHz. Appropriate filters were selected to optimize measurements made with a particular type of pulse. The spectral bandwidths of the data channels ranged from 250 kHz on the BKR ion line to 5 MHz at the upshifted and downshifted CLP plasma lines. The three pulse types were used to extract different kinds of information about the processes occurring in the Ba^+ plasma. Power profile (i.e. power versus range) measurements made with the BKR pulse had the best detection sensitivity with moderately good altitude resolution (600 m). Better altitude resolution (150 m) and wideband spectral information were obtained with the CLP with some loss of sensitivity when signals were strong. The MRACF yielded ion-line spectral information with poor (38 km) altitude resolution but with extremely good temporal resolution (6 s). A concise description of the above radar techniques is furnished by Sulzer [1989].

An important feature of the GRI data-acquisition program was that raw, unintegrated voltage samples were preserved on all data channels throughout the experiment period (~ 45 min). This made it possible to optimize temporal integration periods after the fact, change digital processing techniques as desired, and examine radar returns on a pulse-by-pulse basis to explore interesting events.

4.1.3 Radar Results

As noted above, the AA-1 and AA-7 releases occurred at altitudes too high to readily generate plasma striations. This was confirmed with in 2-D simulation of the CRRES release conducted by J. D. Huba of the Naval Research Laboratory. Nevertheless, extremely interesting plasma heating phenomena were observed with the Arecibo radar. The absence of plasma striations will simplify the interpretations of these results.

Figure 2 shows backscatter power measured with the 430 MHz radar during the AA-1 experiment. These data were acquired with BKR pulses. Figure 2 is a temporal expansion of the AA-1 data presented in Section 1 (Figure 2, Section 1). The ionospheric backscatter power is directly proportional to electron density and inversely proportional to the quantity $[1 + T_e/T_i]$, where T_e and T_i are the electron and ion temperatures, respectively. During the observations of Figure 2, the radar beam was initially positioned at a zenith angle of 15° and at the azimuth of the nominal release location (1.8° azimuth). Azimuth scans were initiated at 212 s relative time in Figure 2. The release event occurred at 138 s. The faint, vertical streak seen near 138 s at ~250 km altitude is the rocket and/or release event as seen through a high order sidelobe of the radar beam. This echo lasts for about 1 s (141.3 s after launch until 142.2 s after launch). It is currently not known whether this echo is caused by the rocket body itself or by a strong specular return off the early time Ba^+ cloud. It appears that the echo is closely tied to the release event itself. Within ~2 s of the release, a decrease is backscatter cross section is evident over roughly a 10 km altitude band centered on 250 km altitude. This depletion persists for approximately 10 s; thereafter an enhancement in backscatter cross section is evident. A series of electron density profiles obtained near the time of release is displayed in Figure 3. Times are referenced to the release event, and the electron density scale applies to all of the data shown except for the enhancement at the rocket/release event and the depletions evident at this altitude immediately thereafter.

The increase in backscatter cross section signals the arrival of Ba^+ ions in the radar field-of-view. As noted above, the horizontal separation between the release point and radar beam location at the release height was ~16.4 km. The Ba^+ ions required ~12 s to reach the radar beam after the release. This implies a travel speed of 1.4 km/s. Notice that the depletion in cross section persists at altitudes immediately below the Ba^+ cloud.

An essential question to be addressed is whether the depletion in cross section during AA-1 is caused by a reduction in electron density, an increase in the T_e/T_i ratio, or a combination of the two effects. To resolve this issue, spectral information at the

radar center line (so-called ion line) must be examined. This was done by processing data acquired with coded long-pulse (CLP) pulses. To obtain reasonable statistical accuracy for this measurement, radar data were averaged over the time interval 4.8 s to 10.2 s after the release. During this period, the depletion was most pronounced and had the best altitude definition. Random measurement errors were further reduced by averaging the spectral data in altitude. (Statistically independent CLP spectra are obtained at 150-m range intervals.) A BKR electron density profile obtained for the time period is mentioned above is shown in Figure 4. Spectra acquired with the CLP technique during the period are displayed in Figure 5. The three data panels show the incoherent backscatter spectrum below the depletion, in the center of the depletion, and above it. Notice the large change in spectral shape within the depletion.

When analyzed and interpreted within the context of incoherent scatter theory, the results of Figure 5 indicate that natural O^+ ions represent the dominant ion constituent at all altitudes shown. This verifies that large numbers of Ba^+ ions had not yet reached the radar viewing location. The temperature measurements above and below the depletion (T_e = 821 and 816 K; T_i = 714 and 788 K) are characteristic of the background ionosphere under summertime conditions at dawn. The incoherent scatter spectrum obtained within the depletion indicates that both T_e and T_i are elevated above their respective background values, with the electron temperature being greatly enhanced. The increase in T_i is consistent with the expected energy transfer between the hot electron gas and the ion gas through local collisional processes.

The ratio of T_e/T_i obtained within the depletion region (T_e/T_i = 2.6) can be used to correct the incoherent scatter cross section for its dependence on T_e/T_i (discussed above). When this correction is made, it is found that the depletion of Figure 4 is totally explained on the basis of an elevated T_e/T_i ratio alone and that no significant depletion in electron density has occurred. Thus, the background electron density profile (dot-dash curve in Figure 4) has not changed. Similar studies indicate that depletions in incoherent scatter cross section observed at lower altitudes after the Ba^+ ions arrive are also caused by increased values of T_e/T_i in a plasma that contains primarily O^+ ions.

The early time response of ionospheric plasma during AA-1 can be characterized as follows. There was no change in the background plasma viewed by the Arecibo radar within 2 s of the release. During the period 2 - 12 s after the release, greatly elevated electron temperatures were observed over an ~10 km altitude interval (centered on the release altitude). This occurs in advance of the bulk of the Ba^+ cloud, which arrives in the radar field-of-view ~12 s after the release. Even in the presence of the Ba^+ cloud, enhanced electron temperatures persist in the background ionosphere below the cloud.

This temperature enhancement disappears approximately 20 s after the arrival of the Ba^+ ions.

Electron heating prior to the arrival of Ba^+ ions in the radar field-of-view was also observed during the AA-2 experiment (Section 2). However, the AA-2 release occurred in a background ionospheric plasma having significantly less electron density than with AA-1. As a result, the statistical measurement errors were somewhat greater. In the case of AA-7, no such measurements were possible because the flight path of the rocket came much closer to the Arecibo radar beam at the release altitude. This is illustrated in Figure 6, which offers expanded altitude coverage of the AA-7 data shown in Section 1 (Figure 3, Section 1). The large echo from the rocket body saturates the radar receiver at the release altitude for ~8 s following the release. Initially, the radar beam was pointed at a fixed location (zenith angle = 15°, azimuth = 3.9°), but at 241 s relative time azimuth scans across the Ba^+ cloud were initiated. During the first return scan across the cloud, a large depletion in backscatter return is evident above the cloud. The corresponding magnetic flux tube maps to lower altitudes behind the cloud. The development of a large depletion above the Ba^+ cloud appears to be primarily a late time phenomenon. In Figure 6, a mild depletion forms above the cloud within a minute of the release, but large depletions are only observed in the late time environment (> 5 min after release). This type of effect was observed both during AA-7 and AA-1.

An example of an electron density profile illustrating the depletion in backscatter cross section is provided in Figure 7. The large peak near 240 km is the Ba^+ cloud; the cloud has sunk in altitude relative the release height because of gravity. In Figure 7, the measured backscatter is correctly represented as electron density at all altitudes except between 255 and 300 km, where a depletion is evident relative to the background profile (dashed curve in Figure 7 measured ~2 min earlier). As noted above, a depletion in incoherent backscatter may arise because of elevated T_e/T_i and/or a reduction in electron density. Spectral analyses of the incoherent scatter "ion line" are required to make this determination.

In Figure 8, CLP spectral measurements simultaneously made during the observing period of Figure 7 are presented. Analyses of these spectra within the context of incoherent scatter theory yield the physical parameters of interest to this study [e.g., Sultan *et al.*, 1992]. The spectrum in the bottom panel was obtained in the topside of the Ba^+ cloud; it shows that the Ba^+ is the dominate ion in the plasma and that the electron temperature is elevated relative to the ion temperature (T_e/T_i = 1.8). The elevated electron temperature is believed to be caused by the continuous "pumping" of the Ba cloud by solar UV radiation. A plasma cloud consisting mostly of Ba^+ (i.e. 94% Ba^+,

6% O^+) is expected because of an "electrostatic snowplow" process that excludes background O^+ ions during cloud formation (e.g., Bernhardt *et al.*, 1991; Schunk and Szuszczewicz, 1991; and references therein). The incoherent scatter spectrum obtained in the middle of the depletion (center panel in Figure 8) indicates that the ion mixture is roughly 50% Ba^+ and 50% O^+ with T_e/T_i near 2.5. These results indicate that most, but probably not all, of the cross section reduction is caused by elevated T_e/T_i. Electron density depletions that are 5 - 20% below background values are consistent random measurement errors and systematic uncertainties in the least-squares fitting of the incoherent scatter spectrum. Finally, the spectral measurements made above the depletion (upper panel, Figure 8) are similar to measurements made in the background plasma (i.e., a plasma containing dominant O^+ ions with $T_e/T_i \sim 1.1$).

4.1.4 Discussion and Conclusions

The principal observational results presented above consist of an early-time electron heating phenomenon and the development of a hot magnetic flux tube behind (i.e. to the north of) the Ba^+ cloud at late times. The hot flux tube probably has reduced electron density relative to the background ionosphere. This notion is supported by data acquired with the Digital Ionospheric Sounding System (DISS) at Ramey, Puerto Rico, which indicates the presence of an ionospheric duct behind the Ba^+ cloud (T. W. Bullett, private communication, 1993).

The causes of the two phenomena are currently not well-understood. The electron heating observed at early times during AA-1 is quite remarkable. Within ~2 s of the Ba release, significant elevations in electron temperature are observed at a point roughly 16 km away from the release point! The temperature increase is confined to a ~10 km altitude interval centered on the release altitude. The direct horizontal path between the release location and observation point crosses geomagnetic field lines at nearly a right angle.

Initially, the neutral Ba cloud undergoes photoionization because of the presence of solar UV radiation at wavelengths between 310 and 200 nm. However, the motion of the photoelectrons are restricted by the geomagnetic field (e.g., the electron gyroradius of a 10 eV electron traveling perpendicular to the geomagnetic field is ~2 cm). Neutral waves (e.g., shock waves) initiated by the release could readily move across field lines, but this does not provide a reasonable explanation for the radar observations. The associated waves would have to propagate at a very large velocity (~8 km/s). Moreover, significant ion heating that would be expected to accompany a large shock wave is not observed. In addition, the observed electron temperature enhancement occurs over a

relatively-narrow, sharply-defined altitude interval rather than a broad, extended height range anticipated for a spherically expanding wavefront.

Impulsive electric/electromagnetic fields generated by the release event might serve as a source for the observed electron heating. In this case, wave propagation speeds and the rate of collisional dissipation of the wave(s) would determine the onset time of the electron heating measured with the radar. Because the electron temperature enhancement is narrowly confined to altitudes surrounding the release height, propagational geometries perpendicular, or nearly perpendicular, to the geomagnetic field are needed. For example, the impulsive emission of large amplitude upper hybrid waves/electron Bernstein modes could provide the source for the electron temperature enhancement. The source mechanism is currently the subject of a highly focused study.

The late-time formation of a hot flux tube adjacent to the Ba^+ cloud is also an unanticipated result with no readily available interpretation. Presumably, this situation arises, at least in part, because of electrodynamical and chemical processes that take place in the ionosphere. It is possible that the radar consistently viewed the southward portion of the Ba^+ cloud, and that the northward extension of the cloud crosses the observed hot flux tube. This could provide the source of electron heating. Analyses of optical observations made during AA-1/AA-7 are needed to establish the location of the radar beam within the Ba^+ cloud. At the time of this writing, a detailed explanation of the late-time radar observations does not exist.

4.2 Arecibo Radar Measurements in Support of AA-3b

Geospace Research, Inc. supported the AA-3b release with observations made with the 430 MHz incoherent scatter radar at Arecibo Observatory. This included the development of a measurement strategy, the acquisition of the radar data, and analysis of selected results. To date, these analyses have been limited to key features in data acquired during release A. This release occurred on the upleg of the AA-3b rocket and could be directly viewed with the Arecibo radar.

4.2.1 Description of the AA-3b Releases

Three release events took places as part of the AA-3b experiment. The payload for release A consisted of 712 g of Ba and 38 g of Li. This release was performed on the upleg of the flight near 290 km altitude. Rocket-borne diagnostics were positioned to view this release parallel to geomagnetic field lines. The chemical payload for release B was identical to that of A. Release B occurred at an altitude near 359 km shortly after the

rocket passed through apogee. The *in situ* diagnostic package also viewed this release along geomagnetic field lines. Finally, the contents of canisters C and D were simultaneously discharged on the downleg near 243 km altitude. Each canister contained 1,471 g of Ba and 19 g of Sr. The canisters were both ejected in the same direction across geomagnetic field lines; the diagnostic payload viewed this release perpendicular to the geomagnetic field. Release A could be observed directly with the Arecibo 430 MHz radar. However, the pointing limitations of the Arecibo antenna allowed only the magnetic flux tubes on which releases B and C+D took place to be viewed by the radar.

The focus of Arecibo radar operations was on release A. The launch of AA-3b occurred at 04:37:30 AST on June 6, 1992. Release A took place 180 s into the flight (04:40:30 AST) near the projected release altitude of 290 km. At the time of release, the solar depression angle was ~15.4°.

4.2.2 Arecibo Radar Operations

The radar observing program for AA-3b was designed to provide high temporal and spatial resolution data important for studies of the early-time release physics. This was accomplished with two types of radar pulses: a 13-baud Barker-coded pulse (BKR) having a baud length of 4 μs; and a 512-baud, pseudo-random phase-coded pulse (1-μs bauds), generically termed a coded long-pulse (CLP) [e.g., Sulzer, 1986, 1989]. Two BKR pulses and one CLP pulse were cyclically transmitted within a "frame time" of 30 ms. A frame consisted of three 10 ms interpulse periods (IPPs). During the AA-3b experiment, the ionospheric return from the BKR pulses were sampled at the radar center frequency (so-called ion line). Backscatter from CLP pulses was monitored across a 1-MHz bandpass at the ion line and across a 5 MHz-bandpass at the downshifted plasma line (centered at 430 MHz - 5 MHz). The CLP center line measurements yielded standard incoherent scatter ion-line spectra with 150-m range resolution, whereas the plasma line channel was used to monitor echoes generated by suprathermal electrons.

4.2.3 Radar Results

During the AA-3b experiment, the Arecibo radar beam was initially directed toward the exact location of release A (zenith angle = 14.6°, azimuth = 28.2°). This was accomplished with an updated estimate of the rocket trajectory 60 s into the flight. The radar pointing remained fixed until 307 s after launch (04:42:37 AST). Thereafter, the beam was steered toward the geomagnetic flux tube of release B (zenith angle = 14.6°, azimuth 9.1°) and subsequently scanned in azimuth.

Backscatter power measured with the Arecibo incoherent scatter radar during the Ba/Li releases is displayed in Figure 9. These data were acquired with BKR pulses. Releases A and B take place at 180 s and 365 s, respectively, in this display. The figure shows radar backscatter power (color scale) versus altitude and time relative to the launch at 04:37:30 AST. After launch, the radar beam was steered to the projected point of the first release. In so doing, the radar was aimed directly at the rocket. At the earliest times in the figure, only noise is evident because the radar receiver was taken off line during the period of re-pointing. The large echo with the curved trajectory is caused by the rocket passing through the main lobe of the radar beam. The rocket echo saturated the sensitive radar receiver, and in this case the color scale at right is wrapped many times. The weaker streaks seen below the rocket are believed to be echoes from payload doors ejected earlier in the flight.

During release A, approximately 712 gm of Ba and 38 gm of Li were explosively released in the middle of the radar beam at 290 km altitude. Surprisingly, this release produced a decrease in radar backscatter rather than an increase expected because of the rapid ionization of neutral Ba. As noted above, the radar beam remained pointed at the release location until 307 s after launch; subsequently the beam was repositioned in azimuth to intersect the geomagnetic flux tube of the second release point (which could not be viewed directly by the radar). As the radar beam was moved, backscatter from the rocket was once again detected near 368 km altitude.

Figure 10 shows a sequence of electron density profiles beginning at the time of release A (0 s relative time in the figure). Each profile is the result of integrating 1000 BKR pulses over a 15-s interval. The saturated echo from the rocket is intentionally clipped for display purposes. In Figure 10, a depletion in backscatter is clearly evident over ~15 km altitude interval centered on the release height. As noted in the earlier discussions of AA-1/AA-7, a reduction in backscatter power may be the result of either a decrease in electron density or an elevation in T_e/T_i. Notice that the expected enhancement in electron density from the Ba^+ cloud never develops, even at late times after the release. This is somewhat surprising in light of the results of AA-2, AA-1, and AA-7.

To determine the cause of the reduction in backscatter cross section, one must perform an incoherent spectral analysis similar to that employed for AA-1. Figure 11 shows the electron density profile recorded during a time interval selected for spectral analysis. This period was chosen to be as close as possible to the release event, while avoiding unwanted saturation effects from the rocket echo (a problem for CLP analyses). The spectral results for this time period are shown in Figure 12. At the time of this

writing, no incoherent scatter analyses of these spectra have been performed. However, based on the shapes of the spectra a qualitative analysis can be performed. The spectrum in the bottom panel of Figure 12 is a background spectrum obtained below the depletion. Its shape indicates that $T_e \sim T_i < 1000$ K, under the usual assumption that O^+ is the dominant ion in the ambient ionosphere. The middle and upper panels of Figure 12 show spectral measurements obtained at the center of the depletion and the upper edge of the depletion (see Figure 11). A background measurement immediately above the depletion was not possible because of the presence of the rocket. The spectra obtained in the depletion do not exhibit features associated with a greatly elevated T_e/T_i ratio. In particular, enhanced acoustic sidebands similar to those found in the center panel of Figure 5 are absent. The spectrum in the middle panel resembles the background spectrum with the top sawed off. This spectrum is not amenable to a qualitative description within the context of incoherent scatter theory. The upper spectrum is not unlike the result expected for an O^+ plasma with $T_e/T_i \sim 1.1$. Thus, the qualitative analysis seems to imply that the depleted backscatter is largely due to a reduction in electron density. However, more detailed studies involving incoherent scatter analyses are required before this conclusion can be firmly established.

For completion, we include the results of a spectral analysis of an unsaturated echo from the "rocket." Results obtained 25 s after release A are displayed in Figure 13. This figure clearly shows that three objects constitute the "rocket" echo, each at different ranges with slightly varying Doppler shifts. One might speculate that this is the rocket payload (largest echo), canister B, and a remnant of canister A.

4.2.4 Discussion and Conclusions

Preliminary results from the AA-3b experiment indicate that release A created an ionospheric depletion rather than the expected enhancement from an ionized Ba cloud. The reason for this is currently not well-understood. At the time of the release, the height of the UV terminator is calculated to be ~258 km. Thus, the neutral Ba cloud at 290 km altitude was adequately illuminated by ionizing solar radiation.

The *total* amount of Ba in the release canister (712 gm) was much less than that of AA-1/AA-7 (22 kg) or AA-2 (35.3 kg). During AA-3b, a significant amount of Li (38 g) was released with the Ba. On the basis of test releases performed at NASA/Wallops Island Flight Facility on November 20, 1985, we assume that the vaporization efficiency of Ba is 40%. For Li, the corresponding value is ~100%. Consequently, $\sim 1.2 \times 10^{24}$ atoms of Ba and $\sim 3.3 \times 10^{24}$ atoms of Li were vaporized during release A. The mean velocity of the Li atoms is roughly four times greater than

that of the Ba atoms, which is assumed to be of the order of 1-2 km/s. This type of mixture may have pushed background O^+ outside of the region of release, while depositing only a small amount of Ba^+ in return. Once the observed large-scale (15-km) depletion develops, its lifetime (determined by cross-field plasma diffusion) is expected to be very long (> 1 hr). This assumes that no new ionization source is present. The degeneration of the depletion evident in Figure 10 is probably not related to the lifetime of the depletion. This effect is caused by the **E x B** drift of the depletion outside the volume viewed by the radar.

Optical and *in situ* data obtained in support of release A may provide important clues for understanding the development of a electron density depletion. In the near future, it is anticipated that the complete data set will be assembled. Our overall objective is to use theoretical models developed as part of the NASA/CRRES program to interpret the AA-3b radar results.

REFERENCES

Bernhardt, P. A., P. Rodriguez, C. L. Siefring, and C. S. Lin, Field-aligned dynamics of chemically induced perturbations to the ionosphere, *J. Geophys. Res.*, *96*, 13887, 1991.

Schunk, R. W., and E. P. Szuszczewicz, Plasma expansion characteristics of ionized clouds in the ionosphere: Macroscopic formulation, *J. Geophys. Res.*, *96*, 1337, 1991.

Sultan, P. J., M. Mendillo, W. L. Oliver, and J. M. Holt, Detection of artificially created negative ion clouds with incoherent scatter radar, *J. Geophys. Res.*, *97*, 4085-4097, 1992.

Sulzer, M. P., A phase modulation technique for a sevenfold statistical improvement in incoherent scatter data-taking, *Radio Sci.*, *21*, 737-744, 1986.

Sulzer, M. P., Recent incoherent scatter techniques, *Adv. Space Res.*, *9*, (5)153-(5)162, 1989.

FIGURE CAPTIONS

Figure 1. Overview of the AA-1 and AA-7 release geometries. The locations of Arecibo Observatory (AO), the Arecibo HF facility (HF), a digisonde/optical observing site at Ramey (RA), and the launch site at Tortuguero, Puerto Rico (TO) are displayed in the figure. A distance scale along the geomagnetic meridian crossing Arecibo Observatory is included for reference. The locations of the two Ba releases are shown (AA1rel and AA7rel) along with the observing points of the Arecibo diagnostic radar at the release altitudes (AA1dia and AA7dia).

Figure 2. Backscatter power measured with the Arecibo incoherent scatter radar during the AA-1 Ba release. BKR pulses were used for this display. The figure shows radar backscatter power (color scale) versus altitude and time relative to 05:01:15 AST. The actual launch time was 3 s earlier. Radar power is expressed as a signal-to-noise ratio and plotted in dB.

Figure 3. Consecutive series of electron density profiles (linear scale) measured during the AA-1 release. Individual profiles are offset by two tick marks (8×10^5 cm^{-3}). Each profile represents the average of 100 radar pulses recorded over a 3-s period. Times shown inside the plot frame are referenced to the release time; they represent the beginning times of integration periods. Error bars are ~10% of the electron density values displayed. A background profile is plotted as a dotted line for reference.

Figure 4. Electron density profile obtained shortly after the AA-1 release. A pronounced reduction in backscatter is evident near 250 km altitude. For reference, a background profile is plotted as a dot-dash line.

Figure 5. Incoherent scatter spectra simultaneously measured during the data integration period of Figure 4 (4.8 s - 10.2 s after release). The spectral data were recorded with 150-m range resolution using the CLP technique. In addition to the temporal integration, spectra from consecutive altitudes were averaged for each display. Altitude ranges of integration are shown in the upper left hand corner of each panel. Values of T_e and T_i (shown at

right) are best fits to the spectral data with an ion composition of 100% O^+.

Figure 6. Backscatter power measured with the Arecibo incoherent scatter radar during the AA-7 Ba release. BKR pulses were used for this display. The figure shows radar backscatter power (color scale) versus altitude and time relative to the launch at 04:58:00 AST. Radar power is expressed as a signal-to-noise ratio and plotted in dB.

Figure 7. Electron density profile obtained ~15-min after the AA-1 release. A pronounced reduction in backscatter is evident above the Ba^+ cloud (large peak near 240 km). For reference, a background profile is plotted as a dot-dash line.

Figure 8. Incoherent scatter spectra simultaneously measured during data integration period of Figure 7 (15 min 3 s - 15 min 18 s after release). Altitude ranges of integration are shown in the upper left hand corner of each panel. Values of T_e and T_i and the percentage of Ba^+ ions (shown at right) are best fits to the spectral data. The balance of the ions are O^+.

Figure 9. Backscatter power measured with the Arecibo incoherent scatter radar during the two Ba/Li releases of AA-3b. BKR pulses were used for this display. The figure shows radar backscatter power (color scale) versus altitude and time relative to the launch at 04:37:30 AST. Radar power is expressed as a signal-to-noise ratio and plotted in dB. The radar directly viewed the first release at 180 s after launch. For the second release (365 s relative time), the radar was pointed at the geomagnetic flux tube along which the release took place. During the first release, backscatter from the rocket saturates the radar receiver, creating an echo that is extended in range. As the radar beam was moved to monitor the second release, backscatter from the rocket was once again detected near 368 km altitude.

Figure 10. Consecutive series of electron density profiles (linear scale) measured during the release A. Individual profiles are offset by one tick mark (4 x 10^5 cm^{-3}). Each profile represents the average of 1000 radar pulses

recorded over a 15-s period. Times shown inside the plot frame are referenced to the release time; they represent the beginning times of integration periods. Error bars are ~3% of the electron density values displayed. The rocket echo is intentionally clipped in this display. For reference, a background profile is plotted as a dotted line.

Figure 11. Electron density profile highlighting the reduction in radar backscatter caused by release A. An echo from the rocket is evident beginning at 311 km altitude. For reference, a background profile is plotted as a dot-dash line.

Figure 12. Incoherent scatter spectra simultaneously measured during the data integration period of Figure 11 (23.2 s - 53.2 s after release A). Altitude intervals used for integration are shown in the upper left hand corner of each panel. Values of T_e and T_i and the percentage of Ba^+ ions have not yet been determined.

Figure 13. Analysis of the "rocket" echo recorded shortly after release A. Spectral power is shown versus Doppler frequency and radar range. These data were acquired with the CLP technique.

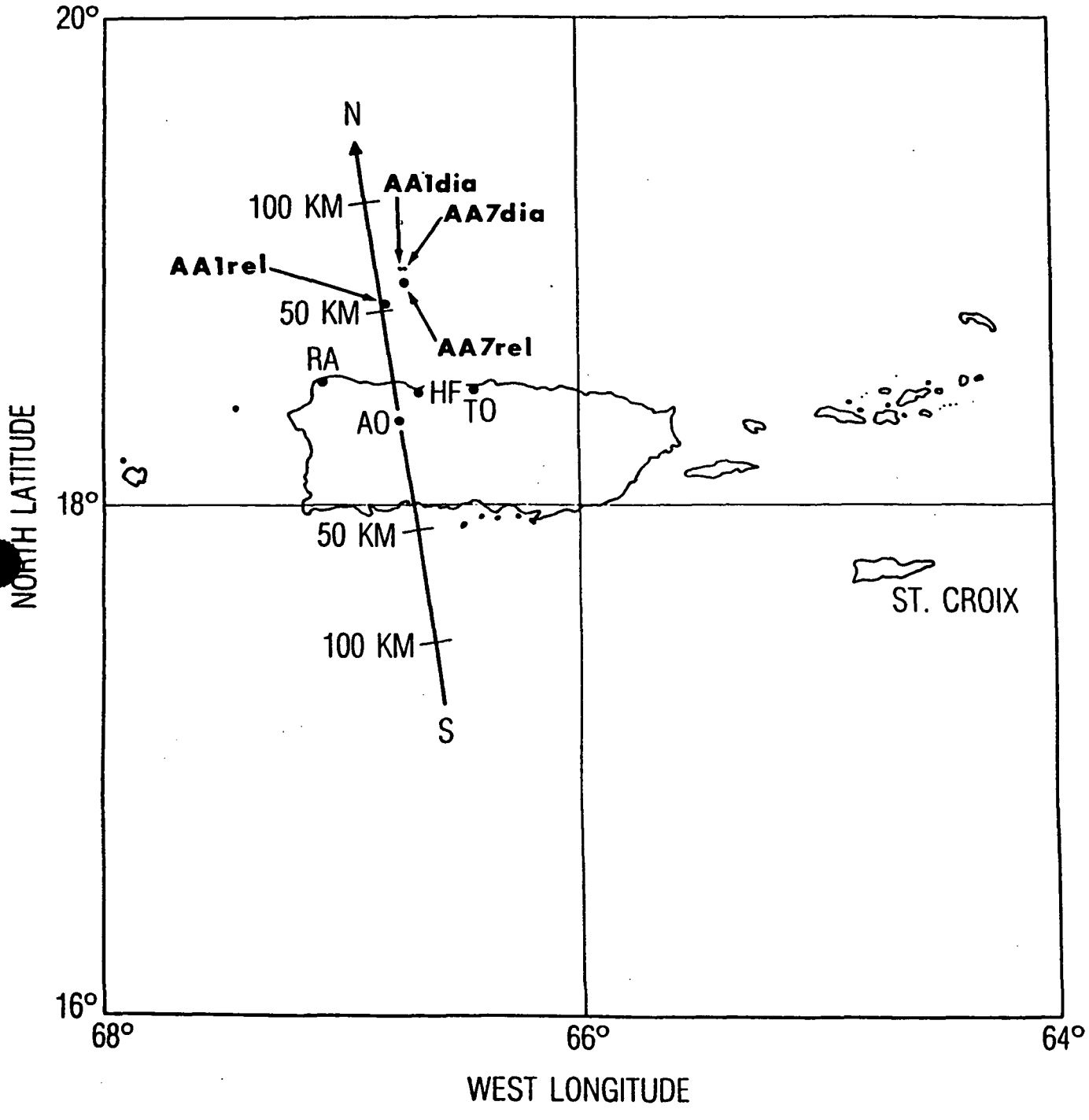
20°
18°
16°
68°
66°
64°
NORTH LATITUDE
WEST LONGITUDE
N
S
100 KM
50 KM
50 KM
100 KM
AA1dia
AA7dia
AA1rel
AA7rel
RA
HF
TO
AO
ST. CROIX

Figure 1

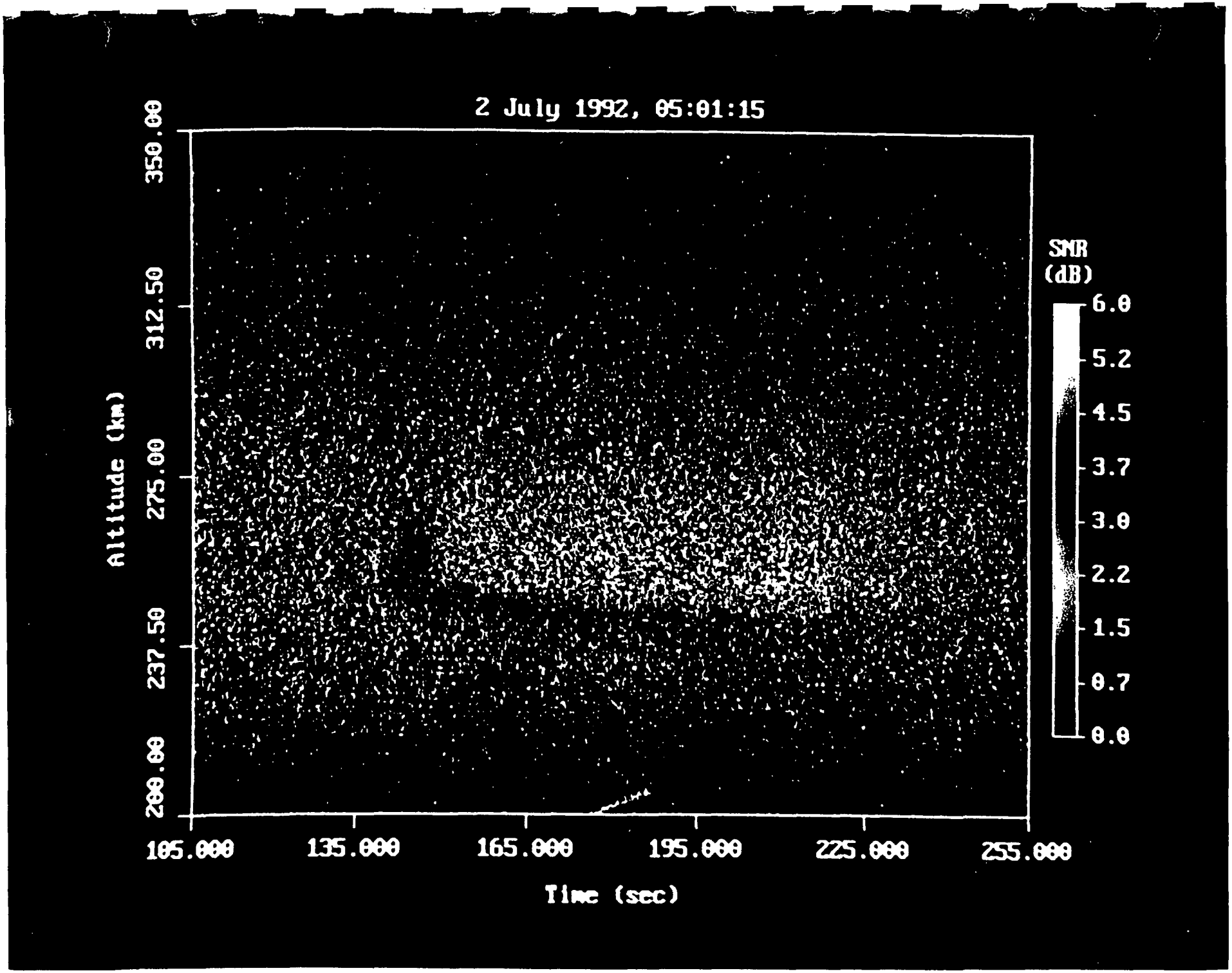
2 July 1992, 05:01:15
Altitude (km)
350.00
312.50
275.00
237.50
200.00
105.000
135.000
165.000
195.000
225.000
255.000
Time (sec)
SNR
(dB)
6.0
5.2
4.5
3.7
3.0
2.2
1.5
0.7
0.0

Figure 2

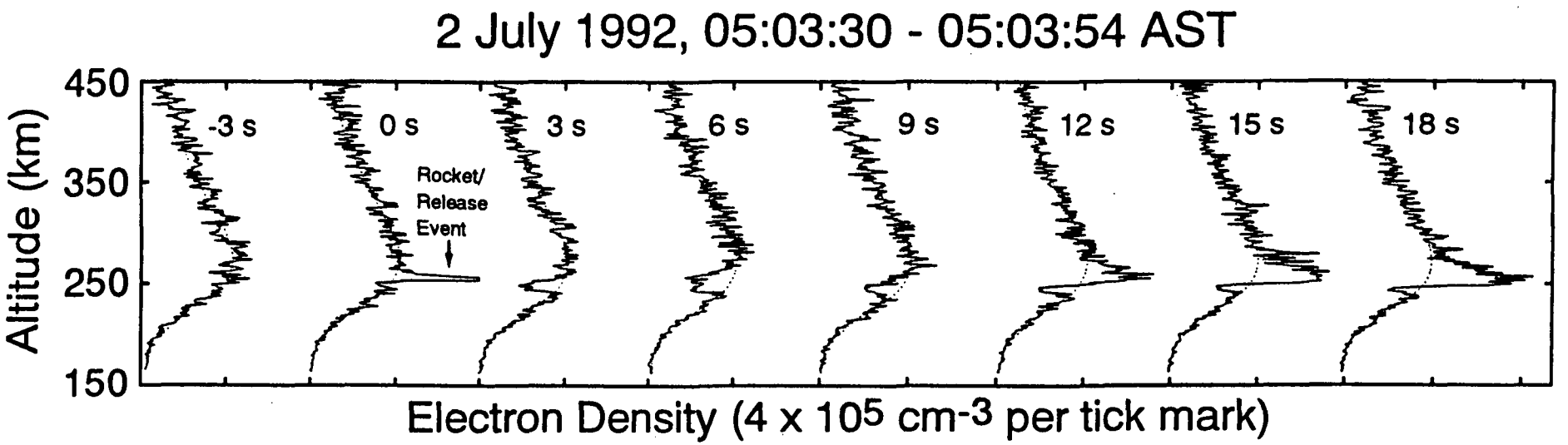
2 July 1992, 05:03:30 - 05:03:54 AST
Altitude (km)
450
350
250
150
-3 s
0 s
3 s
6 s
9 s
12 s
15 s
18 s
Rocket/
Release
Event
Electron Density (4 x 10^5 cm^-3 per tick mark)

Figure 3

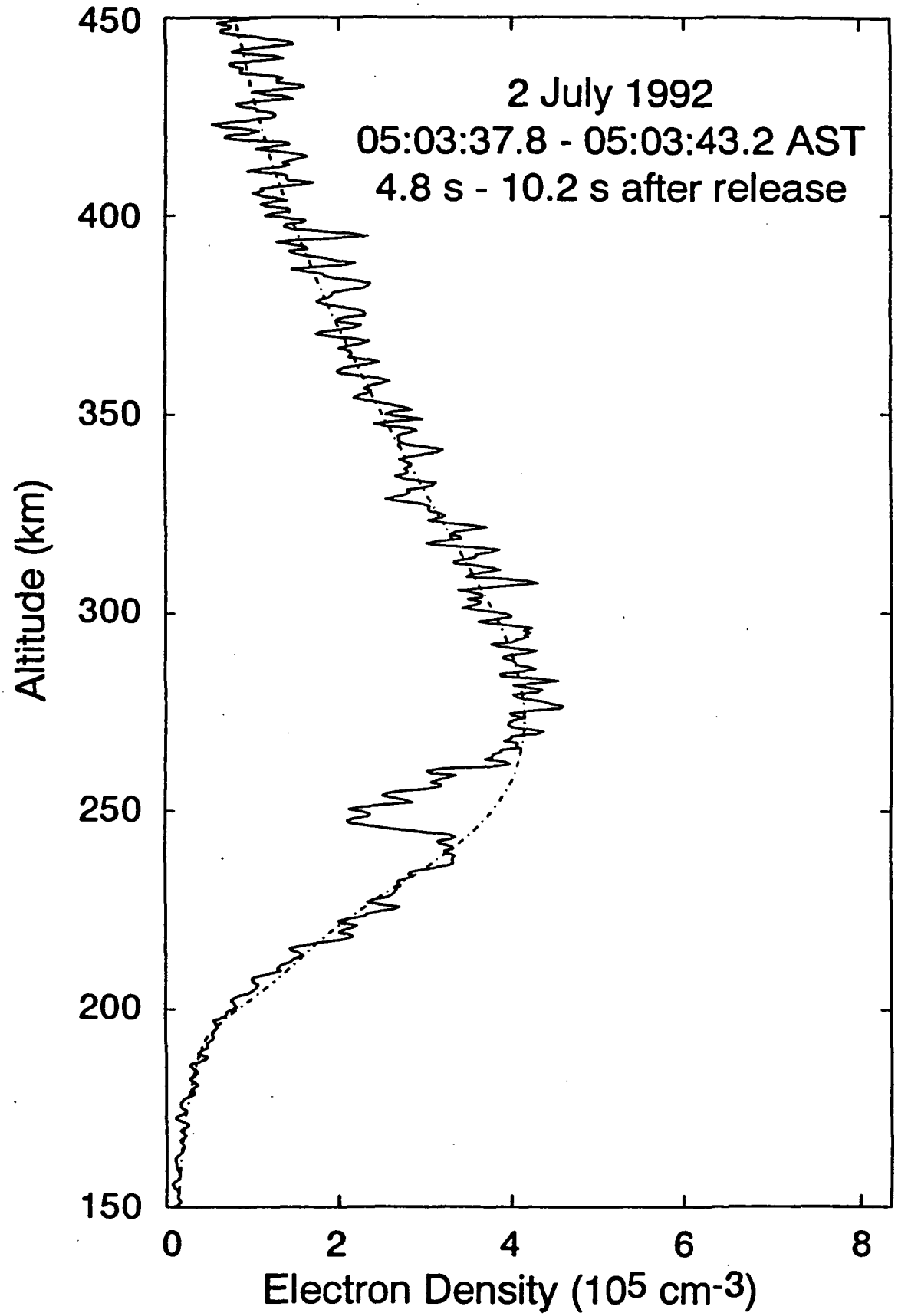
2 July 1992
05:03:37.8 - 05:03:43.2 AST
4.8 s - 10.2 s after release
Altitude (km)
450
400
350
300
250
200
150
0
2
4
6
8
Electron Density (10^5 cm^-3)

Figure 4

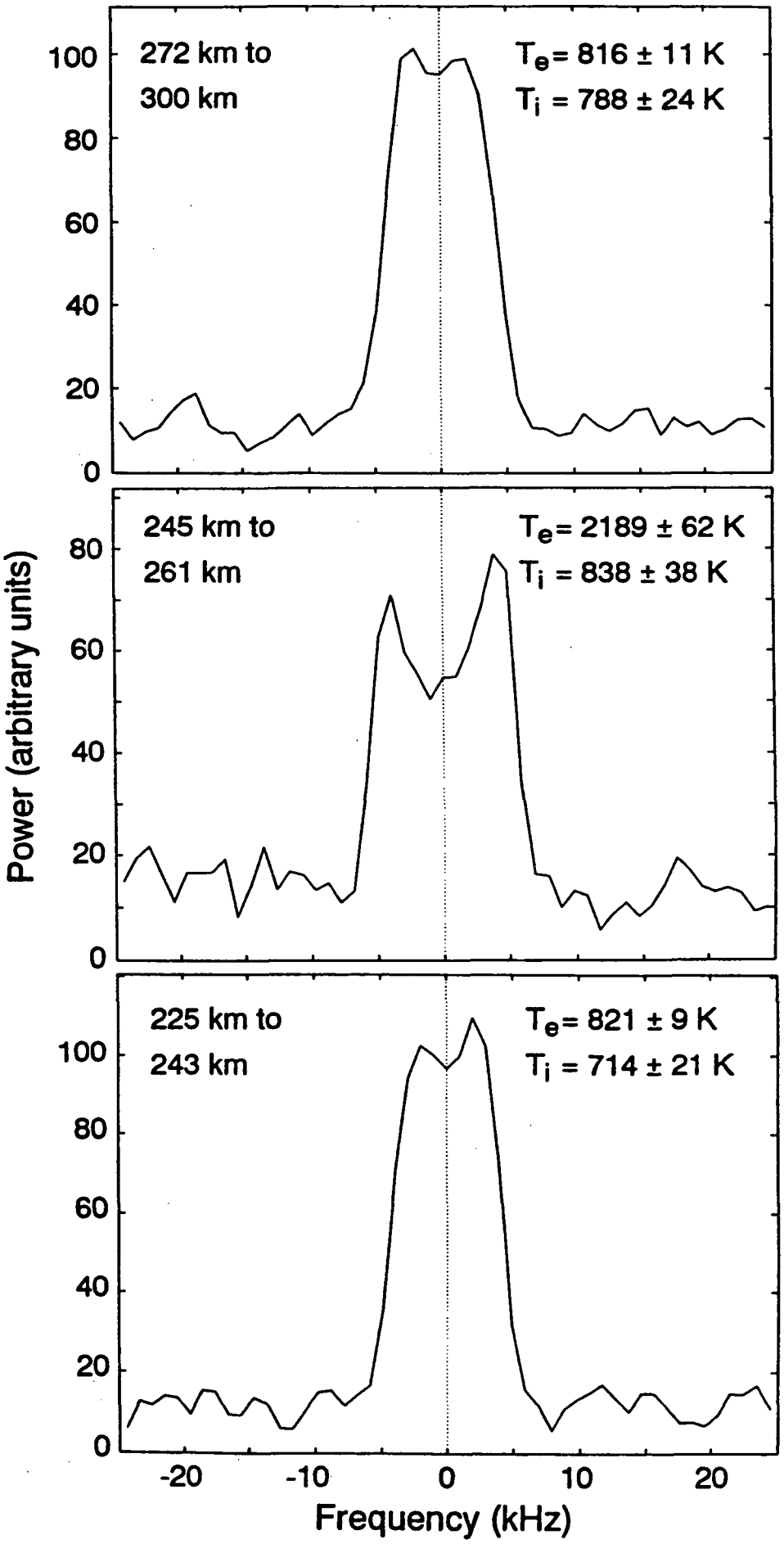
272 km to
300 km
T_e= 816 ± 11 K
T_i = 788 ± 24 K
245 km to
261 km
T_e= 2189 ± 62 K
T_i = 838 ± 38 K
225 km to
243 km
T_e= 821 ± 9 K
T_i = 714 ± 21 K
Power (arbitrary units)
Frequency (kHz)
0
20
40
60
80
100
-20
-10
0
10
20

Figure 5

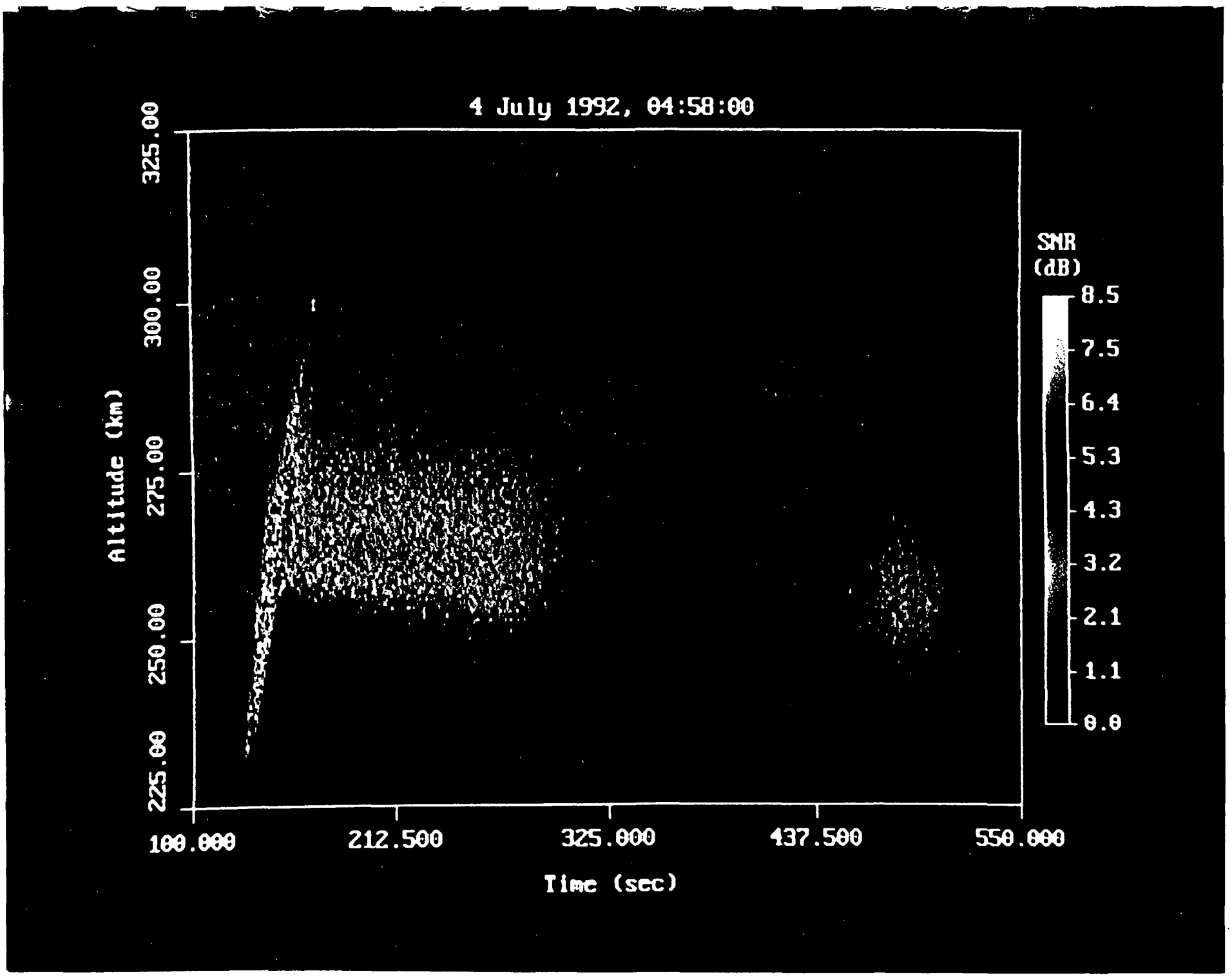
4 July 1992, 04:58:00
Altitude (km)
325.00
300.00
275.00
250.00
225.00
100.000
212.500
325.000
437.500
550.000
Time (sec)
SNR
(dB)
8.5
7.5
6.4
5.3
4.3
3.2
2.1
1.1
0.0

Figure 6

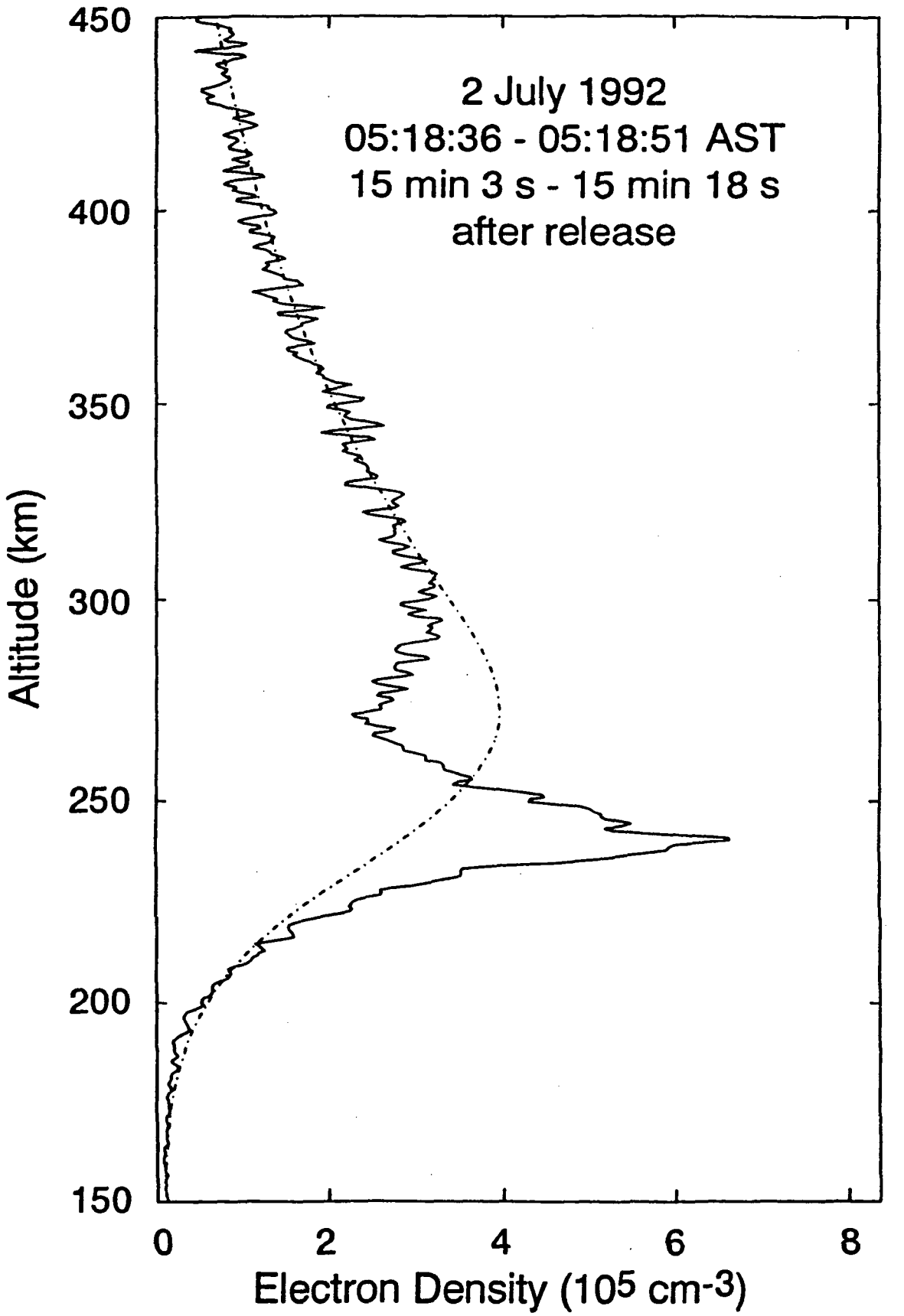
2 July 1992
05:18:36 - 05:18:51 AST
15 min 3 s - 15 min 18 s
after release
Altitude (km)
450
400
350
300
250
200
150
0
2
4
6
8
Electron Density (10^5 cm^-3)

Figure 7

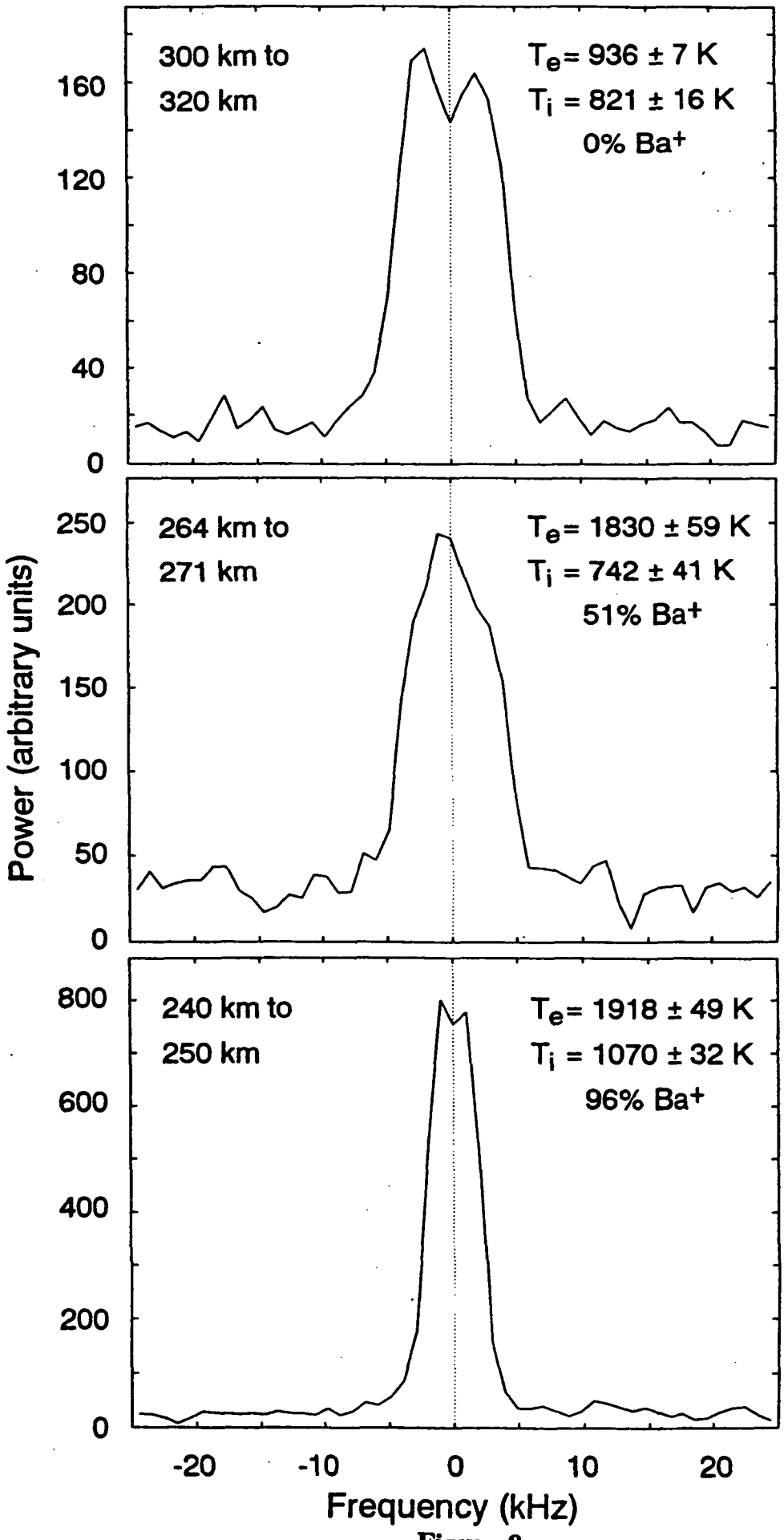
300 km to
320 km
T_e= 936 ± 7 K
T_i = 821 ± 16 K
0% Ba^+
264 km to
271 km
T_e= 1830 ± 59 K
T_i = 742 ± 41 K
51% Ba^+
240 km to
250 km
T_e= 1918 ± 49 K
T_i = 1070 ± 32 K
96% Ba^+
Power (arbitrary units)
Frequency (kHz)
0
40
80
120
160
50
100
150
200
250
200
400
600
800
-20
-10
0
10
20

Figure 8

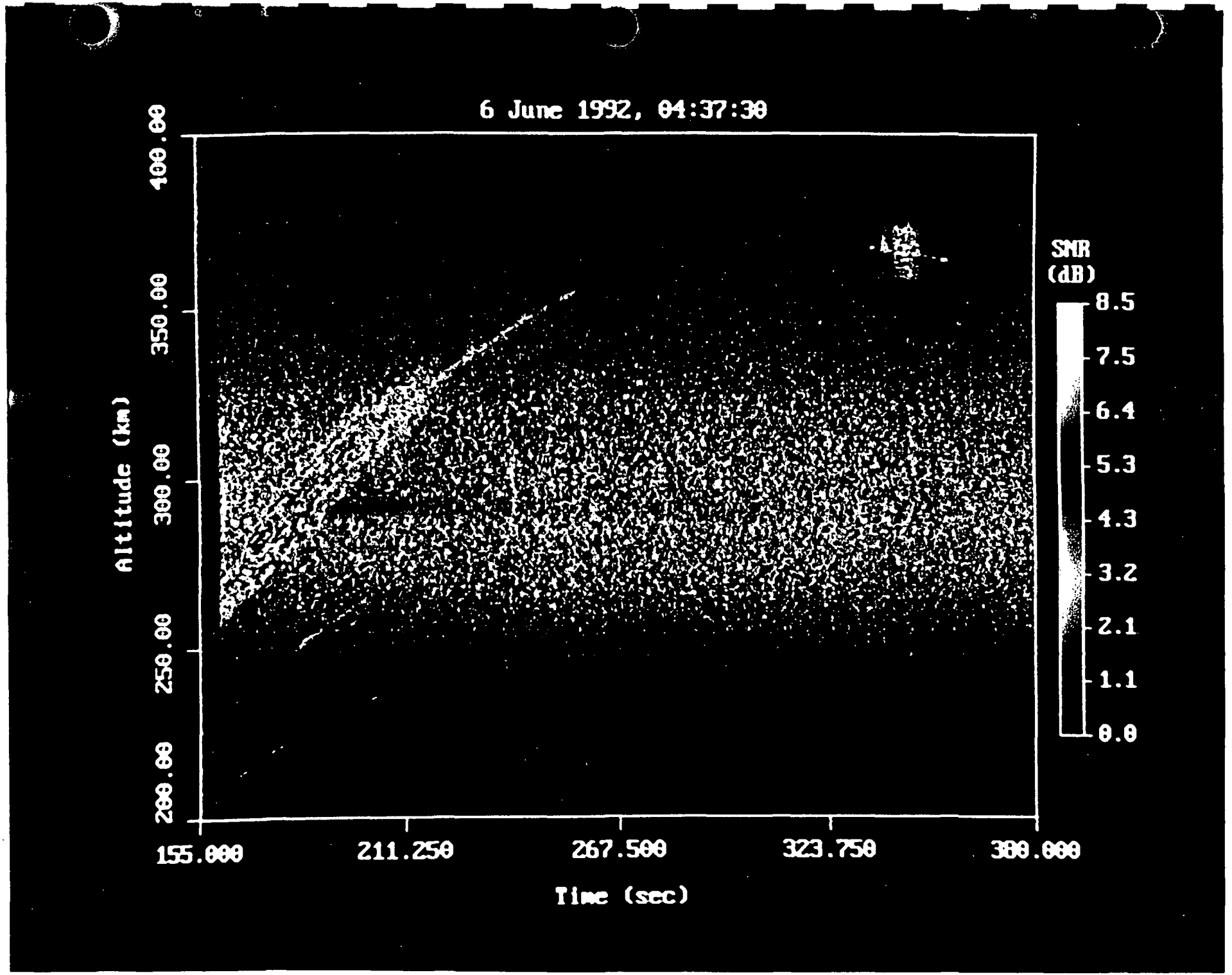
6 June 1992, 04:37:30
Altitude (km)
400.00
350.00
300.00
250.00
200.00
155.000
211.250
267.500
323.750
380.000
Time (sec)
SNR
(dB)
8.5
7.5
6.4
5.3
4.3
3.2
2.1
1.1
0.0

Figure 9

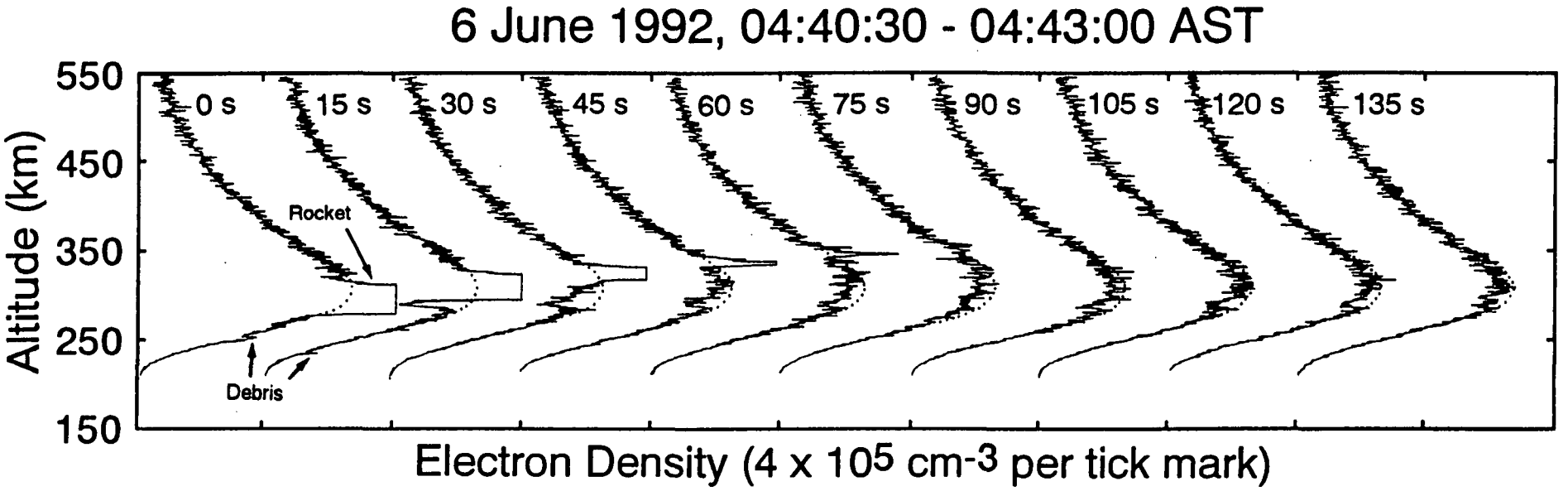
6 June 1992, 04:40:30 - 04:43:00 AST
550
450
350
250
150
Altitude (km)
0 s
15 s
30 s
45 s
60 s
75 s
90 s
105 s
120 s
135 s
Rocket
Debris
Electron Density (4 x 10^5 cm^-3 per tick mark)

Figure 10

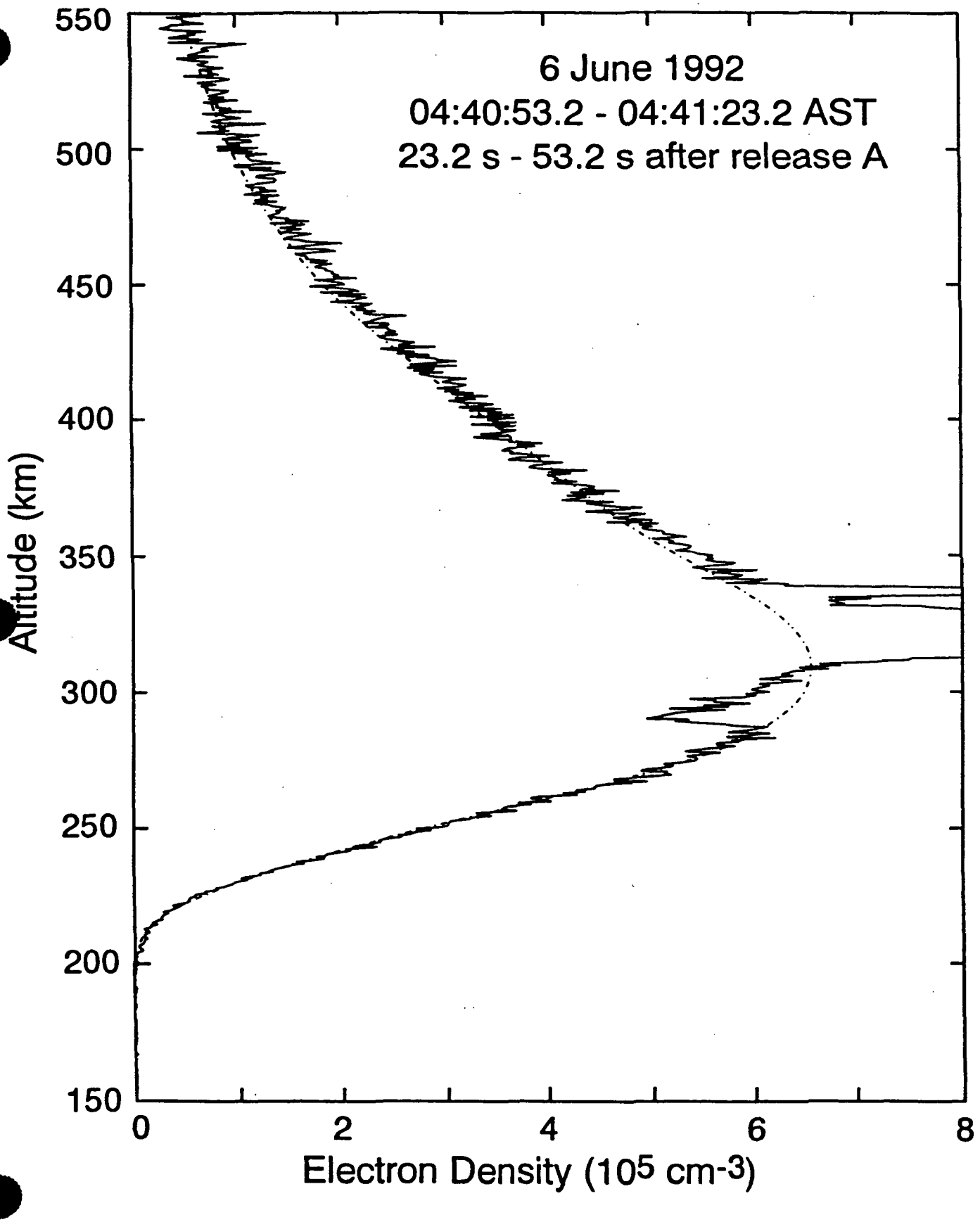
6 June 1992
04:40:53.2 - 04:41:23.2 AST
23.2 s - 53.2 s after release A
Altitude (km)
550
500
450
400
350
300
250
200
150
0
2
4
6
8
Electron Density (10^5 cm^-3)

Figure 11

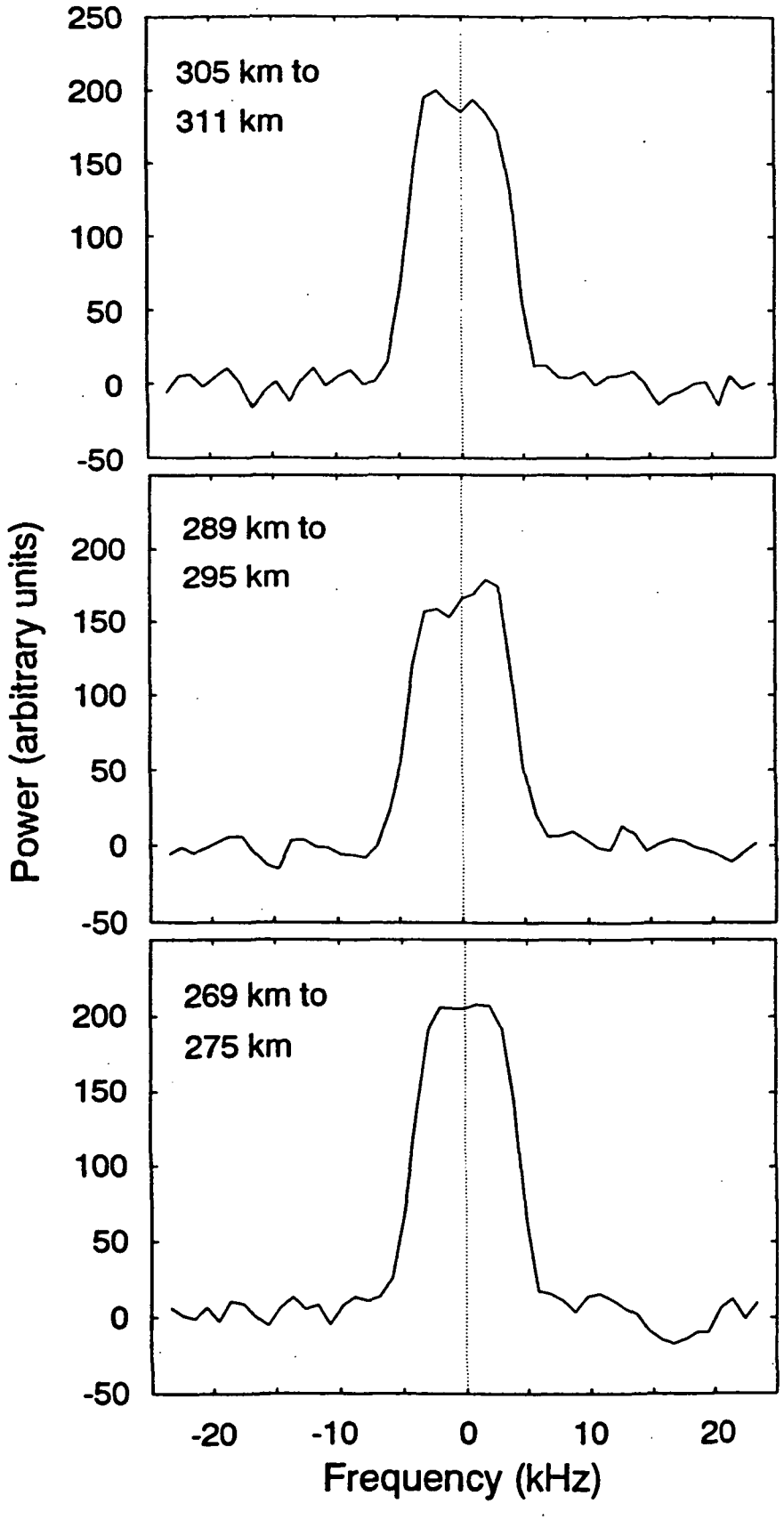
305 km to
311 km
289 km to
295 km
269 km to
275 km
Power (arbitrary units)
250
200
150
100
50
0
-50
-20
-10
0
10
20
Frequency (kHz)

Figure 12

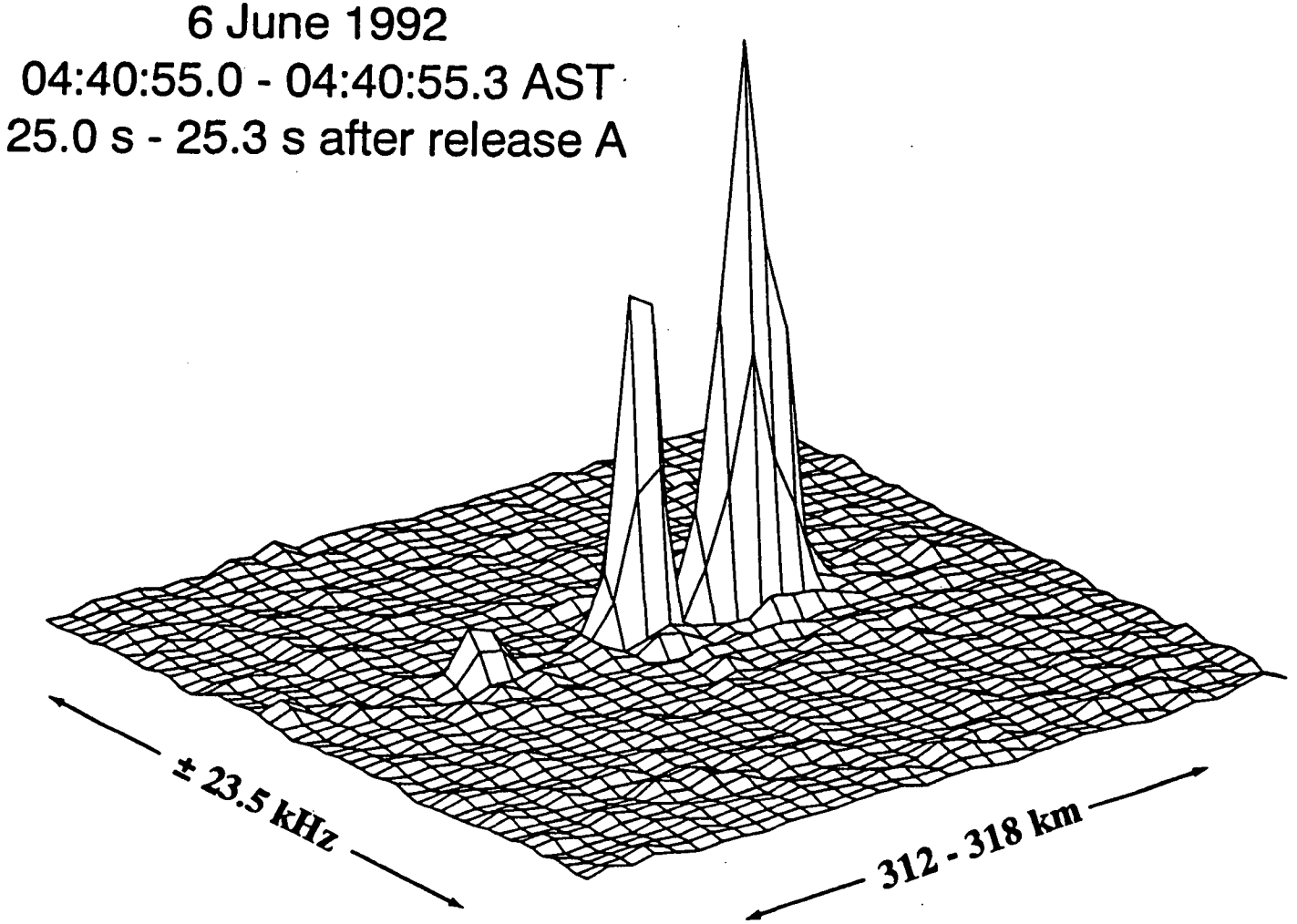
6 June 1992
04:40:55.0 - 04:40:55.3 AST
25.0 s - 25.3 s after release A
± 23.5 kHz
312 - 318 km

Figure 13

5. Spin-off Science Fostered by the *El Coqui* Campaign

Prior to the *El Coqui* Campaign, experiments were performed at Arecibo Observatory to verify radar performance in support of the proposed CRRES observing programs. The measurements were made in May 1991 and involved a collaborative effort between F. T. Djuth of Geospace Research, Inc. (GRI) and M. P. Sulzer of Arecibo Observatory. Data were acquired both with the Arecibo data-taking system and with a high-speed radar processor deployed at the Observatory by GRI. This setup was identical to the actual data acquisition scenario adopted for the *El Coqui* experiments. Several of the CRRES experiments entailed rocket-borne releases of barium in sunlight (at dawn), which was expected to yield prodigious amounts of photoelectrons. We performed tests in the noontime ionosphere to simulate ionospheric conditions appropriate for the CRRES releases. The test results indicated that the methodology developed for CRRES was an extremely valuable tool for studies of natural ionospheric phenomena.

The paper presented below describes the test results and illustrates how they can be used in investigations of the natural environment. This work is published in *Geophysics Research Letters.*, *21*, 2725, 1994.

Application of the Coded Long-Pulse Technique to Plasma Line Studies of the Ionosphere

F. T. Djuth[1], M. P. Sulzer[2], and J. H. Elder[1]

[1] Geospace Research, Inc., 550 N. Continental Boulevard, El Segundo, CA 90245

[2] Arecibo Observatory, Arecibo, Puerto Rico 00613

ABSTRACT

Recently, the coded long-pulse radar technique was tested at Arecibo Observatory, Puerto Rico using photoelectron-enhanced plasma lines in the daytime ionosphere. The technique immediately proved to be a powerful diagnostic tool for studying natural ionospheric phenomena. Our initial observations indicate that extremely accurate measurements of absolute electron density (0.01 to 0.03 % error bars) can be achieved with an altitude resolution of 150 m and a temporal resolution of ~2 s. In addition, the technique provides information about electron density structure within a 150-m altitude cell and yields parameters from which the energy spectrum of suprathermal electrons ($\geq$ 5 eV) can be deduced. Our initial measurements are used to illustrate applications of the coded long-pulse technique to several aeronomic/ionospheric areas of current interest. These include studies of neutral wave motions in the lower thermosphere, measurements of ion composition in the F_1 region, and investigations of electron-gas thermal balance and photoelectron energy loss processes. The technique can be utilized to examine irregularity formation in the F region, measure ionospheric currents, probe electron acceleration processes in ionospheric modification experiments, verify the magnetic field dependence of Langmuir wave damping, and more generally test higher order corrections suggested for the Langmuir dispersion relation.

INTRODUCTION

Ground-based incoherent scatter radars make use of well-established radar techniques to obtain information about a wide variety of physical parameters in the upper atmosphere (~70 km to >1000 km altitude). For example, electron density, electron and ion temperatures (T_e , T_i), ion drift velocities, electrostatic electric fields, and, at lower heights, the ion-neutral collision frequency and the concentration of negative ions, can be measured directly by analyzing the ionospheric scatter returned in a narrow frequency band (10 - 20 kHz) surrounding the radar frequency [Evans, 1969]. While much information can be extracted from the radar scatter near the radar transmission frequency (so-called center-line or ion-line scatter), a wealth of additional information is contained in weak broadband echoes surrounding the center-line scatter (i.e. at frequencies in the band $f_r \pm f_p$, where f_r is the radar frequency and f_p is roughly the electron plasma frequency). These signals are referred to as "plasma lines" and are the result of radio wave scattering from Langmuir waves. In the presence of suprathermal electrons, Langmuir waves are greatly enhanced beyond their natural thermal levels [e.g. Yngvesson and Perkins, 1968]. Populations of suprathermal electrons are readily generated in the daytime ionosphere (photoelectrons) and are a common feature of the auroral ionosphere (particle precipitation events). By monitoring plasma line scatter with an incoherent scatter radar, one can make extremely accurate measurements of electron density and electron density gradients, deduce the energy distribution of the suprathermal electrons present in the ionosphere, monitor the motion of electron density irregularities, and obtain a great deal of information about electron transport and elastic and inelastic collision cross sections in the upper atmosphere [e.g., Mantas and Walker, 1976; Abreu and Carlson, 1977; Carlson *et al.*, 1977; Showen, 1979]. When the ion line and plasma line observations are combined, new insights into atmospheric processes are often obtained [Carlson *et al.*, 1977; Wickwar, 1978; Valladares *et al.*, 1988].

DATA-TAKING METHODOLOGY

Several new radar techniques have been developed that provide great improvements in the altitude and temporal resolution of incoherent scatter radar observations and significantly increase the accuracy with which certain ionospheric parameters (such as electron density) can be measured [e.g., Showen, 1979; Birkmayer *et al.*, 1984; Birkmayer and Hagfors, 1986; Heinselman and Vickrey, 1992a]. The development of the "cutoff" technique [Showen, 1979] and its subsequent refinement [Heinselman and Vickrey, 1992a] provide for high-accuracy measurements near the F-region peak The observational technique described by Birkmayer *et al.* [1984] and Birkmayer and Hagfors [1986] employs a chirped radar approach to greatly improve plasma line measurements of electron density and electron density gradients throughout the F-region ionosphere.

In the current work, we apply the pseudo-random phase-coding technique described by Sulzer [1986] to plasma line measurements in the daytime ionosphere at Arecibo Observatory, Puerto Rico. This radar method is often referred to as the coded long-pulse technique (CLP). During the Arecibo tests discussed below, the 430 MHz incoherent scatter radar was operated at a peak power near 1.5 MW. Radar pulses 512 μs in duration were transmitted within an interpulse period (IPP) of 50 ms. The IPP was initially set to this large value to accommodate the data-taking systems. Each radar pulse had a different phase code imposed on it; the minimum time (baud length) between 180° phase reversals was 1 μs. Complex (in-phase and quadrature) voltages were sampled at a 5 MHz rate so that ~5-MHz segments of the plasma line spectrum could be covered. During the experiment, plasma line sidebands in the frequency range 430 MHz ± (3.5 to 8.5 MHz) were sampled. The low frequency limit (3.5 MHz) coincided with an electron Landau damping cutoff in signal strength; the high frequency limit (8.5 MHz) was set at the point where severe losses are encountered in antenna line-feed gain. This upper frequency restriction will be removed in the near future with the construction of a new

wideband Gregorian feed system at Arecibo. During the Arecibo experiment, independent, wideband (5 MHz) plasma line spectra were obtained every 1-μs in radar time delay, or every 150 m in radar range. The results presented below were obtained at the downshifted plasma line ($f_r - f_p$), where the sensitivity of the Arecibo line feed is the best. The radar beam was pointed vertically.

An example of a plasma line spectrum measured at a single range cell is shown in Figure 1. The tallest spike in the figure is the plasma line signal; the broad hump is caused by plasma line clutter originating at other ranges. Spectra measured at each 150-m range cell can be least-squares fit to determine the frequency of the plasma line peak (approximately equal to the average plasma frequency in a range cell), to establish plasma line spectral width (proportional to the plasma frequency variation within the range cell during the 12.5 s integration period), and to obtain the peak amplitude of the signal as well as the area under the peak (which provides information about the electron energy distribution). Measurements of plasma line frequency, spectral width, and peak area are presented in Figure 2 along with error values for an integration of 250 radar pulses. In general, the error bars at altitudes above 120 km are quite small, and observations in this region can be processed with an automated routine. Currently, radar IPPs as short as 9 ms can be accommodated at Arecibo, so the same quality of results as that shown in Figure 2 is now available after only 2.25 seconds of integration! Below 120 km altitude, error bars can increase significantly because of increased clutter (determined by the shape of the electron density profile) and because electron-neutral collision frequencies become large enough to impact Langmuir wave damping decrements. Measurements below 105 km altitude are extremely difficult to make.

AERONOMIC OBSERVATIONS

By combining the plasma line observations with independent ion-line measurements of electron temperature and solving the Langmuir wave dispersion relationship [Yngvesson and Perkins, 1968], the average electron density in each 150-m range cell can be accurately established. Figure 3 shows an example of an electron density profile calculated in this manner along with the electron density profile obtained from ion-line measurements at about the same time. The normal incoherent scatter ion-line observations have very large random errors compared to the plasma line results. With the CLP plasma line technique, the 1-σ error bars are of the order of 0.03% at lower heights near 120 km and ~ 0.01% at higher altitudes near 210 km. A worst case systematic error for plasma line data at Arecibo can be obtained by ignoring T_e-dependent corrections to the Langmuir wave dispersion relation. This yields systematic electron density errors of ~3% at the lowest heights near 105 km and less than 1% at altitudes above 200 km. Notice that the two data curves in Figure 3 deviate below 200 km altitude. Standard analyses of ion-line data in this altitude region require that an ion composition model be assumed. Errors in the ion composition model result in inaccurate determinations of T_e/T_i, which give rise to the incorrect estimates of electron density in Figure 3. (The discrepancy at E-region altitudes where $T_e/T_i = 1$ indicates that near field correction of the radar beam is not well-understood.) However, one can use the ion line power profile data along with the plasma line observations to deduce the altitude profile of T_e/T_i. This frees up a fitting parameter and allows the mean ion mass to be deduced from the ion line spectrum. Similar strategies can be applied at higher altitudes where the ion mix cannot readily be modeled (e.g. above ~400 km).

The total area of the plasma line peak can be converted into the phase-velocity dependent "temperature" T_p [Yngvesson and Perkins, 1968], which is a physically meaningful way of expressing plasma wave intensity. By plotting κT_p versus plasma wave phase energy one can deduce information about the velocity distribution of

photoelectrons. Figure 4 shows a display of this type obtained using CLP plasma line data. These observations have 100 times better energy resolution and approximately 10 times better temporal resolution than previous measurements of this kind at Arecibo [e.g., Abreu and Carlson, 1977]. This will enable the problem of electron thermal balance in the ionospheric F region [Carlson *et al.*, 1977] to be examined in great detail. Currently, well-known discrepancies [e.g., Swartz and Nisbet, 1973; Carlson *et al.* 1977] arise when model calculations of electron temperature in the daytime ionosphere are compared to temperatures directly measured with incoherent scatter radars for a given value of the solar EUV flux, a measured electron density profile, and measurements of photoelectron-enhanced plasma waves.

The dips in κT_p marked by arrows in Figure 4 are believed to be caused by inelastic collisions between electrons and the neutral gas. Similar "bite outs" were observed between 13 and 15 eV by Abreu and Carlson [1977] with much poorer energy resolution; the bite outs may be related to the dips present in Figure 4. Abreu and Carlson [1977] indicate that these features are not found in theoretically calculated electron fluxes and suggest that relevant atmospheric cross sections be reexamined. Additional theoretical calculations similar to those performed by Jasperse and Smith [1978] would greatly facilitate the interpretation and utility of these data.

Finally, the great precision with which electron density can be measured with the CLP technique is likely to open up new vistas of ionospheric investigation. For example, CLP plasma line studies in the lower thermosphere routinely reveal the presence of gravity waves. In Figure 5, imprints of gravity waves on the electron density profile are readily apparent in the measurements. These profiles were obtained from samples of 250 radar pulses taken every 6 min. Well-defined waves having a vertical wavelength of about 7 km are evident in the early-time observations (11:14 AST, 11:20 AST, and 11:26 AST). In addition, a much longer wavelength disturbance can be seen in the profiles particularly at altitudes between 130 and 140 km. This wave activity gives way

to the formation of an intermediate ion layer beginning at 11:32 AST. It is clear that CLP observations can be a valuable tool for studying the coupling of waves between the mesosphere and thermosphere.

CONCLUSIONS

The application of the coded long-pulse (CLP) technique to daytime plasma line studies at Arecibo provides a powerful new diagnostic tool for probing the upper atmosphere. Although several specific applications have been illustrated in the preceding section, the utility of the technique is not limited to these examples. By simultaneously measuring the upshifted and downshifted plasma lines, ionospheric currents can be measured throughout the ionosphere. Moreover, the technique is sensitive enough to test higher order corrections suggested for the Langmuir dispersion relation [e.g., Heinselman and Vickrey, 1992b; Kofman *et al.*, 1993]. Observations made during radio wave modification of the Arecibo ionosphere have shown that the CLP can readily be used to study electron acceleration processes in the plasma. The technique is well-suited to auroral investigations, where good temporal and spatial resolution is often needed to map out electron density structures and determine electron energy spectra. Other innovative uses of the technique are likely to emerge as more comprehensive data sets are acquired, and new approaches are applied to old problems.

Acknowledgments. Two of the authors (F.T.D. and J.H.E.) acknowledge support from NASA under contract NAS8-39075, the National Science Foundation under grants ATM-9201040 and ATM-9202658, and from The Phillips Laboratory, Hanscom Air Force Base under contract NAS8-39238. The Arecibo Observatory is part of the National Astronomy and Ionosphere Center, which is operated by Cornell University under cooperative agreement with the National Science Foundation.

REFERENCES

Abreu, V. J., and H. C. Carlson, Photoelectron energy loss and spectral features deduced by the plasma line technique, *J. Geophys. Res.*, *82*, 1017-1023, 1977.

Birkmayer, W. T., and T. Hagfors, Observational technique and parameter estimation in plasma line spectrum observations of the ionosphere by chirped I.S. radar, *J. Atmos. Terr. Phys.*, *48*, 1009-1019, 1986.

Birkmayer, W. T., T. Hagfors, and M. P. Sulzer, A new method for accurate ionospheric electron density measurements by incoherent scatter radar, *J. Geophys. Res.*, *89*, 6841-6849, 1984.

Carlson, H. C., Jr., V. B. Wickwar, and G. P. Mantas, The plasma line revisited as an aeronomical diagnostic: suprathermal electrons, solar EUV, electron-gas thermal balance, *Geophys. Res. Lett.*, *12*, 565-567, 1977.

Evans, J. V., Theory and practice of ionosphere study by Thomson scatter radar, *Proc. IEEE*, *57*, 495-530, 1969.

Heinselman, C. J., and J. F. Vickrey, On the spectral analysis and interpretation of incoherent scatter plasma line echoes, *Radio Sci.*, *27*, 221-230, 1992a.

Heinselman, C. J., and J. F. Vickrey, On the frequency of Langmuir waves in the ionosphere, *J. Geophys. Res.*, *97*, 14,905-14,910, 1992b.

Jasperse, J. R., and E. R. Smith, The photoelectron flux in the earth's ionosphere at energies in the vicinity of photoionization peaks, *Geophys. Res. Lett.*, *5*, 843-846, 1978.

Kofman, W., J.-P. St-Maurice, and A. P. van Eyken, Heat flow effect on the plasma line frequency, *J. Geophys. Res.*, *98*, 6,079-6,085, 1993.

Mantas, G. P., and J. C. G. Walker, The penetration of soft electrons into the ionosphere, *Planet. Space Sci.*, *24*, 409-423, 1976.

Showen, R. L., The spectral measurement of plasma lines, *Radio Sci.*, *14*, 503-508, 1979.

Sulzer, M. P., A radar technique for high range resolution incoherent scatter autocorrelation function measurements utilizing the full average power of klystron radars, *Radio Sci.*, *21*, 1033-1040, 1986.

Swartz, W. E. and J. S. Nisbet, Incompatibility of solar EUV fluxes and incoherent scatter measurements at Arecibo, *J. Geophys. Res.*, *78*, 5640, 1973.

Valladares, C. E., M. C. Kelley, and J. F. Vickrey, Plasma line observations in the auroral oval, *J. Geophys. Res.*, *93*, 1997-2003, 1988.

Wickwar, V. B., Plasma lines in the auroral *E* layer, *J. Geophys. Res.*, *83*, 5186-5190, 1978.

Yngvesson, K. O., and F. W. Perkins, Radar Thomson scatter studies of photoelectrons in the ionosphere and Landau damping, *J. Geophys. Res.*, *73*, 97-110, 1968.

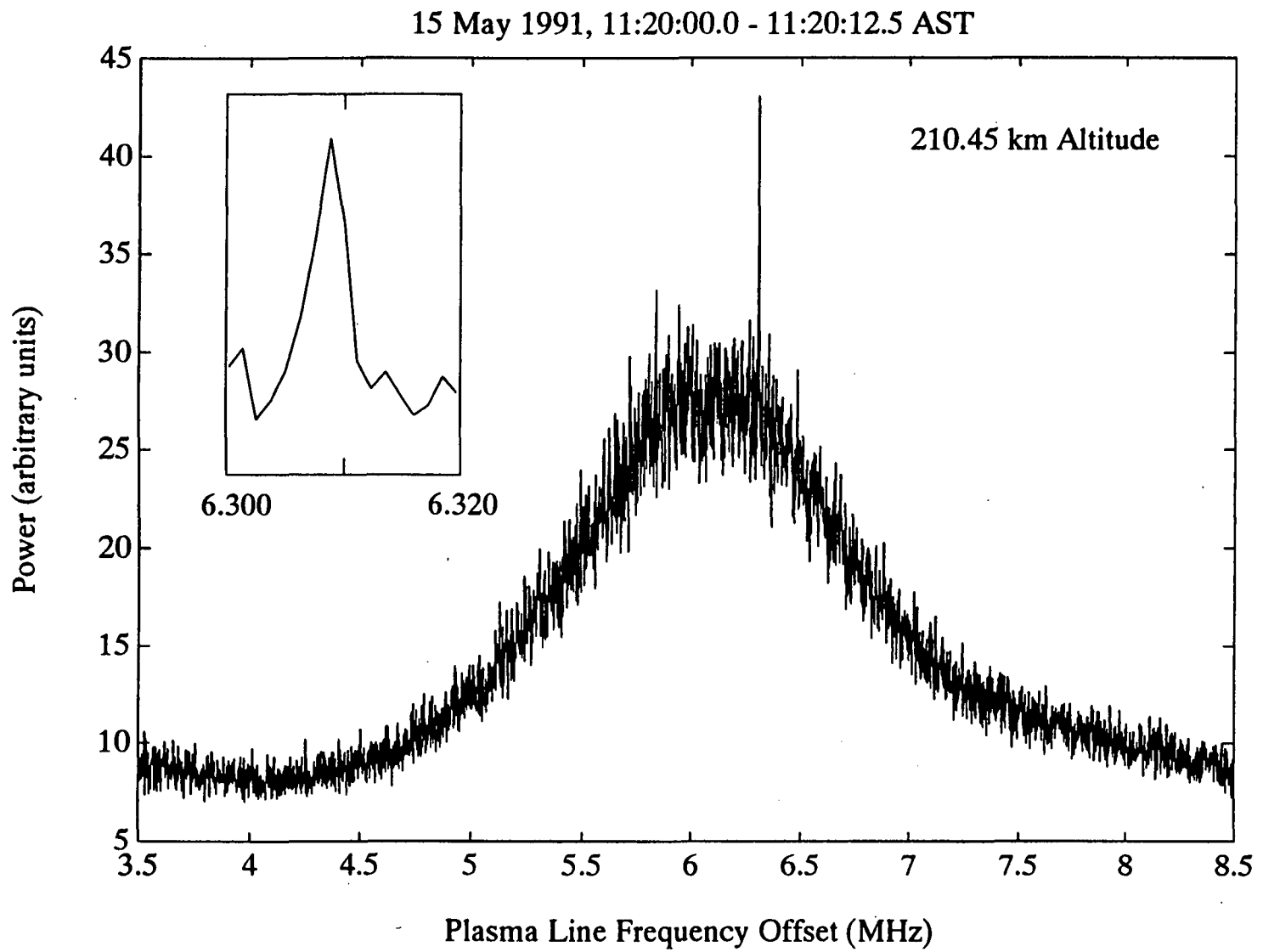

Fig. 1. Example of a wideband plasma line spectrum measured in a single 150-m range cell during the May 1991 tests. The band pass displayed extends from 430 MHz - 3.5 MHz to 430 MHz -8.5 MHz. The tallest spike in the figure is the daytime photoelectron-enhanced plasma line signal; the broad hump is caused by plasma line clutter originating at other ranges. Inset shows plasma-line peak in greater detail.

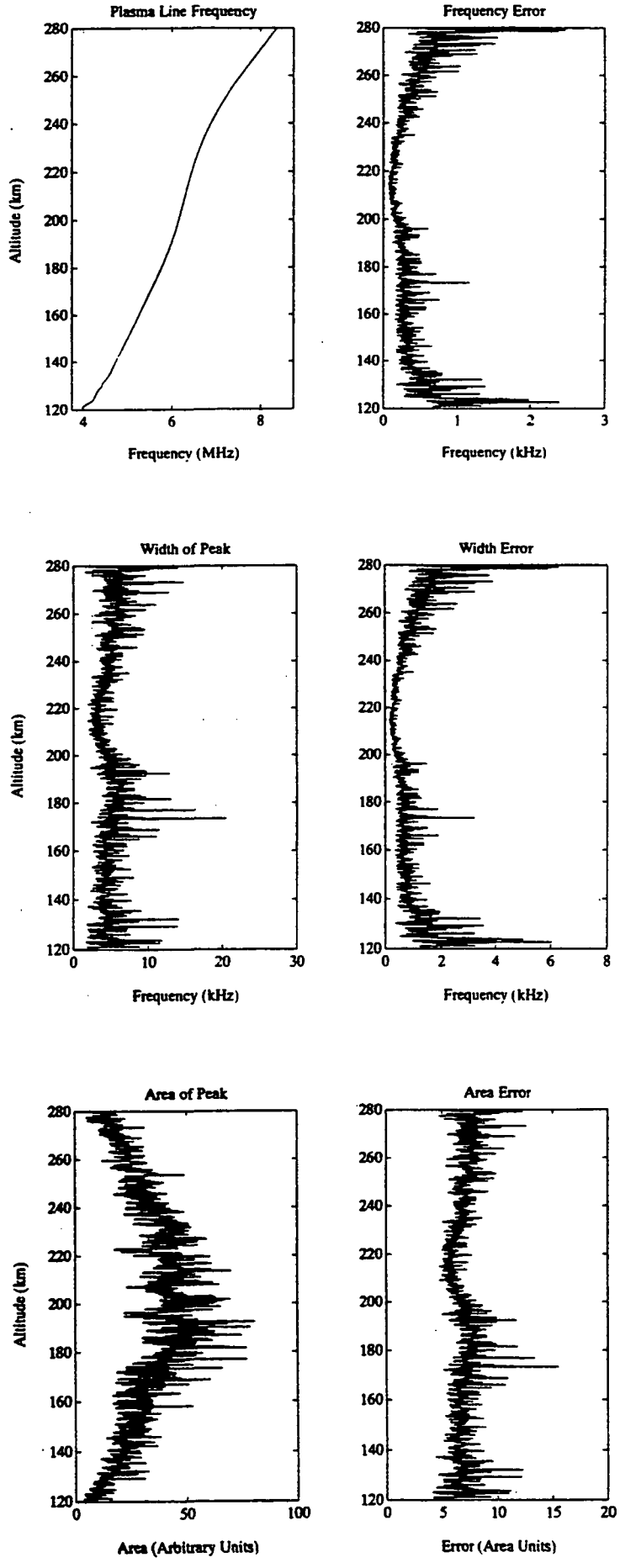

Fig. 2. Frequency of plasma line peak, peak width, and area of peak versus altitude for data obtained on 15 May 1991, 11:20:00.0 - 11:20:12.5 AST (panels on left). One-sigma error bars calculated as part of the nonlinear least-squares fitting process are shown in panels at right.

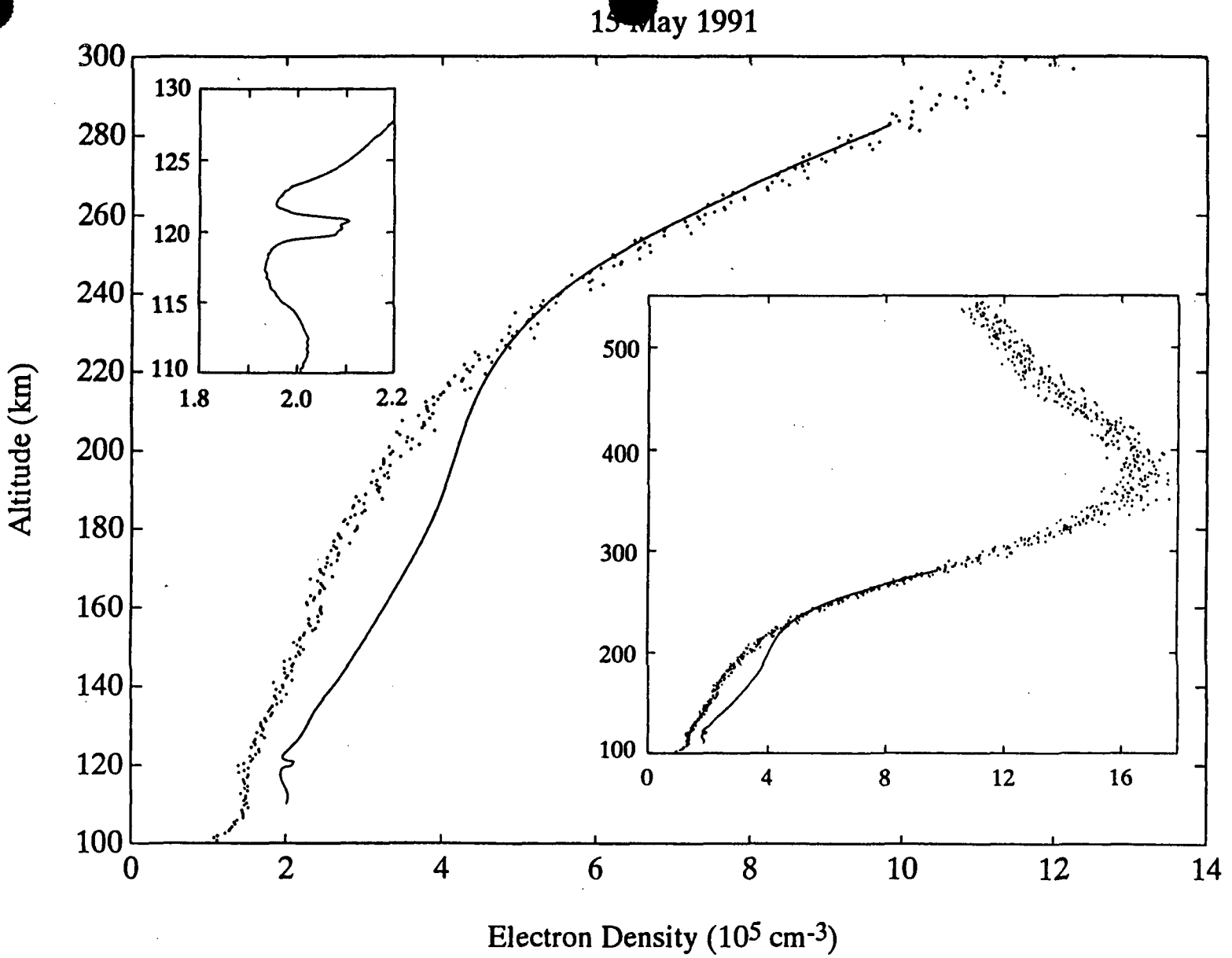

Fig. 3. Electron density profile measured using the downshifted plasma line on 15 May 1991, 13:24:00.0 - 13:24:12.5 AST with 150-m altitude resolution (solid line), and ion line measurements of the electron density profile made shortly thereafter from 13:32:40.0 to 13:32:52.5 AST with 600-m resolution (dots). The ion line profile has been corrected for range, antenna near-field effects, and T_e/T_i; the peak of the F-layer was calibrated using an f_oF_2 measurement simultaneously made with the ionosonde at Arecibo Observatory. Details of the sporadic-E region are shown in upper left inset, and the full profile is displayed at bottom right.

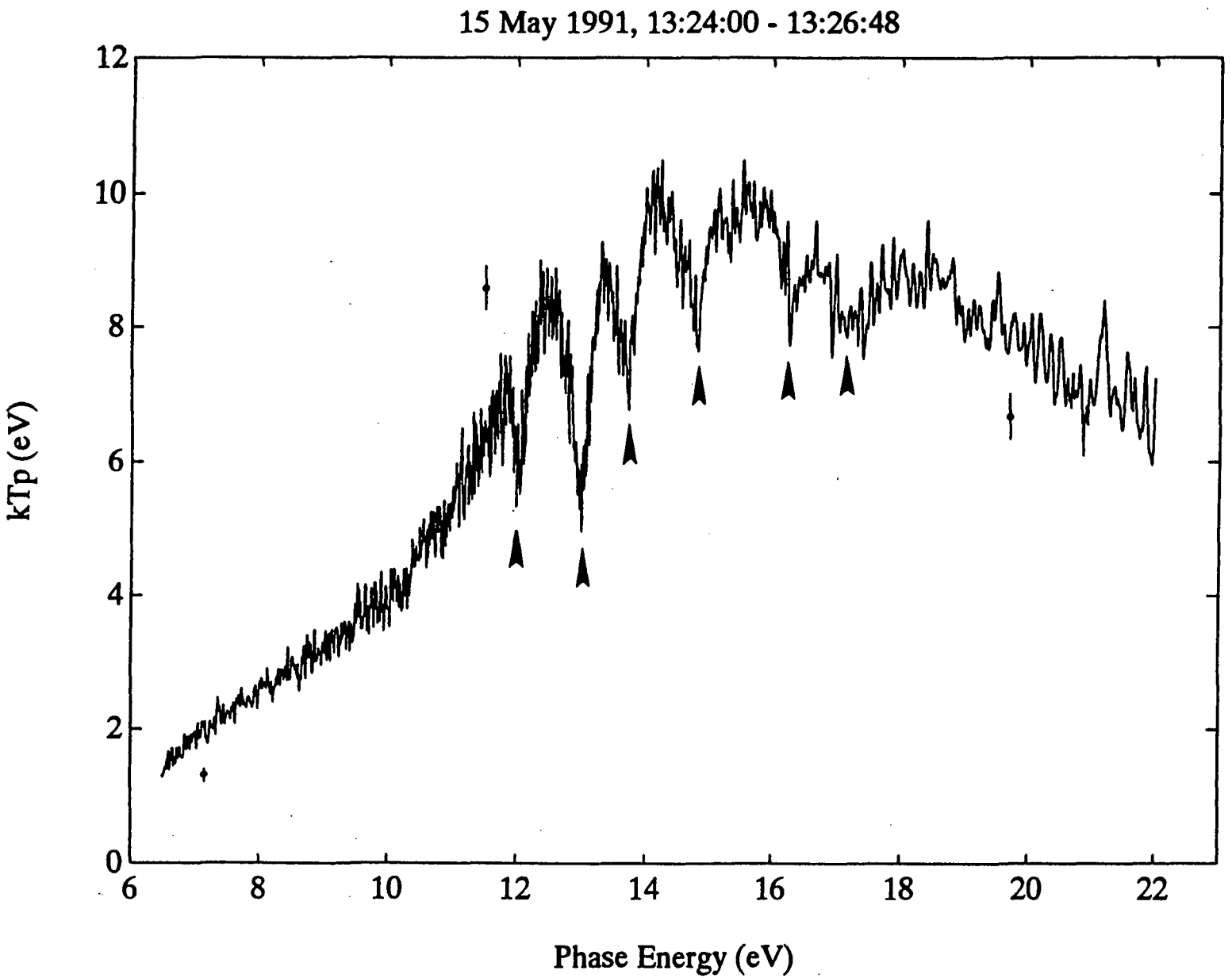

Fig 4. Plasma line intensity in κTp as a function of Langmuir wave phase energy. The lowest energy near 6 eV corresponds to data taken at an altitude of 125 km, whereas the highest energy (25 eV) corresponds to an altitude of about 275 km. Representative 1-σ error bars are shown in three regions of the spectrum.

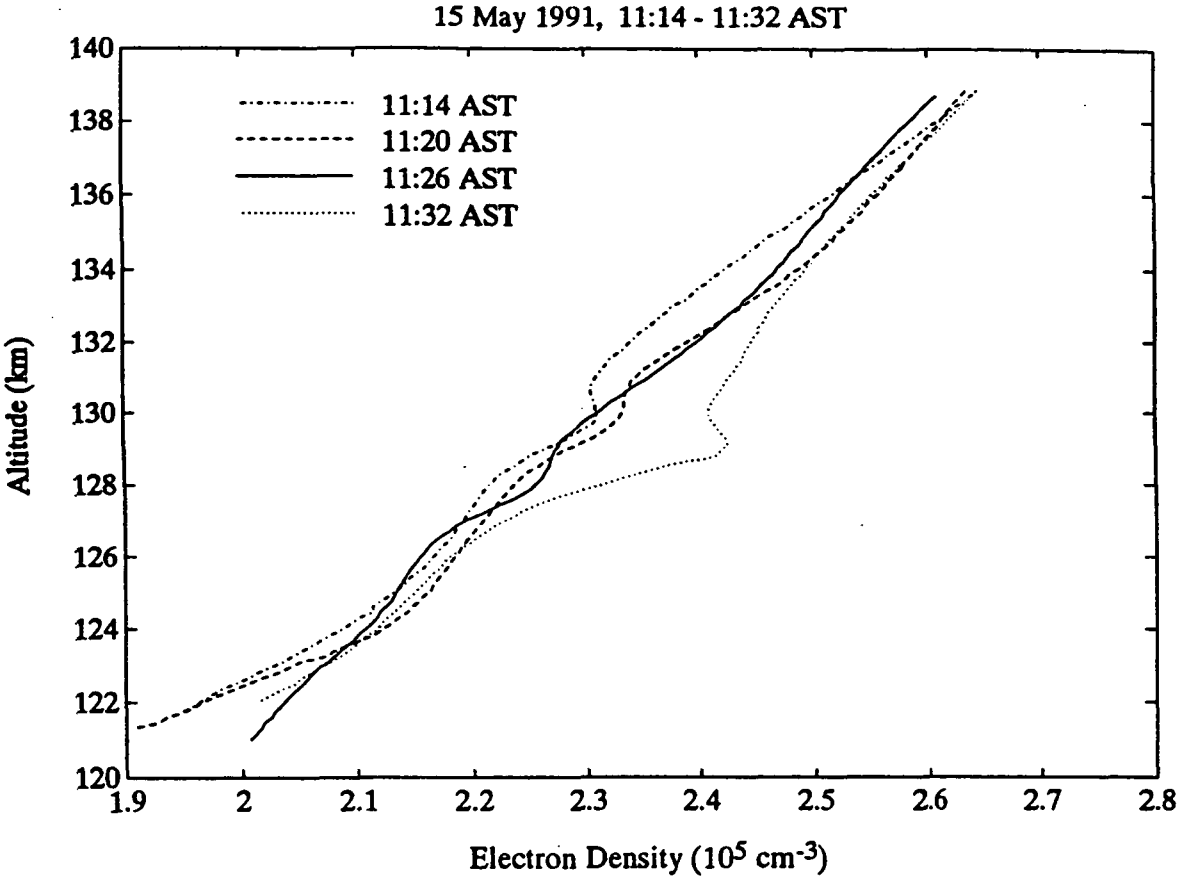

Fig. 5a. Lower thermosphere segment of electron density profiles recorded at six-minute intervals. The data acquisition period for each profile is 12.5 s.

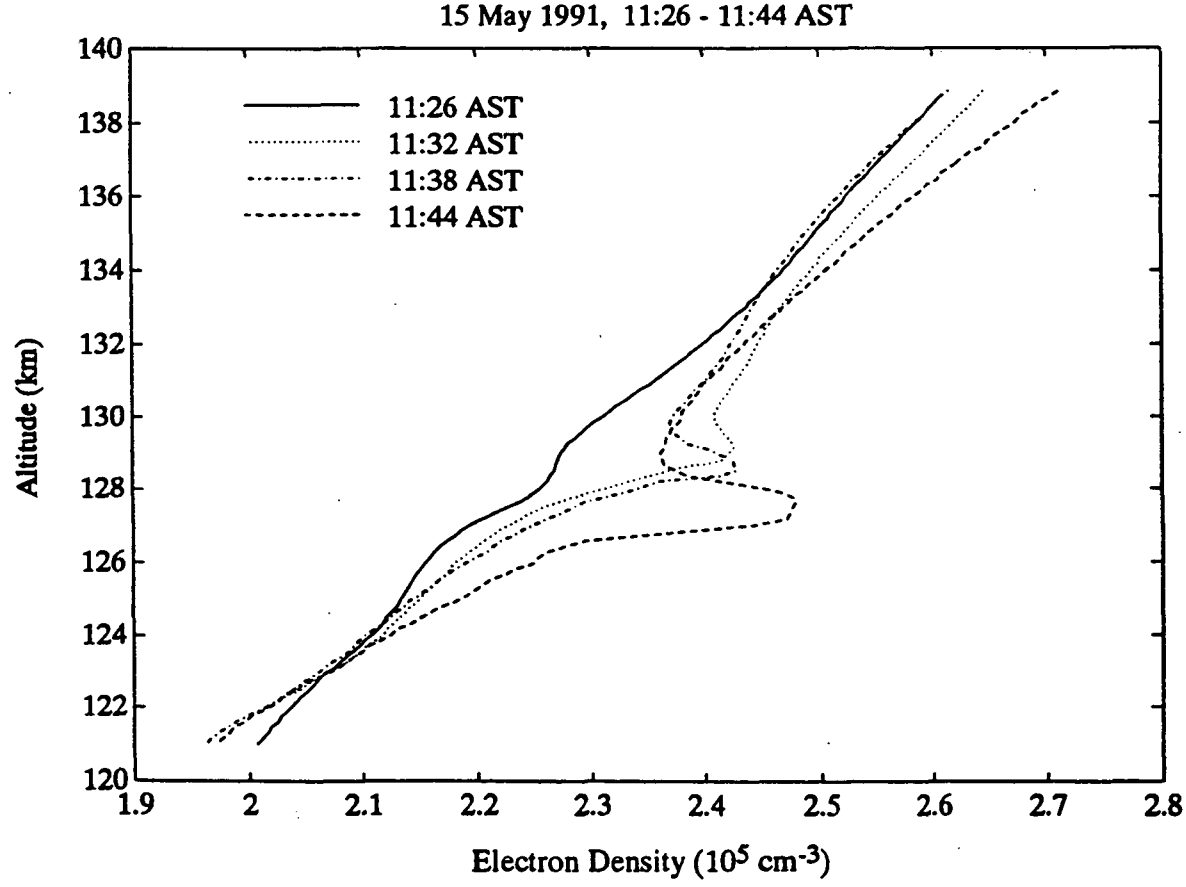

Fig. 5b. Continuation of the measurements shown in Fig. 5a at later times. For reference, the profiles recorded at 11:26 AST and 11:32 AST are repeated in the display.

REPORT DOCUMENTATION PAGE

Form Approved
OMB No. 0704-0188

Public reporting burden for this collection of information is estimated to average 1 hour per response, including the time for reviewing instructions, searching existing data sources, gathering and maintaining the data needed, and completing and reviewing the collection of information. Send comments regarding this burden estimate or any other aspect of this collection of information, including suggestions for reducing this burden, to Washington Headquarters Services, Directorate for Information Operations and Reports, 1215 Jefferson Davis Highway, Suite 1204, Arlington, VA 22202-4302, and to the Office of Management and Budget, Paperwork Reduction Project (0704-0188), Washington, DC 20503.

1. AGENCY USE ONLY *(Leave blank)*	2. REPORT DATE	3. REPORT TYPE AND DATES COVERED
	7 July 1995	Final Report, 21 Aug 1991 through 30 June 1994

4. TITLE AND SUBTITLE

Radar Investigations of Barium Releases over Arecibo Observatory, Puerto Rico

5. FUNDING NUMBERS

NAS8-39075

6. AUTHOR(S)

Frank T. Djuth

7. PERFORMING ORGANIZATION NAME(S) AND ADDRESS(ES)

Geospace Research, Inc.
550 N. Continental Boulevard, Suite 110
El Segundo, CA 90245

8. PERFORMING ORGANIZATION REPORT NUMBER

GRI-CR-95-7110

9. SPONSORING/MONITORING AGENCY NAME(S) AND ADDRESS(ES)

NASA
Marshall Space Flight Center
Marshall Space Flight Center, AL 35812
COTR: Mr. Clarence Gearhart/EM41

10. SPONSORING/MONITORING AGENCY REPORT NUMBER

11. SUPPLEMENTARY NOTES

12a. DISTRIBUTION/AVAILABILITY STATEMENT

Approved for public release; distribution unlimited

12b. DISTRIBUTION CODE

13. ABSTRACT *(Maximum 200 words)*

The NASA Combined Release and Radiation Effects Satellite (CRRES) *El Coqui* rocket campaign was successfully carried out in Puerto Rico during the period 18 May through 12 July 1992. This report describes five chemical release experiments in the upper ionosphere supported by Geospace Research, Inc. during the *El Coqui* campaign. Additional spin-off science is also discussed. The *El Coqui* releases are designated AA-1 (rocket 36-082), AA-2 (rocket 36-081), AA-3b (rocket 36-064), AA-4 (rocket 36-065), and AA-7 (rocket 36-083). Particular attention is paid to releases AA-2 and AA-4. These two experiments involved the illumination of ionospheric release regions with powerful high-frequency (HF) radio waves transmitted from the Arecibo HF facility. In the AA-2 experiment, mircroinstabilities excited by the HF wave in a Ba^+ plasma were examined. This release yielded a smooth plasma cloud that helped clarify several fundamental issues regarding the physics of wave-plasma instabilities. During AA-2 extremely strong HF-induced Langmuir turbulence was detected with the Arecibo 430 MHz radar. CF_3Br was released in the AA-4 study to create an ionospheric hole that focused the HF beam. This experiment successfully explored wave-plasma coupling in an O^+ ionosphere under conditions of very high HF electric field strengths.

14. SUBJECT TERMS

Ionosphere, Chemical Releases, Active Experiments, Ionospheric Irregularities, Plasma Instabilities

15. NUMBER OF PAGES

156

16. PRICE CODE

17. SECURITY CLASSIFICATION OF REPORT	18. SECURITY CLASSIFICATION OF THIS PAGE	19. SECURITY CLASSIFICATION OF ABSTRACT	20. LIMITATION OF ABSTRACT
Unclassified	Unclassified	Unclassified	SAR